Applications for liquid chromatography coupled to isotope ratio mass spectrometry and evaluation of the oxidation processes towards compound specific δ^{15}N analysis

Dissertation

zur Erlangung des akademischen Grades eines

Doktors der Naturwissenschaften

– Dr. rer. nat. –

vorgelegt von

Daniel Köster

geboren in Paderborn

Fakultät für Chemie

der

Universität Duisburg-Essen

2020

Die vorliegende Arbeit wurde im Zeitraum von April 2015 bis Dezember 2018 im Arbeitskreis für Instrumentelle Analytische Chemie von Prof. Dr. Schmidt in der Fakultät für Chemie der Universität Duisburg-Essen durchgeführt.

Tag der Disputation: 15.06.2020

Gutachter: Prof. Dr. Torsten C. Schmidt

Prof. Dr. Oliver J. Schmitz

Vorsitzender: Prof. Dr. Rainer U. Meckenstock

DOI: 10.17185/duepublico/71933
URN: urn:nbn:de:hbz:464-20211109-145728-3

Table of Content

Summary

LC-IRMS has become a valuable tool in analytical chemistry since it was established in 2004. With more than 70 published applications in peer reviewed journals in the past 15 years, the main fields of application are in authenticity control, degradation of environmental contaminants, and the measurement amino acid in the context of nutrition, archeology, or forensics. As demonstrated in the present work by the elucidation of the plant origin of xylitol in chewing gums, compound specific $\delta^{13}C$ analysis by LC-IRMS is able to deliver precise carbon isotopic information with a simple sample preparation procedure and an online combination of analyte separation and measurement. With the developed method and sample preparation, xylitol in chewing gum formulations based on wood material could be discriminated from the cheaper substituent which is based on corn husks. Many applications using $\delta^{13}C$ analysis could benefit from an additional determination of the $\delta^{15}N$ information, which can increase the power to discriminate between analyte sources or serve as an additional information in the monitoring of the degradation of pollutants.

To develop a LC-IRMS system based on the persulfate oxidation process in combination with a membrane gas separation unit for $\delta^{15}N$ measurements, the oxidation process in the interface under standard $\delta^{13}C$ measurement conditions was thoroughly evaluated. Special focus of the work on the oxidation efficiency was on the interaction of the interface oxidation parameters, as these are commonly not evaluated in existing publications. The obtained results show that accurate isotopic signatures for carbon can be obtained even though the transformation to CO_2 is not 100 % complete if the principle of identical treatment of the analytes and reference substances is applied. In addition, the common assumption that a linear correlation between analyte concentration and signal intensity in LC-IMRS indicates complete conversion of the analyte could be disproved. Only with the developed combination of TOC measurement and the LC-IRMS interface or separate referencing with a carbonate standard, exact information about the oxidation efficiency in the interface can be obtained. Based on the standard oxidation conditions in the interface, batch experiments with nitrogen containing model analytes were performed in a large scale reaction vessel to obtain a time resolved speciation of the nitrogen containing reaction products formed during the mineralization. For the analysis of the remaining organic analyte, the total bound nitrogen, ammonium, nitrate, and nitrite, analytical methods were developed on a combined TOC/TNb instrument and two IC systems for anion and cation chromatography. The main challenge for the method

development were the high background of sodium or potassium as well as sulfate and persulfate that originates from the oxidation agent which is present in large excess (g L^{-1} for the oxidation agent vs. low mg L^{-1} for the nitrogen containing mineralization products). The TNb measurement was strongly affected by the presence of persulfate especially for ammonium and organic nitrogen, whereas nitrate was not affected at the tested conditions. Based on the TOC and the ion chromatography based measurements, nitrate and ammonium could be identified as the main products of the mineralization. The results were evaluated with a nitrogen mass balance approach which indicated, that for the tested model compounds, overall nitrogen recoveries between 91 and 102 % could be obtained. Under the standard oxidation conditions, ammonium oxidation to nitrate was not fast enough for the application in an online-reactor setup, which could be applied for the δ^{15}N measurement by LC-IMRS.

As a result of the mixed production of ammonium and nitrate under acidic conditions the reaction conditions had to be adapted and oxidation of nitrogen containing analytes in an alkaline medium was evaluated. Initially, ammonium and nitrate were observed as the main reaction products, but the subsequent oxidation of ammonium to nitrate is comparably faster at alkaline conditions. The alkaline oxidation conditions were transferred from the batch reactor system to the LC-IMRS interface. At combined system flow rates of 275 µL min^{-1}, more than 62.5 % of the initially introduced nitrogen could be recovered with a setup using a commercially available interface. For amino acids e.g. glycine, nitrate recovery rates of 85.5 % could be obtained. It could be shown, that increased residence times in the oxidation reactor (by reduction of the system flow) could lead to increased recoveries for the model compounds. Based on the evaluation of the persulfate oxidation reaction in the LC-IRMS interface and the results obtained for the oxidation under alkaline reaction conditions, nitrate could be utilized as an intermediate species used for quantitative conversion of the analyte nitrogen to an IRMS measureable gaseous form. The problem of the formation of two intermediate species (ammonium and nitrate) as observed for the oxidation under acidic conditions could be overcome by the new reaction conditions. The alkaline oxidation was successfully tested for model compounds in a commercially available LC-IRMS interface.

Zusammenfassung

Die LC-IRMS Kopplung hat sich seit der Einführung des ersten kommerziell verfügbaren Systems im Jahr 2004 zu einer analytischen Methode mit breitem Anwendungsfeld entwickelt. Mehr als 70 Anwendungen wurden in den letzten 15 Jahren im Bereich der Authentizitätskontrolle, der Überwachung des Abbaus von Umweltschadstoffen und der Untersuchung von Aminosäuren im Kontext der Ernährungswissenschaften, der Archäologie, sowie der Forensik veröffentlicht. Wie in dieser Arbeit am Beispiel der Untersuchung der pflanzlichen Herkunft von Xylit aus Kaugummis gezeigt werden konnte, lassen sich mit Hilfe der LC-IMRS Technik präzise Kohlenstoffisotopenverhältnisse mit einer einfachen Probenvorbereitung und kombinierter Trennung und substanzspezifischer Detektion ermitteln. Mit der entwickelten Methode und Probenvorbereitung lässt sich zwischen dem in Kaugummis verwendeten Xylit welches aus Holz hergestellt wurde, und dem günstigeren Alternativprodukt aus Nebenerzeugnissen der Maisproduktion unterscheiden. Viele der zur Zeit genutzten Applikationen der δ^{13}C Messungen könnten von einer zusätzlichen Bestimmung des Stickstoffisotopenverhältnisses profitieren, wodurch zum Beispiel die Unterscheidung zwischen der Quelle von Kontaminanten oder die Überwachung von Abbauprozessen der Analyten verbessert werden könnte.

Für die Weiterentwicklung des LC-IRMS Systems zur komponentenspezifischen δ^{15}N Messung basierend auf der Oxidation der Analyten mit Persulfat in der flüssigen Phase und einer darauf folgenden Abtrennung der entstandenen Gase per Membran musste zunächst der Oxidationsprozess unter Standardbedingungen für die δ^{13}C Messungen genau untersucht werden. Der Fokus der Arbeit zur Untersuchung der Oxidationseffizienz im Interface lag dabei auf der Interaktion der einzelnen Methodenparameter, da diese in der Literatur bisher nicht ausführlich untersucht wurde. Mit den Ergebnissen konnte gezeigt werden, dass unter Berücksichtigung der identischen Handhabung von Analyten und Referenzmaterialien bei der Messung für Kohlenstoff akkurate Ergebnisse erzielt werden könne, auch wenn die oxidative Umsetzung im Interface nicht komplett ist. Zusätzlich konnte gezeigt werden, dass die häufig getätigte Annahme, dass ein linearer Zusammenhang von Analytkonzentration und Intensität des Messsignals ein Indiz für eine vollständige Umsetzung im Interface sei wiederlegt werden. Mit der entwickelten Kombination von TOC Messungen und LC-IRMS Interface oder der separaten Referenzierung über einen Karbonatstandard lassen sich exakte Informationen über die Oxidationseffizienz im Interface erhalten.

Um die Entstehung der stickstoffhaltigen Oxidationsprodukte währen der Mineralisierung stickstoffhaltiger organischer Verbindungen unter den standardmäßigen Oxidationsbedingungen im Interface zeitlich aufgelöst verfolgen zu können, wurde die Oxidation im größeren Maßstab in einem externen Reaktor durchgeführt. Zur Analyse des verbliebenen organischen Kohlenstoffs, des gesamt Stickstoff, Ammonium, Nitrat und Nitrit wurden analytische Methoden auf einem TOC/TNb Analysator und zwei IC Systemen zur Anionen- und Kationenchromatographie entwickelt. Ein Hauptaugenmerk bei der Methodenentwicklung lag auf dem großen Hintergrund an Natrium und Kalium sowie Sulfat und Persulfat aus dem Oxidationsmittel, der im großen Überschuss zu den Analyten in den Proben vorhanden ist (g L^{-1} an Oxidationsmittel im Gegensatz zu mg L^{-1} für die stickstoffhaltigen Oxidationsprodukte). Die TNb Messungen wurden stark vom Überschuss an Oxidationsmittel beeinflusst, wobei es vor allem zu Unterbefunden bei Ammonium und organisch gebundenem Stickstoff kam, die Nitratmessung war unter den getesteten Bedingungen nicht beeinflusst. Mithilfe von TOC und IC Messungen konnten Nitrat und Ammonium als die Hauptreaktionsprodukte der Mineralisierung identifiziert werden. Die Ergebnisse wurden über eine Stickstoffmassenbilanz ausgewertet, die zeigen konnte, dass Wiederfindungsraten von 91 - 102 % für Stickstoff erreicht werden konnten. Unter den standardmäßigen Oxidationsbedingungen wurde das gebildete Ammonium nicht schnell genug in Nitrat umgesetzt um eine Realisierung der Oxidation in einem Durchflussreaktor zu ermöglichen, der für den Einsatz in einem Interface für die δ^{15}N Analytik eingesetzt werden könnte.

Als Ergebnis der Bildung von Ammonium und Nitrat aus der Mineralisierung unter sauren Bedingungen wurden die Reaktionsbedingungen angepasst und Versuche zur Oxidation unter alkalischen Bedingungen durchgeführt. Auch hier wurden bei den Batch-Versuchen zunächst Ammonium und Nitrat als Hauptprodukte identifiziert, allerdings konnte gezeigt werden, dass die Oxidation von Ammonium zu Nitrat unter alkalischen Bedingungen deutlich schneller abläuft. Die Oxidationsbedingungen aus den Reaktorversuchen wurden auf die Oxidation im Durchflusssystem des LC-IRMS Interfaces übertragen. Bei Gesamtflüssen von 275 µL min^{-1}, konnten mehr als 62.5 % des vorhandenen Stickstoffes aus den Analyten zu Nitrat umgewandelt werden. Für Aminosäuren wie z.B. Glycin, konnten sogar Umsatzraten von bis zu 85.5 % erreicht werden. Es konnte gezeigt werden, dass für eine Verbesserung der Oxidationseffizienz vor allem eine Erhöhung der Aufenthaltszeit im Reaktor (über einen niedrigeren Fluss) ausschlaggebend ist.

Auf der Grundlage der Erkenntnisse aus der Untersuchung der Oxidationseffizienz im LC-IRMS Interface und den Ergebnissen der Versuche zur alkalischen Oxidation, hat sich gezeigt, dass Nitrat als Zwischenstufe für die möglichst quantitative Umsetzung des im Analyten gebundenen Stickstoffes zu einem mittels IRMS messbaren Gas sehr gut geeignet ist. Die Problematik der parallelen Bildung von Ammonium und Nitrat unter sauren pH Bedingungen kann so unter den neu entwickelten Reaktionsbedingungen vermieden werden. Die Oxidation unter alkalischem pH konnten in einem kommerziell verfügbaren LC-IMRS System mit verschiedenen Modellsubstanzen erfolgreich getestet werden.

Chapter 1: Introduction

In contrast to classical tools in analytical chemistry, which are mainly designed for the precise quantification or identification of substances, stable isotope analysis offers an additional dimension of information that can be obtained from the involved molecules themselves. Processes such as phase transfer or chemical reactions can introduce changes to the isotopic composition of an analyte by fractionation processes. With the help of stable isotope analysis (SIA), these small changes in the isotopic composition can be measured to get an insight into the history of a substance which has been imprinted into the ratio of heavy to light isotopes. In many fields of research, such as geochemistry, archeology, nutrition, doping control, and food authenticity, SIA has become a valuable tool. Isotope ratios can be determined from bulk samples such as hair or whole plant material, but additional information can be gained by compound specific isotope analysis (CSIA), where individual substances are chromatographically separated prior to analysis. Separation is mainly performed by gas chromatography or liquid chromatography coupled to isotope ratio mass spectrometry (GC-IRMS & LC-IRMS).[1] In case of GC-IRMS methods for the measurement of hydrogen, carbon and nitrogen isotope ratios are well established. In contrast, the coupling of LC with IRMS was developed more recently due to technical challenges and is only available for the determination of carbon isotope ratios. For many applications LC-IRMS offers the advantage that polar non-volatile compounds can be directly analyzed, whereas GC-IRMS measurement would require derivatization of the analytes to perform isotope analysis.

1.1 Stable isotopes

The term isotope refers to a nuclide of a chemical element having the same atomic number (number of protons, Z) but a different mass number (number of neutrons + number of protons, A)[2] For example, the two stable isotopic forms of carbon are commonly expressed in the form ${}^{A}_{Z}C$ as ${}^{12}_{6}C$ for the light isotope and ${}^{13}_{6}C$ for the heavy isotope of carbon. From the nearly 2500 known nuclei, 250 nuclei are considered to be stable based on their half-life being greater than 500 x 10^6 years.[3] Distribution of the heavy to the light isotope varies between the elements. For hydrogen, carbon, nitrogen, and oxygen, the light isotope accounts for more than 95 % of all isotopes, whereas the opposite is true for lithium and boron, where >80 % of the element is represented by the heavy isotope form.[4] The abundance of the most relevant elements in environmental stable isotope analysis are shown in **Table 1.1**.

Table 1.1: Isotopic abundance of the elements commonly used in SIA expressed as mole fractions[5]

Element	Analyte gas	m/z measured	Mass number	Stable isotope	Representative isotopic composition (mole fraction)
Hydrogen	H_2	2, 3	1	^{1}H	0.999885(70)
			2	^{2}H, D	0.000115(70)
Carbon	CO_2	44, 45, 46	12	^{12}C	0.9893(8)
			13	^{13}C	0.0107(8)
Nitrogen	N_2	28, 29, 30	14	^{14}N	0.99636(20)
			15	^{15}N	0.00364(20)
Oxygen	CO	28, 29, 30	16	^{16}O	0.99757(16)
			17	^{17}O	0.00038(1)
			18	^{18}O	0.00205(14)

In a molecule, the isotopic composition can either differ in the number of isotopic substitutions or the position of the isotopic substitution. Molecules that only differ in the number of isotopic substitutions are termed isotopologues.[1] Methane for example can be present in ten isotopologue forms with different amounts of substitution of ^{13}C and ^{2}H isotopes. If the overall mass of a molecule is constant, and the position of the isotopic substitution in the molecule changes, the term isotopomer (isotopic isomer) is commonly used.[6] These can occur as isotopic constitutional isomers as well as in the form of isotopic stereoisomers. Different isotope effects during chemical reactions or phase transfer processes lead to the enrichment of the heavy or light isotope compared to the global mean composition of an element. Measurement of the extent of these effects are used in a variety of applications, for example to identify the geographical, chemical, and biological origin of substances. With these techniques, samples which would commonly be referred to as "chemically identical" can be differentiated.[7]

Isotopic abundances are commonly expressed as isotope ratios of the heavy to the light isotope $R(\,^{h}E/\,^{l}E)$ which represents the number of entities of the heavy isotope in a relation to the number of entities of the light isotope in a sample.[1] For the comparison of isotopic data between laboratories, the δ-notation for the expression of an isotope ratio in comparison to the ratio of an isotope reference material was introduced in the 1940s and first used in a publication by McKinney *et al.* in 1950.[8] The δ-value of a compound $R(\,^{h}E/\,^{l}E)_c$ in respect

to the substance defining the isotopic reference scale $R(^{h}E/\ ^{l}E)_{ref}$ is defined by **Equation 1.1.**

$$\delta^{h}E_{c,ref} = \left(\frac{R(^{h}E/\ ^{l}E)_{c}}{R(^{h}E/\ ^{l}E)_{ref}} - 1\right) \times 10^{3} \qquad \textbf{(1.1)}$$

Commonly, δ-values are reported in parts per thousand or per mil using the symbol ‰. According to **Equation 1.1**, a positive δ-values indicates that the ratio of the heavy to the light isotope in the sample is higher, than in the reference material. Whereas negative δ-values suggest, that the sample is depleted in the heavy isotope in comparison to the reference material.[6] The δ-notation has the great advantage that very subtle changes in the isotopic composition which are found in natural processes can be displayed without direct comparisons of isotope ratios. Most elements of interest in CSIA show a significant difference in the ratio of heavy to light isotope **(Table 1.1)** which leads to very small numbers for the corresponding ratios.[9] By **Equation 1**, a measured $^{13}C/^{12}C$ ratio of 0.0112361 in a sample results in a $\delta^{13}C$ value of +5 ‰ in comparison the carbon reference material VPDB ($^{13}C/^{12}C$ = 0.0111802).[1] The δ-scale is limited to the isotope ratios commonly observed in natural variations for elements such as carbon, nitrogen, oxygen, and sulfur. For hydrogen, due to the high natural variations, as well as for isotopic tracer studies, the δ-scale can lead to errors. In these cases, isotope amount fractions have to be employed. An overview of the observed isotope ratios and $\delta^{13}C$ values measured against the international VPDB scale for carbon in different parts of the global carbon pool is given in **Figure 1.1**.

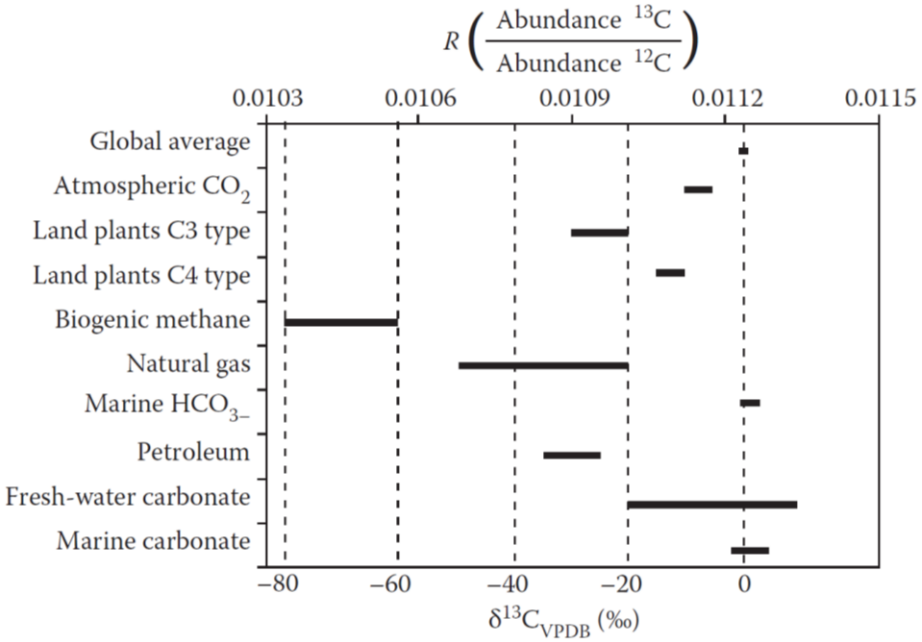

Figure 1.1: Comparison of the isotope ratios and $\delta^{13}C$ values observed as the global mean value as well as in different compartments of the global carbon cycle.[10]

For carbon, significant differences between $\delta^{13}C$ values of the individual source material allow a differentiation, e.g. between different photosynthetic pathways (C3 and C4 plants). Other applications are used to measurement the $\delta^{13}C$ value of atmospheric CO_2 which enables the connection of rising atmospheric CO_2 concentration to the combustion of fossil fuels such as natural gas or petroleum.[10]

1.2 Isotope fractionation

Isotope effects, which are responsible for the variation of isotopic signatures of individual subsamples from the global mean value of an element can be classified as equilibrium isotope effects (EIE) or kinetic isotope effects (KIE). The EIE is defined as the influence of an isotopic substitution on an equilibrium constant, for example in isotope exchange reactions or partitioning.[6] In contrast, the KIE is the effect of an isotopic substitution on a rate constant which can effect effusion, diffusion, evaporation and chemical reaction rates.[1] Isotope fractionation as a result of thermodynamic processes is mainly a product of the differences in vibrational energy between isotopically unsubstituted (light) molecules and molecules substituted with one or more heavy isotopes. The molecule containing the heavier isotopes vibrates at a lower frequency compared to the unsubstituted molecule, which results in a reduced zero point vibrational energy.[11-12] This process continues as multiple heavier isotopes

are added into a molecule, whereby the effect on the substitution of an additional heavy isotope to a molecule that already contained a heavy substitution shows a non-linear trend towards lower vibrational energies.[13] The reduced vibrational energy of isotopically substituted molecules results in a difference in bond dissociation energies, where the lighter molecules would show lower dissociation energies than the heavier substituted molecules.[1] The effect of equilibrium isotope fractionation also depends on the temperature in a defined system. For carbonates, it was observed that at higher temperatures, the isotopic fractionation decreases with a roughly linear relation when plotted against T^{-2}.[12] During the reaction of isotopologues, KIE can occur as a result of direct isotopic substitution at the site of the reaction (primary isotope effect) as well as by indirect effects of isotopic substitution close to the reactive site (secondary isotope effect). In many observed fractionation processes, the kinetic isotope effect is a result of a series of reaction steps. In this case the term apparent kinetic isotope effect is recommended to be used.[14]

Isotope fractionation between two substances (A and B) is commonly expressed by the isotope fractionation factor ($\alpha^{h}E_{A/B}$) as expressed in **Equation 1.2**.

$$\alpha\,{}^{h}E_{A/B} = \frac{R({}^{h}E/\,{}^{l}E)_A}{R({}^{h}E/\,{}^{l}E)_B} \qquad \textbf{(1.2)}$$

In this equation, the term $R({}^{h}E/\,{}^{l}E)_A$ and $R({}^{h}E/\,{}^{l}E)_B$represent the isotope ratios of the individual substances. In combination with **Equation 1.1**, and after rearranging, the isotope fractionation factor can be expressed by the δ-value of the individual substances as shown in **Equation 1.3** below.

$$\alpha\,{}^{h}E_{A/B} = \frac{R({}^{h}E/\,{}^{l}E)_A}{R({}^{h}E/\,{}^{l}E)_B} = \frac{(\delta\,{}^{h}E_A+1)\times R\,({}^{h}E/\,{}^{l}E)_{ref}}{(\delta\,{}^{h}E_B+1)\times R\,({}^{h}E/\,{}^{l}E)_{ref}} = \frac{\delta\,{}^{h}E_A+1}{\delta\,{}^{h}E_B+1} \qquad \textbf{(1.3)}$$

Special attention has to be given as isotope fractionation factors can be defined differently for equilibrium and kinetic isotope fractionation. In addition, the definition of the direction of a chemical equilibrium reaction has to be taken into account as reversing the direction of the reaction produces an inverse value of the fractionation factor.[1, 6]

1.3 Instrumentation for SIA

Besides isotope ratio mass spectrometry, several techniques have been established to determine stable isotope ratios. For the determination of carbon isotope ratios in gaseous CO_2, cavity ring-down spectroscopy as well as mid-infrared laser spectroscopy have successfully been applied.[15-16] Cavity ring-down spectroscopy has additionally been used for the measurement of hydrogen and oxygen isotope ratios, where the results obtained were found to be comparable in delta value and precision to routine IRMS methods.[17] Spectroscopic methods offer the advantage that they are more portable in comparison to traditional IRMS methods and can be used in field applications. In addition, the conversion step to the IRMS measurement gas (e.g. CO, H_2) can be avoided, which was found to be one of the limiting steps in achieving higher precisions by IRMS.[17] Nuclear magnetic resonance (NMR) in terms of site-specific natural-isotope fractionation (SNIF-NMR) has been used for the determination of hydrogen isotope ratios since the 1980s, but has also been shown to be applicable for the measurement of carbon isotope ratios at natural abundance levels.[18] The main advantage of NMR techniques over IRMS is, that position-specific isotope information of complex organic molecules can be obtained.[18] By IRMS, this is only possible after labor intensive chemical degradation of the analyte.[19-20] Drawbacks of the SNIF-NMR techniques are mainly the high costs of the instrumentation and long analysis times required for high precision results. A major drawback of the spectroscopic methods is, that they can until now not be hyphenated with chromatographic sample separation techniques. On-line combinations of chromatography and isotope ratio analysis are commonly performed by IRMS coupled to either gas chromatography or liquid chromatography. For the measurement of bulk isotope ratios, elemental analyzer systems coupled to IRMS are commonly used. Detailed information about the specific techniques are given in the following chapters.

1.3.1 Isotope ratio mass spectrometry

For the measurement of isotope ratios at natural abundance levels, specialized instrumentation is necessary in order to achieve the required precision of the measurement. Although regular MS systems like quadrupole, time of flight, or Orbitrap MS are able to resolve isotopic information, the isotopic composition cannot be determined with a precision of standard deviations in the range from four to six significant figures required for SIA.[9] For stable isotope ratio measurements of all elements, three main types of mass spectrometers are employed. Thermal ionization mass spectrometry (TIMS) and inductively coupled plasma mass spectrometry (ICP-MS) are commonly used for metal analysis, whereas special static gas instruments are designed for the determination of isotope ratios in noble gases.[21-22] For the measurement of isotope ratios in light elements, gas isotope ratio mass spectrometry (GIRMS/IRMS) is used. The high precision of IRMS instruments is achieved by using a magnetic sector field for the separation of the ions and subsequent continuous detection by independent Faraday cups arranged in the focal plane of the mass spectrometer. In **Figure 1.2**, a schematic overview of an IRMS system for the determination of carbon isotope ratios is presented.

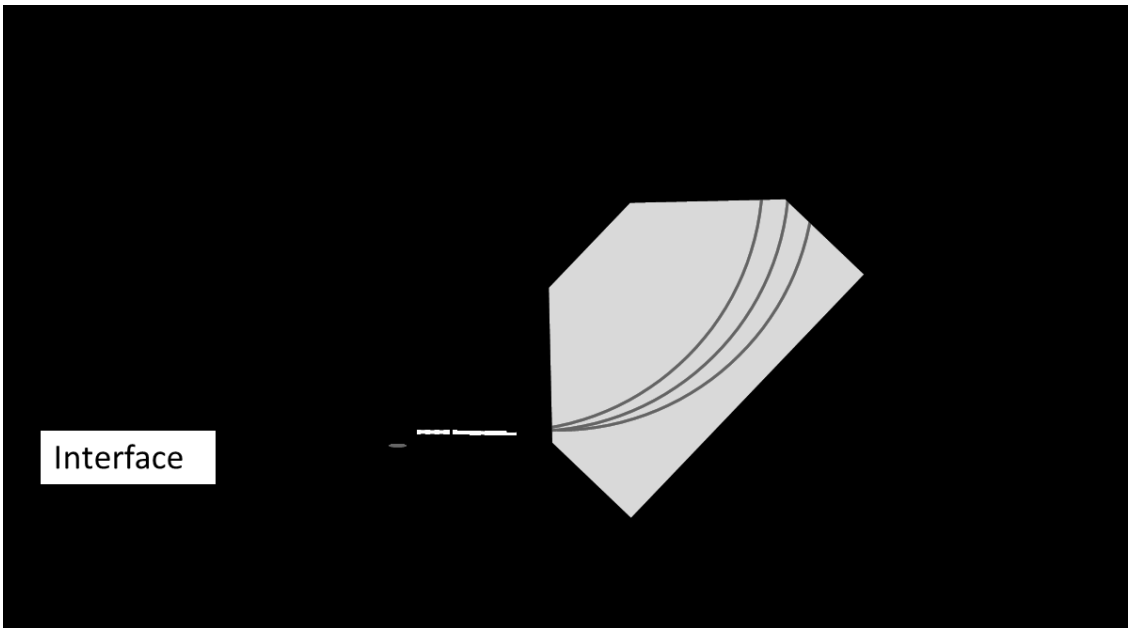

Figure 1.2: IRMS system for the measurement of carbon isotope ratios

Due to the high specialization of this type of instrument, only a limited number of gas species (depending on the element to be analyzed) can be measured. Target analytes have to be transformed into a measurement gas that represents the original isotopic composition of the

sample. For most applications, determination of ^{13}C, ^{2}H, ^{15}N, and ^{16}O isotope ratios is performed from gases of CO_2, H_2, N_2, N_2O, NO, O_2, and CO.[9] This transformation can be performed by various offline methods as well as in online interfaces as employed for CSIA. For the transfer of the measurement gas into the IRMS, an open split system is commonly used for the online conversion systems of IRMS in the combination with elemental analyzer or chromatographic systems. Highest precision can be obtained by the use of a dual inlet system, which can only be used in combination with an offline purification of the measurement gas that is not applicable for hyphenation with chromatographic separation systems.[8, 23-24] With the open-split setup, the measurement gas as well as the reference gas are introduced into the ion source of the IRMS (**Figure 1.2 a-e**) in a stream of helium carrier gas. In the ion source, gas molecules are ionized by electron impact (EI) ionization. The electrons are emitted from a filament commonly consisting of a thin tungsten or thorium wire. On impact with the analyte gas molecules, radical cations are formed ($CO_2^{+\bullet}$). In addition, fragmentation of the analyte gas occurs, so that that for example $CO^{+\bullet}$ is also formed from CO_2 to a certain extent. Due to the closed ion source design for IRMS systems a high ionization efficiency of roughly one ion per 1000 molecules of analyte gas entering the IRMS source can be obtained in comparison to ionization rates of one ion per 10^6 molecules produced in a conventional EI ion source.[9] The produced ions are focused in an ion optic and accelerated towards the magnetic sector field mass analyzer. In the magnetic field, the trajectory of the ion beam is influenced according to the mass-to-charge ratio of the individual ions. Thereby the ion beam for species of distinct masses are spatially separated so that they can be simultaneously detected by individual faraday cup detectors. The signal from the faraday cups are amplified for each ion species and recorded for the calculation of the isotopic composition of the measurement gas.

1.3.2 Elemental analyzer isotope ratio mass spectrometry

The hyphenation of an elemental analyzer to isotope ratio mass spectrometry (EA-IRMS) is mainly used for the measurement of bulk isotope ratios. Complex samples such as whole hair or tissue samples can be measured to obtain an overall mean of the isotope ratio in the sample.[25-26] The EA-IRMS system can be used for CSIA in cases where the analyte has been isolated in an offline separation or for the measurement of pure compounds as reference material for the use in other SIA systems. In the EA-IRMS, a high temperature catalytic conversion is used to completely oxidize the sample. A schematic overview of the Pyrocube

EA system (Elementar Analysensysteme GmbH, Langensebold, Germany) for the measurement of carbon and nitrogen isotope ratios is shown in **Figure 1.3**. Sample preparation for the EA-IRMS system includes the drying and homogenization of the sample and subsequent weighing of the samples into small tin cups. The tin cups are folded, so that ambient air is displaced from the cups. The autosampler of the instrument directly injects the tin cups into the oxidation reactor. After the introduction of the sample, an oxygen gas pulse is delivered to the helium carrier gas of the instrument to combust the sample at 920 °C to CO_2, N_2, NO_x, and H_2O. Copper oxide in the reactor acts as an additional oxidation agent and reservoir for oxygen. Silver wool is added to the oxidation reactor to trap sulfur and halogens if present in the analytes. After the oxidation of the sample, the gases are transported into a copper filled reduction reactor heated to 600 °C. Excess oxygen is removed in this step, in addition, NO_x species from the combustion of the sample are transformed to the N_2 measurement gas used for the $\delta^{15}N$ measurement.

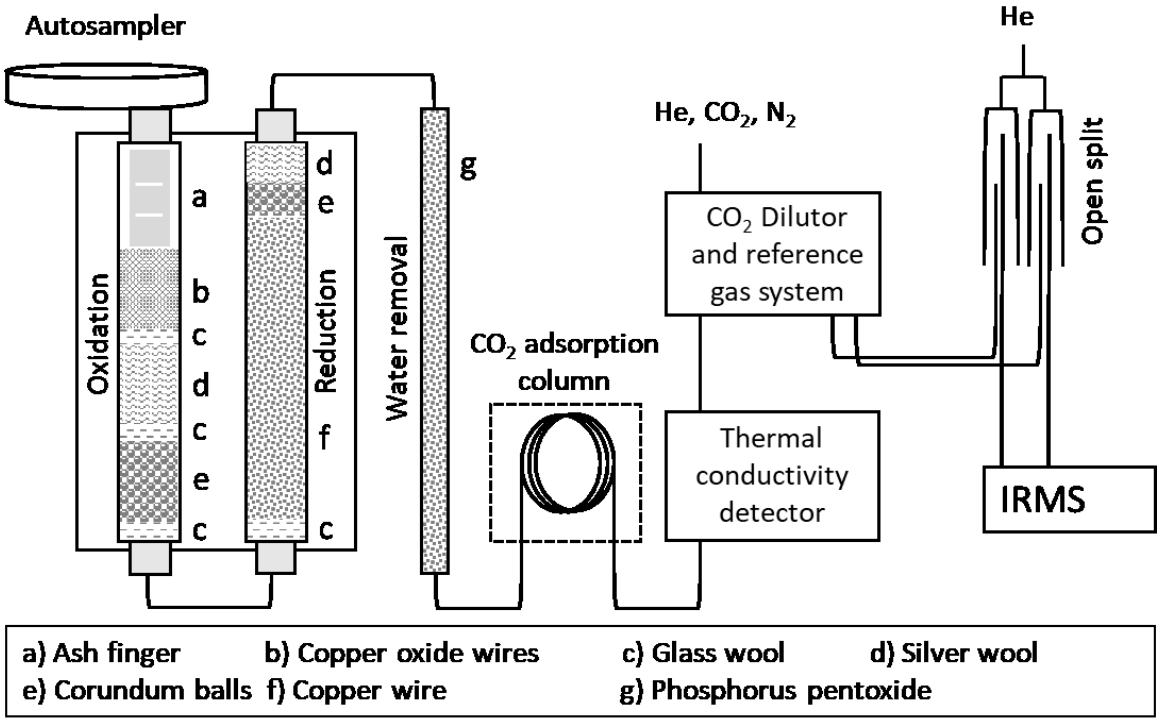

Figure 1.3: EA-IRMS system for the parallel bulk measurement of $\delta^{13}C$ and $\delta^{15}N$ isotope ratios

After the reduction tube, water formed during the oxidation of hydrogen containing compounds has to be removed before entering the CO_2 adsorption column. This step is performed with the help of a glass tube filled with phosphorous pentoxide on a support material. In the next step, CO_2 is trapped from the carrier gas stream onto an adsorption column, as CO_2 and N_2 cannot be measured simultaneously by the IRMS system. CO_2 is later

on desorbed by heating of column from 30 to 110 °C. With the help of the exact mass of the sample and the thermal conductivity detector (TCD) positioned directly after the adsorption column, total amounts of nitrogen and carbon in the sample can be obtained via an external calibration. This is especially important during the method development for bulk samples with unknown or varying carbon and nitrogen contents, as the amount of sample introduce for the IRMS measurement has be in the linear range of the MS system. After the TCD, the N_2 measurement gas passes the dilutor and reference gas system and is transported to the IRMS by the open-split. For CO_2, the gas stream is diluted by the addition of helium into the gas stream. As the carbon content in common organic analytes is mostly higher than the nitrogen content, the dilutor is necessary for the simultaneous measurement of ^{13}C and ^{15}N isotope ratios to obtain roughly equal signal intensities for both measurement gas species. With modifications to the oxidation and reduction setup, EA-IRMS systems are also suitable for the measurement of hydrogen, oxygen, and sulfur isotope ratios but these techniques were not used in the presented work.[27-28]

1.3.3 Gas chromatography coupled to isotope ratio mass spectrometry

Gas chromatography coupled to isotope ratio mass spectrometry (GC-IRMS) was the first commercially available hyphenation of chromatographic system with IRMS. It is widely applied in the field of geochemistry, archeology, environmental chemistry and food authenticity.[29-31] GC-IRMS is mainly applied for volatile, temperature stable analytes and current interfaces enable the online measurement of ^{13}C, ^{15}N, ^{2}H, ^{18}O isotope ratios.[29] Initially unsuitable polar or temperature sensitive compounds can be derivatized to lower their boiling point or increase the temperature stability to be suitable for GC-IRMS analysis.[32-33] Carrier gas options are limited to helium in GC-IRMS, as hydrogen would react in the oxidation reactor of the GC interface, and nitrogen cannot be used as a carrier gas as it would make the determination of ^{15}N ratios impossible and would lead to problems in the ion source of the IRMS system. The separation of the analytes is performed on a classical GC column which is attached to an oxidation reactor at the outlet of the GC column. The oxidation reactor consists of a alumina tube filled with platinum, copper, and nickel wires which is held at around 950 °C (**Figure 4**).[34]

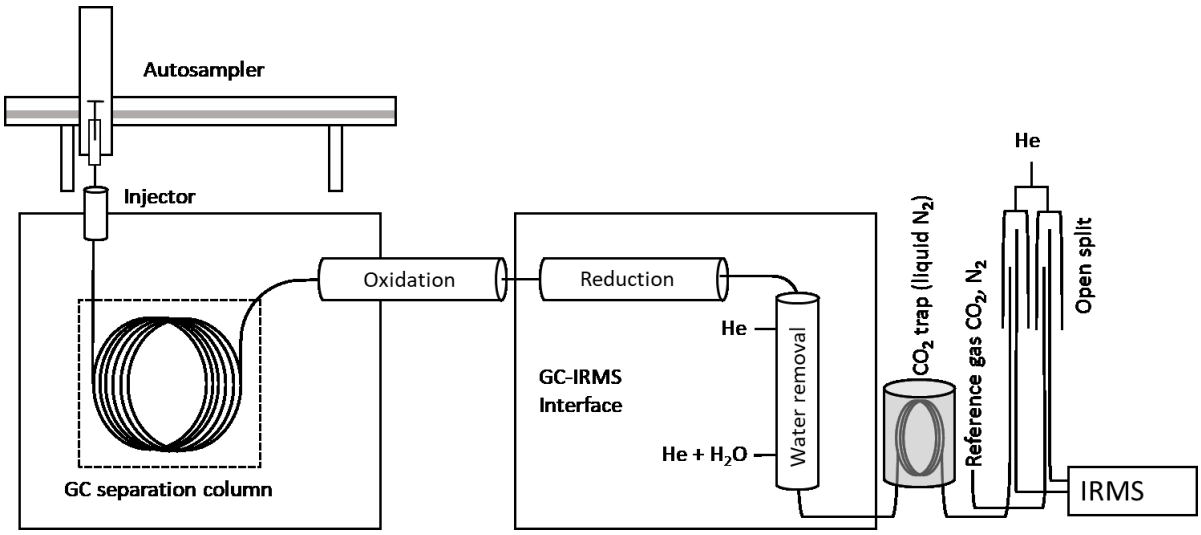

Figure 1.4: GC-IRMS system for the component specific measurement of ^{13}C and ^{15}N isotope ratios

The oxidation is followed by a reduction reactor filled with copper wires, which removes excess oxygen and reduces NO_x species formed during the oxidation to N_2. Water is removed from the carrier gas stream with the help of a Nafion® membrane tube that is placed in a flow of dry helium. For $\delta^{15}N$ measurements, CO_2 is removed from the carrier gas stream by trapping in a capillary immersed in liquid nitrogen. Via the open split system, the measurement gas and the reference gas are introduced into the IRMS.

1.3.4 Liquid chromatography coupled to isotope ratio mass spectrometry

In liquid chromatography coupled to isotope ratio mass spectrometry (LC-IRMS), analytes are separated on a high performance liquid chromatography (HPLC) system and subsequently oxidized to the CO_2 measurement gas used for the determination of compound specific carbon isotope ratios. In contrast to conventional HPLC, specific restrictions apply to the LC-IRMS system. Eluents for the HPLC separation have to be strictly carbon free, so common organic mobile phases used in HPLC cannot be used. In addition, eluents have to be degassed using vacuum and ultrasound to remove residual dissolved air and especially CO_2 which is important for neutral to alkaline eluents. With these restrictions, mainly pure water, carbon free buffer solutions, or diluted inorganic acids can be used as HPLC eluents. The choice of HPLC columns for applications in LC-IRMS is therefore also limited, as many reversed phase (RP) columns cannot be used with pure aqueous mobile phases without the addition of organic modifiers. In addition, high temperature gradients are commonly used in LC-IRMS to modify the polarity

of the aqueous mobile phase without addition of organic eluents, which is not tolerated by standard HPLC columns.[35] Due to the construction of the interface, it is not possible to use higher flow rates than 700 µL min^{-1} in combination of the HPLC pump and the oxidation agent and acid delivered by two independent pumps in the interface.[36] Sodium peroxydisulfate ($Na_2S_2O_8$) is commonly used as an oxidation agent, whereas phosphoric acid is used to acidify the sample. Both reagents are added to the HPLC stream before entering the oxidation reactor in the LC-IRMS interface (**Figure 1.5**).

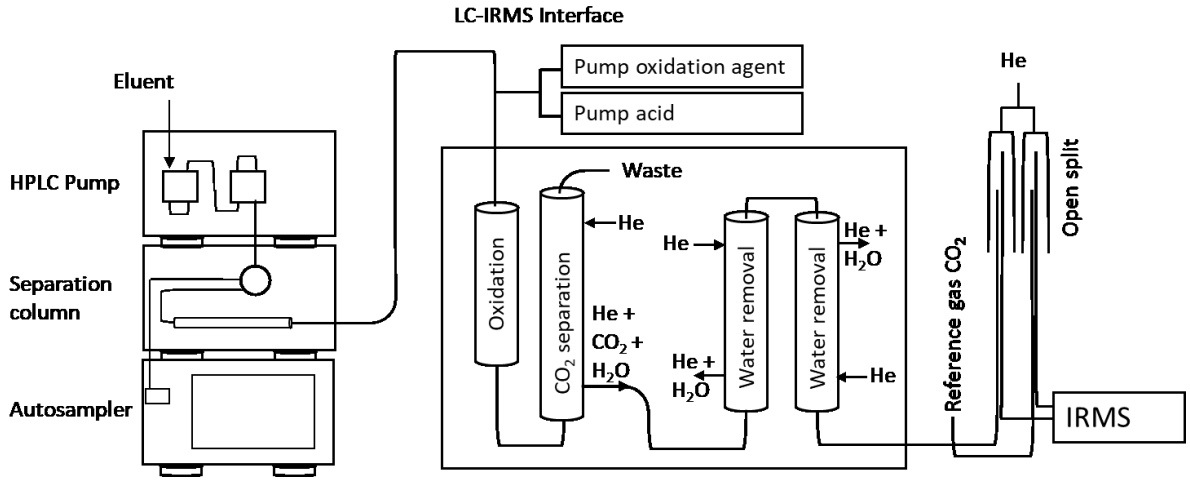

Figure 1.5: LC-IRMS system for the compound specific determination of ^{13}C isotope ratios

The oxidation reactor in the interface consists of a stainless steel capillary of approximately 196 mm^3 volume that is heated to 100 °C. Under these conditions, sulfate radicals are formed, that unselectively oxidize the present carbon in the eluent stream.[36] After passing the oxidation reactor, the sample enters the membrane gas exchange unit, where the CO_2 is transferred from the liquid stream into a countercurrent stream of helium by pervaporation. The helium stream including residual H_2O from the gas exchange process and the CO_2 measurement gas is dried using two Nafion® membrane gas drying units, operated with a countercurrent stream of dry helium. From the interface, the carrier gas enters the IRMS via an open split system. CO_2 reference gas is introduced with the help of an individual open split directly into the ion source of the IRMS.

1.4. Developments in the field of LC-IRMS

The combination of gas chromatography with isotope mass spectrometry with the help of an on-line combustion system was already realized in the late 1970s by two independent groups.[37-38] In contrast to GC-IRMS, the combination of LC-IRMS presents some additional challenges. After the GC separation, the analytes are already present in a gaseous state and can be oxidized in a high temperature gas reactor in the carrier gas stream eluting from the GC. After the removal of residual moisture, the He stream can directly be delivered to the IRMS. In contrast, in liquid chromatography, the analytes are present in a dissolved state in the mobile phase of the LC. Oxidation of the analytes can be performed by wet chemical oxidation (WCO) inside the mobile phase of the HPLC. A second approach is to evaporate the water prior to the oxidation, or combust the sample in a high temperature rector (HTC) where the mobile phase is instantaneously vaporized. In any case, the measurement gas (CO_2 for compound specific carbon isotope analysis) has to be separated from the large excess of water in the mobile phase. During these steps, the analytes should be quantitatively transformed and separated into the gas phase without a loss of the chromatographic separation obtained by the LC.

The first combination of LC with IRMS for measurement at natural isotope abundance levels was described in 1993 by Caimi and Brenna.[39] The transfer and oxidation of the analyte from the HPLC eluent to the IRMS was realized by a moving wire interface. Therefore, a stainless steel wire was coated with the eluent of the LC and the mobile phase was evaporated. The deposited analytes were subsequently oxidized in a combustion furnace and transported to the IRMS in a He carrier gas stream. Major drawbacks of this method were the low fraction of analytes that could be deposited on the wire and isotopic fractionation during the solvent removal in the drying step.[40] Teffera, Kusmierz and Abramson presented a continuous-flow LC-IRMS system based on a chemical reaction interface in 1996.[41] The system was based on an interface for the isotope selective detection of deuterated cortisol metabolites which consists of nebulizer, a momentum separator, and the reaction chamber where the analytes are converted to CO_2 by a microwave-induced helium plasma in the presence of oxygen.[42] As for the moving-wire interface, the CRI showed low sensitivity and fractionation of low molecular weight compounds. Due to these drawbacks, neither of the two methods has been commercially available.[40] In 2004, Krummen *et al.* presented an LC-IRMS interface based on WCO that was made commercially available under the name LC-IsoLink®, by Thermo Fisher

(Bremen, Germany).[36] The oxidation by sulfate radicals is widely applied in the analysis of total organic carbon (TOC) and has already been reported for the isotopic δ^{13}C analysis of dissolved organic and inorganic carbon.[43-44] The system can be used for CSIA when connected to a separation system as well as for BSIA without prior separation of the analytes. (FIA, flow injection analysis or µ-EA mode)[36, 45] As a result of the commonly observed high O_2 background obtained by the WCO-LC-IRMS interface, a copper reduction reactor similar to GC-IRMS applications was successfully integrated into the LC-IRMS setup to improve the results and increase filament lifetimes in the instrument.[46] Since 2010, a second commercially available LC-IRMS interface (LiquiFace®) based on WCO is available by Elementar Analysensysteme (Langenselbold, Germany).[47] In comparison to the IsoLink, only smaller changes to the setup such as different pumping systems, membrane materials, and general dimensions of the components were made. An LC-IRMS interface for the δ^{13}C and δ^{15}N measurement based on the HTC approach was developed by Federherr and co-workers in 2016.[48] The instrument is based on a HTC-EA system that has been adapted for liquid sample introduction.[49-50] High precision δ^{13}C and δ^{15}N results could be obtained by FIA and in LC-IRMS mode, but applications including LC separation of multi component samples have not been performed so far. A major challenge for the HTC-LC-IRMS interfaces is the high amount of water vapor and inorganic constituents of the mobile phase which have to be separated from the measurement gas before entering the IRMS system.

1.5 Chromatographic methods in LC-IRMS

As classical organic eluents cannot be employed for the HPLC separation in LC-IRMS, the selection of stationary phases and complementary carbon free eluents is a challenge during method development. Common eluents used for LC-IRMS separations use pure water, phosphate buffer, diluted phosphoric or sulfuric acid, and sodium or potassium hydroxide solutions. These eluents are combined with stationary phases, which use ion interaction, size exclusion, mixed-mode, or reversed phase separation mechanisms. In addition, the column geometry has to be adapted to the low flow rates tolerated by the LC-IRMS system which are usually between 300 and 600 µL min^{-1}.

For the analysis of sugars, alcohols, sugar alcohols, and organic acids, a number of separations based on ion interaction have been described in literature. Anion exchange columns like the CarboPac PA20 (Thermo Fisher, Bremen, Germany) were used for the determination of glucose and galactose in plasma as well as for the separation of eight carbohydrates.[51-53] Cation exchange columns such as the Alltech 700 CH were used for the separation of sucrose, glucose, and fructose, as well as mannitol and sorbitol.[36] Ligand exchange columns like the Hyper REZ XP Carbohydrate Ca^{2+} (Thermo Fisher, Bremen, Germany) were employed for separation of sugars in honey and the measurement of ethanol in wine.[54-55] These polymer based columns offer the advantage, that they also separate based on a size exclusion mechanism, which enables the separation of mono- and disaccharides like maltitol and xylitol.[56] The compound specific analysis of amino acids by LC-IRMS is performed on mixed mode stationary phases. These reversed phase columns offering additional acidic ion pairing groups, combine hydrophobic interactions with a cation exchange mechanism. The Primesep A (Sielc, Wheeling, USA) column is used in a number of methods resolving amino acids from protein hydrolysate of various origins.[57-59] Classical C_8 or C_{18} columns are not commonly used for LC-IRMS applications, as the alkyl chains on the column particles tend to collapse without a certain amount of organic solvent in the eluent. More recently, RP materials for pure aqueous separations have been designed, which enables the use of RP columns for LC-IRMS. Nevertheless, the elution strength of pure aqueous mobile phases limits the applications to more polar compounds like organic acids or alcohols.[36, 60-61] High temperature HPLC separation was introduced to the field of LC-IRMS in 2008 by Godin *et al.*, by increasing the column temperature, lower viscosities of the eluent and a lower polarity of the aqueous eluent can be achieved.[62] A variety of RP columns have been evaluated for the high temperature LC-IRMS approach, and new methods for the measurement of steroids and pharmaceutical on RP columns by high temperature LC-IRMS were developed.[35, 45, 63]

1.6 Applications of LC-IRMS

1.6.1 Archeology

Isotopic analysis in the field of archeology mainly focuses on the use of radiocarbon dating (^{14}C) and the determination of bulk isotope ratios for the reconstruction of dietary habits.[64-65] Compound specific stable isotope ratios for individual amino acids have been determined by GC-IRMS for palaeodietary reconstruction.[66] This requires derivatization of the amino acids prior to the GC separation which can lead to a shift in in the $\delta^{13}C$ ratio because of the addition of carbon by the derivatization agent. In addition, reactions at the amino group can lead to fractionation and effects of the derivatization on the observed $\delta^{15}N$ ratio.[67] With the availability of the LC-IRMS interface, methods were developed to separate underivatized amino acids from bone collagen.[68] The separation of amino acids on the LC system was further optimized and applied to determine $\delta^{13}C$ ratios for individual amino acids from hair keratin, which was shown to be a proxy for bone collagen values and therefore usable as a tool for dietary reconstruction.[58, 69-70] With the help of compound specific amino acid $\delta^{13}C$ signatures, distinct groups of terrestrial, omnivore, and marine diet could be distinguished using threonine $\delta^{13}C$ as well as $\Delta^{13}C_{\text{Glycine-Phenylalanine}}$ signatures.[69] The possibility to combine the information obtained from essential amino acids (e.g. phenylalanine) and non-essential amino acids (e.g. glycine) is a major advantage compared to bulk methods which showed overlap between marine and C4 carbon consumers.[66] Besides amino acids, Blyth *et al.* demonstrated, that LC-IRMS in flow injection mode (bulk measurement) can be used to determine $\delta^{13}C$ records in calcite samples from speleothems which can possibly be used as palaeoenvironmental records.[71-72]

1.6.2 Physiology and nutrition

Analytes of interest for applications in the field of nutrition and physiology share the characteristic, that they are mostly small, organic, and polar compounds which are present in complex matrices such as blood plasma, intracellular fluids, or protein hydrolysates.[73] For these analytes, LC-IRMS offers the advantage, that sample derivatization can be avoided and sample preparation protocols can be simplified. In 2005, Godin *et al.* showed, that mucoprotein synthesis rates in a rat model could be determined using ^{13}C labeled threonine with comparable precision to established GC-IRMS methods.[40] The fractional synthesis rate of

glutathione was determined by LC-IRMS analysis of blood samples as a marker for oxidative stress.[74] The study was conducted on neonates that were supplied with ^{13}C-labeled glycine. Initially, glycine was determined after derivatization by GC-IRMS, whereas glutathione was transferred into its oxidized dimeric form (GSSG) and measured by LC-IRMS. The LC separation was optimized for a second study to perform both, the glycine and GSSG measurement by LC-IRMS.[75] Human glucose metabolism was studied after the administration of ^{13}C-labeled glucose to the same group of newborns, therefore blood glucose levels and δ^{13}C values were determined by LC-IRMS. The sample preparation time was reduced in comparison to existing GC-IRMS methods and the performance of the LC-IRMS method was found to be superior to the GC method.[51] Glucose could also be utilized as a marker for diabetes, therefore ^{13}C labeled bicarbonate was orally administered and the δ^{13}C level of glucose in the saliva was determined. The isotopic composition of glucose in the saliva measured by LC-IRMS was found to be suitable to present a non-invasive approximation of blood sugar δ^{13}C levels. A significant increase of the δ^{13}C signature in glucose in the saliva could be interpreted as a sign for early diabetes.[76] Compound specific amino acid analysis was used to study the protein metabolism in fish. Therefore, diets consisting of different mixtures of essential and non-essential amino acids were administered to a population and shifts from the initial δ^{13}C level of amino acids to those incorporated in the fish tissue were analyzed by LC-IRMS.[57, 77]

1.6.3 Geochemistry, hydrology, and soil science

First applications in the field of soil science were published by Heuer *et al.* (2006), developing a method for the compound specific analysis of volatile fatty acids in the sediment and pore-water system. Acetate carbon isotope ratios could be used to cluster the origin of pore water samples and relate the obtained δ^{13}C signatures to the different biogeochemical acetate production and consumption processes.[78] The established methods were used for a larger study of pore-water in seafloor sediments that related acetate δ^{13}C signatures to sediment DOC for the identification of production and degradation pathways of acetate.[79] LC-IRMS analysis of amino sugars extracted from the extracellular polymeric substances (EPS) of soil bacteria communities was developed by Bodé *et al.* in 2009.[80] The method for the analysis of glucosamine, galactosamine, and muramic acid was used as a tool to study the microbial carbon cycle in soil by applying ^{13}C-labeled substrate and measuring incorporation of the label into the EPS.[81-83] Due to the high sample throughput achievable by flow injections using the

LC-IRMS interface, it was possible to analyze the spatial distribution of $\delta^{13}C$ signatures of DOC in pore water.[84] Analysis of DOC and DIC by flow injection has since then been used in several studies.[85-87] This technique was further improved to separate DOC classes based on molecule size classes, which was achieved by size exclusion chromatography.[88-89]

1.6.4 Food quality control

In food quality control, LC-IRMS is used as a tool for the differentiation between origins of plant based material. This could be a differentiation between different plant species, or the distinction between synthetic or natural ingredients in a food product. The process is based on the three main photosynthetic pathways found in plant species. C3 plants, which use the Calvin-Benson cycle, show $\delta^{13}C$ bulk isotope ratios of -22 to -34 ‰ (-25 ‰ on average) depending on the individual plant species and growth conditions.[90-92] The second big family of plants, the C4 plants are enriched in ^{13}C and were found to have $\delta^{13}C$ bulk isotope ratios of -6 to -20 ‰ (-13 ‰ on average).[90-92] CAM plant account for a small class of plants that show an enrichment of ^{13}C in comparison to C3 plants but cannot always be differentiated from C4 plants, as the $\delta^{13}C$ varies to a large extend between plant species and with the growth conditions of the plants.[93] Relevant representatives of the C3 family are most cereals or grains, sugar beet, and trees, whereas sugarcane and corn belong to the C4 family. CAM plants which are relevant in food authenticity studies are pineapple, agaves, and orchids such as vanilla. First applications for LC-IRMS in the field of food authenticity were the detection of adulteration in honey. Cabañero *et al.* (2006) developed a method for the simultaneous determination of carbon isotope ratios of sucrose, fructose, and glucose.[54] With the help of the difference of the individual isotopic signatures as well as $\Delta^{13}C_{Fructose\text{-}Glucose}$, $\Delta^{13}C_{Fructose\text{-}Sucrose}$, and $\Delta^{13}C_{Glucose\text{-}Sucrose}$ adulteration by C4 and C3 plant sugar in the honey could be detected with the help of this method. Further studies on honey authenticity focused on the measurement of a large variety of geographically and botanically different honeys, the measurement of $\delta^{13}C$ values for extracted honey protein and the additional measurement of $\delta^{2}H$ and $\delta^{18}O$ values by EA-IRMS.[94-97] Another important field is the detection of adulterations in alcoholic beverages. Compound specific LC-IRMS techniques were used to measure ethanol, glycerol as well as fructose and glucose to detect adulteration prior and after the fermentation.[55, 98-99] The LC-IRMS was also used as a µ-EA system in the bulk analysis of alcoholic beverages by flow injection.[100] Zhang *et al*. (2011) developed a method for the compound specific analysis of

caffeine from various types of coffees, teas, and energy drinks and was able to separate products based on natural caffeine from products with added synthetic caffeine.[101] Additional applications for the detection of food adulteration by LC-IRMS were developed to distinguish synthetic and natural vanillin flavor in chocolate products as well as the addition of foreign citric acid to commercial lemon juices.[102-104]

1.7 Referencing and normalization for LC-IRMS applications

For the comparability of isotope measurements between laboratories, results have to be normalized against international reference standards. This relative comparison to an international scale is necessary, as absolute isotope ratios can only be determined with comparably high uncertainties, e.g. ±2.5 ‰ for NBS-19 reference material for the VPDB scale.[105] The international scale for carbon isotope ratios was initially based on cretaceous belemnite material from the Pee Dee formation in South Carolina (PDB for Pee Dee Belemnite). Since the PDB material is not available anymore, exact values for δ^{13}C and δ^{18}O of the NBS-19 reference material were assessed relative to PBD. This new international scale which is in use up to day was termed VPDB (Vienna PDB) based on the role of the IAEA (International atomic Agency) located in Vienna.[23] Besides NBS-19, a number of certified secondary reference material are available for the use in LC-IRMS. These are for example, glutamic acid (USGS 40, 41a), sucrose (IAEA-CH-6), caffeine (IAEA-600), benzoic acid (IAEA-601), and different carbonates ($LiCO_3$ (L-SVEC), $CaCO_3$ (IAEA-CO-1, NBS-18), $BaCO_3$ (IAEA-CO-9)).[106] Key questions for the normalization approach are the type of reference material and the mathematical methods used for the normalization. Based on the principle of identical treatment, the reference material should undergo the same chemical transformation during the measurement as the analytes.[23, 107] For LC-IRMS measurements, the analyte as well as the reference material should pass the wet chemical oxidation process and the gas separation in the interface to compensate for possible fractionation during these steps. In addition, the reference material should be structurally as similar as possible to the analyte to achieve equal behavior during the oxidation step. If certified secondary standards are not available for the analyte in question, it is common practice to measure in house standards of the analyte for example with an EA-IRMS in relation to the international scale. EA-IRMS is more suited for the measurement of these third level in house standards, as the high temperature combustion process employed does not lead to significantly different results between compound classes.

When it comes to the statistical methods for the normalization, four options are commonly used in the literature. The simplest form of normalization is the use of certified reference gas for the normalization of measured isotope ratios. If the true δ-value of the reference gas is known, the measured δ-values of the sample can be corrected by **Equation 1.4**.[108]

$$\delta^{h}_{t}A = \delta^{h}_{m}A + \delta^{h}_{t}RG + \frac{\delta^{h}_{m}A\,\delta^{h}_{t}RG}{1000} \qquad \textbf{(1.4)}$$

Using the measured δ-value of the sample ($\delta^{h}_{m}A$) and the true δ-value of the working gas calibrated against an international reference scale ($\delta^{h}_{t}RG$), δ-value of the sample in comparison to the same scale can be obtained ($\delta^{h}_{t}A$). This procedure is automatically performed by the software packages provided by the instrument manufacturers (e.g. Isodat NT 2.0 by Thermo Fisher, Bremen, Germany). The drawbacks of this method are mainly that slight changes in the composition of the reference gas with changing filling levels of the reference gas storing bottle can have direct effects on the measurement result.[109] In addition, relatively high errors are introduced during the normalization procedure if the isotopic signature of the reference gas is not close to the isotopic composition of the analyte in question. The second option is the use of one reference material of known isotopic composition which is commonly termed single-point anchoring. Individual measurements are performed against the system reference gas, but by the additional use of the reference material, the influence of fluctuation in the gas composition can be compensated. By **Equation 1.5**, the true δ-value of the sample ($\delta^{h}_{t}A$) can be calculated using the certified δ-value of a reference compound ($\delta^{h}_{t}Std$) as well as the measured δ-value of a reference compound $\delta^{h}_{m}Std$ on the system.[108, 110]

$$\delta^{h}_{t}A = \left(\frac{(\delta^{h}_{m}A+1000)\times(\delta^{h}_{t}Std+1000)}{\delta^{h}_{m}A+1000}\right) - 1000 \qquad \textbf{(1.5)}$$

With this approach, the individual measurements are performed relative to the reference gas, but long term shifts in the composition of the reference gas are compensated by the normalization as the final true value of the sample is independent of the actual δ-value of the reference gas. The most commonly used method is the two-point anchoring or linear shift normalization. Therefore two reference substances of known isotopic composition are used which bracket the suspected abundance range of the analytes. With the help of a linear regression, the normalized true δ-value of the sample can be obtained. It could be shown, that the normalization with the help of a two-point approach can improve the consistency of normalized carbon isotope ratio measurements between laboratories by 39-47 %.[106] The calculation of the normalized δ-value of the sample ($\delta\,{}^{h}_{t}A$) is performed according to **Equation 1.6**.[108]

$$\delta\,{}^{h}_{t}A = \left(\frac{\delta\,{}^{h}_{t}Std\ 1 - \delta\,{}^{h}_{t}Std\ 2}{\delta\,{}^{h}_{m}Std\ 1 - \delta\,{}^{h}_{m}Std\ 2}\right) \times (\delta\,{}^{h}_{m}A - \delta\,{}^{h}_{m}Std\ 2) + \delta\,{}^{h}_{t}Std\ 2 \qquad \textbf{(1.6)}$$

Multi-point linear normalization describes the procedure, where more than two certified reference standards are used. It is rarely applied as the high number of measurements required for the normalization does not lead to a significant improvement of the accuracy of the normalization. As different sources publish slightly different delta values for certain reference materials, it is always advisable to state the values assigned for the reference materials that have been used for the normalization.[111]

1.8 Determination of total nitrogen and potential applications in an LC-IRMS setup for the compound specific δ^{15}N analysis

As an alternative to the high temperature combustion approach for the measurement of compound specific nitrogen isotope ratios by LC-IRMS presented by Federherr *et al.* (2016), wet chemical approaches for the transformation of the nitrogen contained in the analyte to an IRMS measureable form have to be evaluated.[48] In environmental and food chemistry, the sum parameter total nitrogen (TN) as well as Kjeldahl nitrogen are routinely used. The original analytical procedure for the Kjeldahl nitrogen determination was already published in 1883.[112] Although different modifications and improvements were performed since then, the essential three step procedure remained unchanged. In a first step, the sample is mineralized by the addition of concentrated sulfuric acid as well as different catalysts. When the mineralization is completed, the pH of the solution is adjusted to alkaline conditions to transform ammonium

to ammonia, which is distilled into an acidic collection medium. The trapped ammonium is quantified by titration in the third step.[113] The main drawback of the Kjeldahl procedure is, that the measured nitrogen content does only represent organic nitrogen and nitrogen bound in ammonium. Nitrate, and nitrite cannot be determined by this procedure as they are not reduced to the ammonia during the procedure which is determined as the only reaction product.[114] For the application in an instrumental setup for the stable isotope analysis of nitrogen containing compounds, nitrate plays an important role as it is measured in the context of the distribution of fertilizers of different origins between plant material, soil, and groundwater.[115] First work on the determination of total nitrogen after the oxidation of organic and inorganic nitrogen by heat activated persulfate in batch experiments was reported in Swedish literature by Koroleff (1970, 1973) and Henrikson (1973).[116-118] For the oxidation of nitrogen containing samples, no single oxidation product could be identified under acidic conditions, where NO_3^-, NOCl, and other intermediate species were suspected to be formed.[119] Under alkaline oxidation conditions, after a reaction time of 15 min at 120 °C, complete oxidation of nitrogen containing substances such as nitrate, nitrite, ammonia, and urea could be obtained.[120] The determination of the total nitrogen in the method proposed by Koroleff is based on the oxidation of the total nitrogen to nitrate, subsequent oxidation of nitrate to nitrite on a cadmium column and photometric determination of the nitrite as an azo dye.[120] As the final recovery of total nitrogen is only based on the photometric measurement of the final reaction product, no conclusion could be drawn which byproducts were responsible for the decreased recovery observed for some compounds. First reports of an online determination of total nitrogen by alkaline persulfate oxidation were presented by Rossi and Savarese in 1997.[121] Recoveries for total nitrogen in sea water ranged from 94 to 107 %, but the instrumental conditions of the reactor (80 m, 2.5 mm inner diameter, 115 °C reaction temperature) are not comparable to required dimensions for the oxidation after a chromatographic system as in the LC-IRMS interface. Nitrate as the final oxidation product was reduced to nitrite for the colorimetric determination after transformation in a reduction column containing copper coated cadmium granules.[121] This procedure would not be applicable, as modern IRMS systems require a gaseous analyte, which has to be separated analog to the procedure for CO_2 in the existing $\delta^{13}C$ LC-IRMS setup. Determination of total nitrogen in online systems by measurement of NO by chemiluminescence is routinely performed after high temperature catalytic conversion, but quantitative online conversion of

nitrate to NO in aqueous solution has not been reported. A comparison of several offline techniques was published by Yang *et al.* (1997), temperature variations as well as different reducing agents were evaluatued.[122] From the evaluated agents, V(III), Ti(III), and a mixture of Mo(VI) and Fe(II) showed almost complete transformation of nitrate to NO at reaction temperatures of 80 °C. In general, higher reaction temperatures were found to increase the yield of NO, which is beneficially, as reaction temperatures in the LC-IRMS interface for the oxidation are routinely around 100 °C. The presented methods for the reduction of nitrate to NO would have to be further evaluated for the combination with a previous alkaline or acidic oxidation by sulfate radicals.

Chapter 2: Scope of the thesis

The scope of this work is to develop new methods for the application of compound specific carbon stable isotope analysis for food authenticity control and the elucidation of the oxidation process taking place during the conversion of analytes into the measurement gas in the LC-IRMS interface. In the context of the development of a system for the determination of nitrogen isotope ratios, a special focus was on the behavior of nitrogen containing analytes and the different nitrogen reaction products formed during the oxidation by sulfate radicals. Different analytical strategies for the measurement of the final and intermediate species formed during the oxidation as well as modifications to the standard reaction conditions in the LC-IRMS interface will be presented and discussed.

In **Chapter 3**, a method for the differentiation of xylitol produced on the basis of wood or corn material in bulk samples, as well as in the form of an ingredient in commercially available chewing gum was developed. The method was applied to a set of 21 chewing gum samples of which 18 could be assigned to one of the crop classes. As corn based material is generally sold as a cheaper alternative to the original wood based xylitol, the presented LC-IRMS method is able to prove the authenticity of the product and identify food fraud. Strategies for the optimization of the oxidation efficiency in the LC-IRMS interface for the determination of carbon isotope ratios are discussed in **Chapter 4**. Three different approaches for the assessment of the oxidation efficiency will be compared in regard to their applicability for method development and improvement of existing LC-IRMS methods. Besides the effect of incomplete oxidation on the determination of δ^{13}C isotope ratios, the effect of nitrogen containing groups on the oxidation efficiency in the LC-IRMS interface under standard carbon measurement conditions will be discussed. In **Chapter 5** methods should be developed to monitor the behavior of nitrogen containing compounds and their oxidation products during mineralization by heat activated persulfate in an offline system and by wet chemical oxidation in the LC-IRMS interface. Therefore, methods for the quantitative determination of the individual nitrogen species by ion chromatographic methods as well as with a total nitrogen analyzer were evaluated. Mass balances for the detected reaction products should be evaluated for different nitrogen containing analytes in order to monitor the oxidation process in the LC-IMRS interface for nitrogen containing analytes in detail. In **Chapter 6** reaction conditions in the oxidation interface of the LC-IRMS should be adapted based on the observations made in the previous chapters. Besides the well documented oxidation of

analytes by heat activated persulfate under acidic conditions which is routinely employed for the measurement of δ^{13}C ratios by LC-IRMS and produces multiple intermediate and stable nitrogen containing reaction products, different reaction conditions in an alkaline environment should be tested that could be more suitable for the measurement of δ^{15}N ratios and could potentially lead to a single oxidation product for further development of the nitrogen LC-IMRS interface. A detailed graphical summary of the topics of the different chapters of this work is given in **Figure 2.1**.

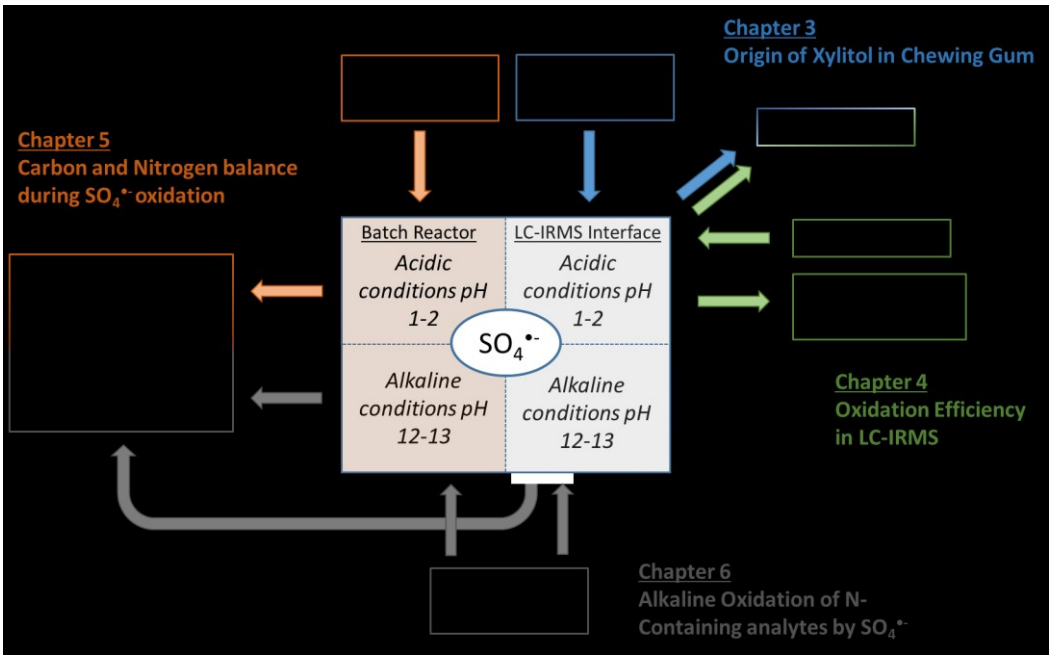

Figure 2.1: Overview of the main chapters presented in the thesis

The determination of compound specific nitrogen isotope ratios in addition to already well established δ^{13}C analysis is of great interest in many fields of research.[33, 123-126] Until now, derivatization of nitrogen containing compounds and subsequent GC-IRMS measurement is the only way to determine compound specific δ^{15}N isotope ratios for polar nitrogen containing compounds. The behavior of these analytes and their reaction products formed during oxidation under LC-IRMS interface conditions has not been investigated in detail so far. The presented work will elucidate the influence of the interface reaction parameters on the oxidation efficiency by evaluating different routes to determine nitrogen and carbon mass balances. The development towards compound specific δ^{15}N analysis by LC-IRMS requires the knowledge about the formation of nitrogen containing end products of the mineralization to finally obtain a single measurable nitrogen species for IRMS analysis.

Chapter 3: The origin of xylitol in chewing gum – a compound-specific isotope technique for the differentiation of corn and wood based xylitol by LC-IRMS

Köster, Daniel[1], Wolbert, Jens-Benjamin[1], Schulte, Marcel S.[2], Jochmann, Maik A.[1] , Schmidt, Torsten C. [1,3]

[1] Instrumental Analytical Chemistry, University of Duisburg-Essen, Universitätsstr. 5, 45141 Essen, Germany

[2] Biofilm Centre, University of Duisburg-Essen, Universitätsstr. 5, 45141 Essen, Germany

[3] University of Duisburg-Essen, Centre for Water and Environmental Research (ZWU) Universitätsstr. 5, 45141 Essen, Germany

Adapted with permission from: D. Köster, J.B. Wolbert, M.S. Schulte, M.A. Jochmann, T. C. Schmidt, *Origin of Xylitol in Chewing Gum: A Compound-Specific Isotope Technique for the Differentiation of Corn- and Wood-Based Xylitol by LC-IRMS, Journal of Agricultural and Food Chemistry, 2018, 66 (8)*, DOI: 10.1021/acs.jafc.7b05212, Copyright 2018 American Chemical Society.

3.1 Abstract

The sugar replacement compound xylitol has gained increasing attention due to its use in many commercial food products, dental hygiene articles and pharmaceuticals. It can be classified by the origin of the raw material used for the production. The traditional “birch xylitol” is considered a premium product in contrast to xylitol produced from agriculture by-products such as corn husks or sugar cane straw. Bulk stable isotope analysis (BSIA) as well as compound-specific stable isotope analysis (CSIA) by LC-IRMS for chewing gum extracts was used to determine $\delta^{13}C$ isotope signatures for xylitol. These were applied to elucidate the original plant type the xylitol was produced from based on differences in the isotope fractionation processes during the photosynthetic CO_2 fixation. For the LC-IRMS analysis, an organic solvent free extraction protocol and HPLC method for the separation of xylitol from different artificial sweeteners and sugar replacement compounds was successfully developed and applied to the analysis of 21 samples of chewing gum from which 18 could be clearly related to the raw material plant class.

3.2 Introduction

As a result of the general trend towards a healthier and more conscious consumption of food products in the western world, the demand for healthy sugar alternatives is constantly increasing. Xylitol is a sugar replacement compound that is widely used in the production of teeth friendly chewing gums and sweets.[127] Structurally it is a pentitol and belongs to the class of the sugar alcohols. In contrast to common high power sweeteners, xylitol has similar properties to conventional sucrose concerning the sweetening power and general taste but also a reduced energy content of around 60 % compared to sucrose.[128] Most of the very potent artificial sweeteners cannot be used to completely replace sugar without altering the overall taste impression of the product.[129] In contrast, xylitol can be used in larger amounts that do not produce unwanted changes in the texture or the taste of the product.

A common source for the xylose which is needed for the production of xylitol is the hemicellulose compound xylan. Xylan can be extracted from a variety of plants where it is used as a building block for plant cell walls.[130] Due to their high xylan content, mostly birch wood and corn husks are used for the commercial production of xylitol.[131-132] The conventional production of xylitol at industrial scale is performed in a four step approach. The first step is the cleavage of the polysaccharides present in the plant material, which is mostly performed by acid or enzyme assisted hydrolysis. After the separation of the xylose from the hydrolysate, it is catalytically hydrogenated followed by crystallization and purification steps to remove the catalyst and remaining educts from the xylitol.[133]

The high energy demand and the difficult purification steps are responsible for the currently high price of xylitol. New approaches using biotechnological methods combined with a variety of new raw material sources are currently under investigation for the cost effective xylitol production from agricultural by-products.[134] Recent studies focus on raw materials such as sugarcane, eucalyptus, rice and wheat straw or microalgae for the xylitol production.[135-139] As corn husks are considered to be a waste product of the agriculture industry and a connection to genetically modified corn crops cannot be excluded, xylitol produced from birch wood is often sold as a premium product with higher retail prices. The different types of photosynthesis pathways in corn (C4 plant) and trees, e.g., birch, beech or oak (C3 plants) lead to a characteristic shift of the δ^{13}C value of the plant material compared to the CO_2 in the atmosphere.[90] This shift in the δ^{13}C isotope ratio is passed on to the biomolecules in the plant

and has been successfully employed in food authenticity studies to elucidate the origin of plant derived products.[55, 94, 100-102] C3 plants, which utilize the Calvin cycle, normally have $\delta^{13}C$ values in the range from -22 to -35 ‰ with average values of -26 ‰, whereas C4 plants, which use the Hatch-Slack pathway, show $\delta^{13}C$ values from -9 to -16 ‰ with an average of -13 ‰.[91, 140-141]

Isotope analysis can be divided into two classes, compound-specific isotope analysis (CSIA) and bulk stable isotope analysis (BSIA). In BSIA, the complete sample (which can be a mixture or a pure compound) is analyzed without separation of the compounds prior to the combustion to low molecular weight gases. In CSIA the sample is separated prior to the combustion, so that isotopic data is obtained specifically for the analyte of interest. In carbon stable isotope analysis, liquid chromatography coupled to isotope ratio mass spectrometry (LC-IRMS) and gas chromatography coupled to isotope ratio mass spectrometry (GC-IRMS) are the most commonly used techniques. LC-IRMS has found many applications in the field of food authenticity control and the detection of alteration of food products. Analytes in this field are often polar and not directly suitable for GC-IRMS due to their high boiling points or low temperature stability. These compounds would require derivatization prior to the analysis which is labor intensive and can introduce isotope shifts that have to be corrected after the analysis.[32] LC-IRMS was first presented in 1993 by Caimi, Brenna and Thomas and made commercially available in 2004 as described by Krummen *et al.*.[36, 142] Since then it has been applied for the detection of adulteration of honey and alcoholic beverages[55, 94, 100] as well as in the determination of the origin of caffeine in energy drinks and teas, vanillin in chocolate and the measurement of $\delta^{13}C$ signatures of amino acids in fish.[57, 101-102]

Until now, sugar replacement compounds have not been in the focus of CSIA studies. Xylitol was chosen as a representative of this class as the production route is of special interest to the customer due to financial and ethical aspects. With reduced production costs, xylitol will find a large application in different food products, currently chewing gums offer a wide variety of samples from different manufacturers that can be used for method development in this specific field and for further applications in the food sector. The aim of this work was to develop a method for the extraction of xylitol from chewing gum formulations and the subsequent measurement of compound specific $\delta^{13}C$ values by LC-IRMS. The LC method development focused on the separation of xylitol from different additional sweeteners such as sorbitol, mannitol and maltitol which are most commonly used in chewing gums and

sweets. For the classification, a combination of statistical evaluation of the $\delta^{13}C$ values from CSIA of the chewing gums and a comparison to bulk isotope measurements by EA-IRMS of samples from known origins as well as different published literature values for raw plant material and xylitol were used.[143]

3.3 Material and Methods

3.3.1 Chemicals and Reagents

The water used as the mobile phase of the HPLC was ultrapure water obtained from an ELGA Purelab Ultra (Veolia Water Technologies, Ratingen, Germany) system. The water was degassed using 1 L screw-cap Schott bottles (Schott AG, Mainz, Germany). The water was degassed under vacuum (Membrane pump, Vacuubrand GmbH & Co., Wertheim, Germany) and was simultaneously treated by an ultrasonic bath (Sonorex RK 100, Bandelin Electronic, Berlin, Germany) for 20 min. Immediately after the degassing and during the whole LC sequence, the mobile phase as well as the reagents used in the LC-Interface were continuously sparged using a low stream of helium (purity 5.0, Air Liquide, Oberhausen, Germany) to prevent gases from the air from dissolving in the reservoir bottles. For the wet chemical oxidation in the interface, sodium peroxydisulfate (99 %, Riedel-de Haën, Seelze, Germany) and ortho-phosphoric acid (85 %, p.a., Merck KGaA, Darmstadt, Germany) were used. For the method development of the HPLC separation, maltitol (≥98%), D-sorbitol (99 %) and D-mannitol (≥98 %) were purchased from Sigma-Aldrich (Steinheim, Germany). Xylitol (for biotechnological applications) was purchased from Fluka (Buchs, Switzerland) as well as two samples of commercially available xylitol from a local shop with declared origin of 100 % birch wood and corn husks respectively (Xucker GmbH, Berlin, Germany). A range of 21 different xylitol containing chewing gums and mints were purchased in various stores in Germany and the Netherlands. A list of the different samples and declared ingredients of the chewing gums is given in **Table 3.1**. The mass fraction of the individual component decreases with the order of appearance in the ingredient list.[144]

Table 3.1: Xylitol containing chewing gum and mint samples and their main ingredients as given by the different manufacturers

Name	*Mass [g]*	*Ingredients*
EPW	2.04	Sweetener (Sorbitol, Xylitol, Maltitol)
MRO	2.06	Sweetener (Isomalt, Mannitol, Sorbitol, Maltitol, Maltitol syrup, Xylitol, Aspartame, Acesulfame potassium, Sucralose)
SMI	0.2	Sweetener (Xylitol 87 %, Aspartame)
MPF5	1.88	Sweetener (Xylitol, Sorbitol, Mannitol, Maltitol, Maltitol syrup, Aspartame, Acesulfame potassium, Sucralose)
RSM	1.43	Xylitol, Sorbitol, Mannitol, Maltitol, Acesulfame potassium, Sucralose
MRE	2.05	Sweetener (Isomalt, Mannitol, Sorbitol, Maltitol, Maltitol syrup, Xylitol, Aspartame, Acesulfame potassium, Sucralose)
SMP	1.15	Sweetener 58 % (Sorbitol, Xylitol, Maltitol molasses, Aspartame, Acesulfame potassium)
EPM	1.48	Xylitol, Sorbitol, Aspartame, Acesulfame potassium
JGW	1.43	Sweetener (Xylitol, Sorbitol, Mannitol, Maltitol, Aspartame, Acesulfame potassium)
FM	1.43	Sweetener 65% (of which Xylitol 99.8 %, Aspartame 0.1 %, Acesulfame potassium 0.1 %)
MSQ	2.07	Xylitol, Mannitol, Sorbitol, Maltitol, Aspartame, Maltitol syrup, Sucralose, Acesulfame potassium
MPF3	2.08	Sweetener (Xylitol, Sorbitol, Mannitol, Maltitol syrup, Maltitol, Aspartame, Acesulfame potassium, Sucralose)
JEU	1.42	Sorbitol, Isomalt, Xylitol, Maltitol
MFO	2.03	Sweetener (Isomalt, Mannitol, Sorbitol, Maltitol, Maltitol syrup, Xylitol, Aspartame, Acesulfame potassium, Sucralose)
MWH	1.53	Sweetener (Xylitol 34 %, Sorbitol, Mannitol, Maltitol syrup, Aspartame, Acesulfame potassium, Sucralose)
X24	1.35	Xylitol 36 %, Sorbitol, Mannitol, Maltitol syrup, Aspartame, Acesulfame potassium
SSP	1.13	Sweetener 60 % (Sorbitol, Xylitol 17 %, Maltitol molasses, Aspartame, Acesulfame potassium)
SPE	2.46	Xylitol, Mannitol, Aspartame, Sorbitol, Acesulfame potassium
FWM	1.42	Xylitol, Dicalciumphosphate 1.3 %, Glycerol, Dyes (Chlorophyllin, Titanium Dioxide), Aspartame
XPM	1.05	Sweetener (Sorbitol, Xylitol 20 %, Aspartame)
JHO	1.43	Sorbitol, Isomalt, Maltitol, Xylitol, Mannitol

3.3.2 Bulk analysis of sweeteners and xylitol by EA-IRMS

$\delta^{13}C$ values for the pure sweetener compounds and the different xylitol samples were measured using a vario PYRO Cube EA system (Elementar Analysensysteme, Langenselbold, Germany) using the C/N mode. The EA was coupled to an IsoPrime 100 isotope ratio mass spectrometer (Elementar Analysensysteme, Langenselbold, Germany) for the isotope ratio measurements. For the analysis, sample amounts between 0.5 mg and 1.0 mg of the pure compound were weighed into tin capsules (4x6 mm) (IVA Analysentechnik GmbH, Meerbusch, Germany) using a Sartorius SE 2 ultra-micro balance (Sartorius AG, Goettingen, Germany). The

experimental $\delta^{13}C$ values were normalized to the international VPDB scale using a two point normalization approach relative to the international reference standards IAEA-CH6 (Sucrose, $\delta^{13}C$ -10.45 ‰) and IAEA-600 (Caffeine, $\delta^{13}C$ -27.77 ‰) (both IAEA, Vienna, Austria) with certified $\delta^{13}C$ values.[23, 106]

3.3.3 Preparation of the chewing gum samples for CSIA by LC-IRMS

For each sample, 1.0 - 2.5 g of chewing gum were crushed with mortar and pestle to break the coating material of the chewing gum and facilitate the dissolution of the water soluble components. The extraction was performed with 50 mL of water which was stirred with the chewing gum for one hour with the help of a magnetic stir bar. The gum base which is not water soluble was discarded and the supernatant was filtered using 0.25 µm syringe filters (polytetrafluoroethylene (PTFE), IVA Analysentechnik GmbH, Meerbusch, Germany). The filtered samples were diluted with water by a factor of 50 and stored in the refrigerator until the analysis was performed.

3.3.4 Instrumentation and conditions for the LC-IRMS measurements

The separation of compounds in the chewing gum extracts was performed on a Reprosil Repromer H (9 µm, 250x4.6 mm) (Dr. Maisch GmbH, Ammerbuch, Germany) column with a flow rate of 600 µL min^{-1} of pure water as the mobile phase. The mobile phase was delivered by a Dionex UltiMate 3000 pump in combination with a Dionex UltiMate 3000 degassing unit both by Thermo Fischer (Scientific, Bremen, Germany). Sample volumes of 5 µL were injected using a Dionex UltiMate 3000 autosampler unit (Thermo Fisher Scientific, Bremen, Germany). The HPLC column was heated to 30 °C using a high temperature HPLC oven (SIM GmbH, Oberhausen, Germany). With the help of the eluent preheating zone, the temperature of the eluent was raised to 30 °C prior to entering the analytical column. For stable isotope analysis an IsoLink interface (Thermo Bremen, Germany) coupled to a Thermo Delta V isotope ratio mass spectrometer (Thermo, Bremen, Germany) was used.

Within the LC-IsoLink interface, organic and inorganic carbon in the eluent stream are converted to CO_2 which is separated from the liquid phase to be introduced into the mass spectrometer in a stream of helium. For the oxidation, sodium peroxydisulfate (100 g L^{-1}) and phosphoric acid (1.5 M) are separately pumped at a flow rate of 50 µL min^{-1} and added to the

HPLC eluate with the help of a T-connector. The oxidation is performed in a heated reactor (100 °C) consisting of a thin metal capillary. After the oxidation, the stream is cooled down to room temperature and enters a gas separation membrane unit. The membrane unit separates the dissolved CO_2 from the liquid phase and transports the CO_2 through two Nafion® gas drying traps and the open split system into the isotope ratio mass spectrometer. More detailed information about the interface can be found in the literature.[36, 40, 62] The LC-IRMS results were normalized to the international VPDB scale using IAEA CH6 sucrose (retention time 429 s, δ^{13}C -10.45 ‰)[106] and xylitol (δ^{13}C -22.5 ‰) which were analyzed using the same method as for the chewing gum extracts to ensure identical conditions. The results were normalized as described in the EA-IRMS section for the two point normalization.

3.4 Results and Discussion

3.4.1 Measurement of bulk xylitol and sweetener samples

To obtain baseline values for pure xylitol of known corn and birch wood origin three xylitol samples as well as the three most common additional sweeteners in chewing gums were analyzed using EA-IRMS. The xylitol of birch origin was found to have a δ^{13}C value of -20.3 ‰, whereas the corn xylitol sample had a δ^{13}C value of -10.4 ‰. Similar isotopic signatures were obtained for 28 commercially available xylitol samples that were studied in South Africa, where xylitol of C3 origin was found to have isotope ratios in the range from -22.3 to -19.7 ‰, and xylitol of suspected C4 origin was found to be in a range from -13.0 to -9.7 ‰.[143]

A summary of these results is presented in **Figure 3.1**. The other sweeteners analyzed by EA-IRMS were found to be in a range from -10.6 to -12.3 ‰ which indicates that they were synthesized based on C4 precursor materials. The xylitol obtained from Fluka (Buchs, Switzerland) showed a lower δ^{13}C value of -22.5 ‰ which indicates a C3 origin of the plant material, although the raw material was not stated on the label of the product.

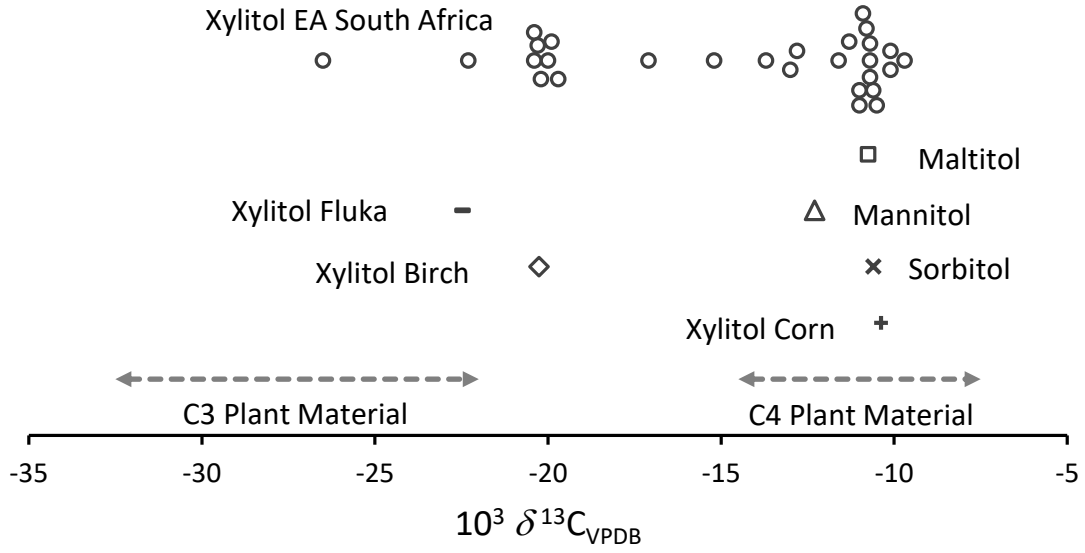

Figure 3.1: $\delta^{13}C$ values obtained from measurements of the pure xylitol and sweetener samples by EA-IRMS. Standard deviations for the EA measurements were below 0.2 ‰. In addition, $\delta^{13}C$ ranges observed for C3 and C4 plants [91, 140-141] and bulk xylitol data obtained by Symes *et al.*, 2017 are plotted.[143]

3.4.2 Development of a HPLC method for the separation of xylitol from other sweeteners in chewing gum

Method development for LC-IRMS applications represents a challenge as the mobile phase has to be completely free of organic solvents, and certain restrictions, e.g., for the flow rates in the system apply. The aim of the method development was to be able to separate xylitol from sorbitol, maltitol and mannitol which are present in larger quantities in chewing gum formulations. To that end, two different cation exchange columns (Repromer H, Repromer Ca, Dr. Maisch GmbH, Ammerbuch, Germany) were tested. Pure water was used as a mobile phase and both column temperature (30-80 °C) and flow rate of the mobile phase (300-600 µL min^{-1}) were systematically evaluated to find the optimal separation conditions. The best results for the separation were obtained at 30 °C and 600 µL flow of the mobile phase using the Repromer H column. Under these conditions sorbitol and mannitol were coeluting with a retention time of 9.9 min and xylitol was eluting at a retention time of 10.9 min. The chromatographic separation of a chewing gum extract by the optimized LC-IRMS method is shown in **Figure 3.2**.

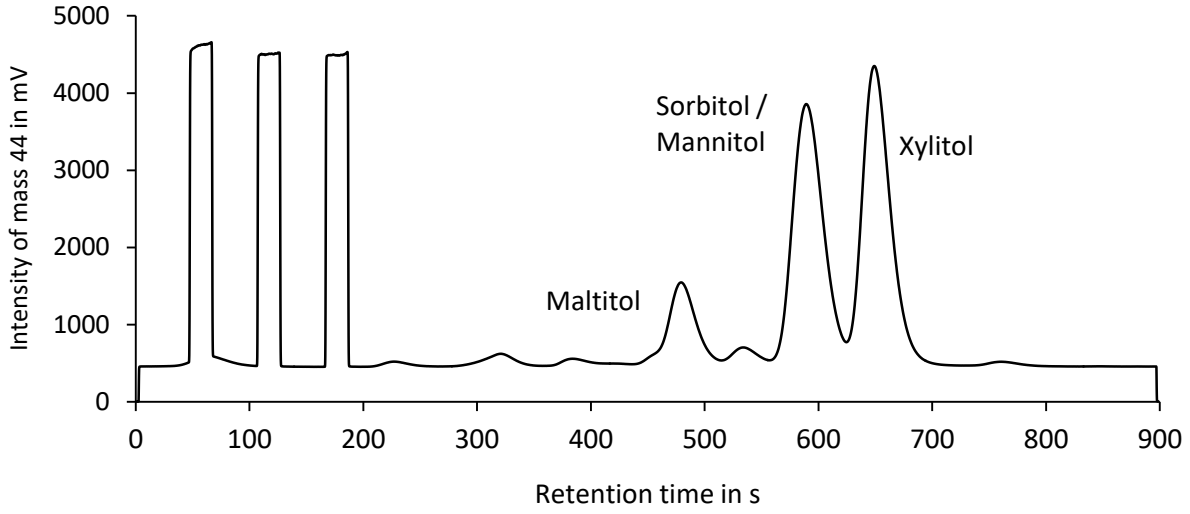

Figure 3.2: Chromatographic separation of xylitol from an aqueous extract of a chewing gum sample (MSQ) containing xylitol, mannitol, sorbitol, maltitol, aspartame, maltitol syrup, sucralose and acesulfame potassium

At equal concentrations of xylitol and sorbitol/mannitol a baseline separation of the compounds could not be achieved. In contrast to GC-IRMS where baseline separation of the analytes is crucial for an accurate determination of δ^{13}C values due to the chromatographic isotope effect [30, 145], this effect is not very pronounced in LC-IRMS so that the results were evaluated and statistically tested for the influence of the coelution. Therefore, samples containing 50 mg L^{-1} of the respective compounds were analyzed and the results obtained for xylitol were compared to samples of pure xylitol at the same concentration. The chromatogram for the mixed sample is shown in **Figure 3.3**. From the repeated measurements of the mix a mean resolution of 1.1 for the xylitol and the sorbitol/mannitol peak was determined (n=4, calculated by full width at half maximum ($W_{0.5H}$), see **Equation 3.1**)

$$R = 1.18 \times \frac{t_R(Xylitol) - t_R(Sorbitol,Mannitol)}{W_{0.5H}(Xylitol) + W_{0.5H}(Sorbitol,Mannitol)} \qquad \textbf{(3.1)}$$

To evaluate the influence of the coelution on the δ^{13}C values for xylitol a two-sample F-test was conducted. At a significance level of α=0.01 there is no evidence that the obtained δ^{13}C value for xylitol measured as a single standard differs from the determined δ^{13}C value in the mixture. During the measurement of the 21 different chewing gum samples no other

constituents of the chewing gum could be identified that interfered with the separation of xylitol from the sample matrix.

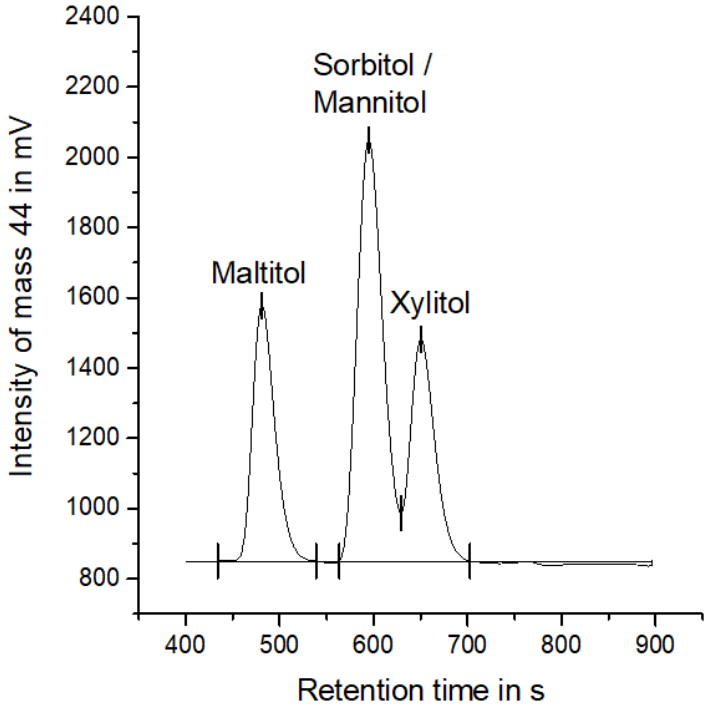

Figure 3.3: Chromatogram obtained for the separation of 50 mg L^{-1} of maltitol, xylitol, mannitol and sorbitol

3.4.3 Measurement of xylitol extracted from chewing gum samples

The extraction procedure developed for the CSIA of xylitol analysis by LC-IRMS offers two main advantages. On the one hand, it is preferable to a preparative separation of xylitol from the matrix and subsequent EA measurement as it saves time and offers less risk for fractionation processes that could occur during the purification of the analyte for analysis by EA-IRMS. On the other hand, the extraction procedure can easily be adapted to varying xylitol concentrations in the chewing gum as the last dilution step can be reduced to obtain up to 50 times higher xylitol end concentrations in the extract. The analysis of xylitol is thereby only limited if a large excess of sorbitol or mannitol is present in the sample. Higher concentrations of mannitol and sorbitol in comparison to xylitol were found to reduce the precision of the measurement. The observed standard deviations were usually lower than 0.3 ‰ for the majority of samples containing less than a threefold excess of sorbitol and mannitol (fraction of the obtained peak areas) over xylitol. Considerably higher standard deviations were

observed for samples with relatively low xylitol concentrations in relation to the sorbitol and mannitol (ratio of sorbitol/mannitol to xylitol between 4.0 and 7.1). In these cases standard deviations from 1.1 to 2.4 ‰ (e.g. samples MRO, MRE, MFO and SMP) were observed. The precision was found to be generally sufficient though for a reliable classification in one of the two categories of origin as the Δ^{13}C between corn and wood based xylitol observed is around 10 ‰ which has also been demonstrated in a larger set of EA measurements in the literature.[143] To statistically evaluate the results and establish threshold values for the C3 and C4 xylitol classes, a one-sided *t*-test was performed with the results obtained for the triplicate measurements of each chewing gum extract. With an error probability of α=0.01, δ^{13}C values below -18.0 ‰ can be identified to be of C3 origin, whereas isotopic signatures above -15.3 ‰ are related to C4 plant material. (Calculation of the threshold values can be found in the supporting information) Chewing gum MWH was the only sample showing an intermediate δ^{13}C value between the two threshold values for xylitol, which could be the result of a mixture of xylitol from different sources used in the production.

As already expected from the list of ingredients the composition of the chewing gums with respect to the ratio of xylitol to the other sweeteners was highly variable. From the set of 21 chewing gums that claimed xylitol as an ingredient, 2 samples were found to contain no xylitol or only very low amounts that could not be determined due to the large excess of the remaining sweeteners. For the remaining 19 chewing gum samples compound specific δ^{13}C values for xylitol could be determined. An overview of the results obtained is given in **Figure 3.4**. With the exception of one sample, all of the analyzed chewing gums fall into two clusters representing the values for C3 and C4 derived xylitol determined by EA-IRMS in this study and in the literature.[143]

The δ^{13}C values obtained for xylitol of C4 origin and the four chewing gum samples which were suspected to contain xylitol of C4 origin were within the δ^{13}C range for C4 plant material commonly observed in literature (-9 to -16 ‰). However, the values obtained for C3 derived xylitol cannot be clearly related to the commonly observed δ^{13}C values for the raw plant material used (-22 to -35 ‰). The reported δ^{13}C values for the raw wood material is more negative than the measured δ^{13}C values for pure xylitol and the extracted xylitol from the chewing gums.

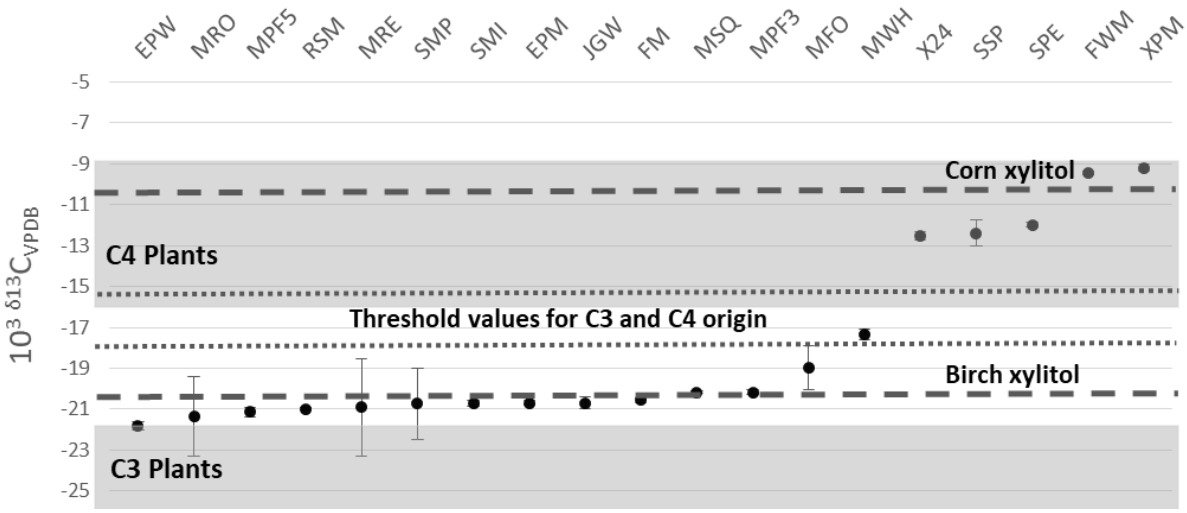

Figure 3.4: δ^{13}C values measured from chewing gum extracts; error bars indicate the standard deviation of the measurement (n=3); grey areas indicate the literature ranges observed for C3 and C4 plants; dotted lines represent the δ^{13}C value measured for pure birch and corn xylitol and threshold values for the differentiation between xylitol of C3 and C4 origin

Isotope data for corn cobs and husks are reported in the range from -11.6 to -13.2 ‰ whereas birch wood was shown to have average δ^{13}C values around -27 ‰.[146-147] The observed offset of around 7 ‰ between the wood xylitol and the raw material cannot easily be explained by the manufacturing process of xylitol as this should result in a comparable shift from C4 plant material to the respective end product. However, Symes *et al.*, (2017) observed a similar trend for the δ^{13}C values of C3 derived xylitol measured as bulk samples by EA-IRMS. By analyzing different size fractions of xylitol crystals, it was proven that the obtained values were not a result of the mixture of xylitol from different sources.[143] It was also suspected that adulteration with undeclared additives could be responsible for the overall higher δ^{13}C value of the xylitol compared to the source, which can be excluded due to the results obtained in this study by CSIA in which possible adulterants would have been separated from the xylitol and the observed trend was still present. Symes *et al.*, (2017) also determined δ^{13}C values for xylose samples of C3 and C4 origin and found that the isotopic signature of the xylose was similar to the xylitol, so that a fractionation process during the hydrogenation of the xylose could be excluded. From these results, it can be concluded that the offset of the observed δ^{13}C values has to be a result of the extraction of the xylans from wood, or the hydrolysis of the xylan to xylose. From results obtained in tree ring studies by SIA, which can be used as a paleothermometer, it has been shown that the lignin fraction of the wood is usually around 3 ‰ lighter than the cellulose fraction.[148-149] Although hemicelluloses or xylan have not been

included in these measurements, there is a high possibility that the hemicellulose fraction also significantly differs from the mean $\delta^{13}C$ value of the whole wood, which could be an explanation of the shift observed for the xylitol. To corroborate this hypothesis it would be necessary to measure isotopic data for the hemicellulose extract as well as for the xylan, which has not been performed until now. Such investigations are currently under way but are out of scope of this study that focused on the source authentication of xylitol rather than explaining isotope shifts in the hemicellulose biosynthesis. In conclusion, real chewing gum samples could be analyzed successfully for their source of xylitol with a very simple sample preparation, which gives another example for the opportunities of LC-IRMS in the field of food authenticity.

Funding Sources

The research was funded by the German Research Foundation (DFG) under the project grants 278676953 and 317438550.

3.5 Appendix to Chapter 3

Setting a threshold for assigning an unknown xylitol sample to wood or corn origin

For the calculation of the one-sided prediction intervals as threshold values for a decision between C3 and C4 based xylitol, the values of the single measurements (*n*=3 for each sample) shown in **Figure 3.4** for the xylitol extracted from chewing gum were used (Except for gum MWH which showed intermediate δ^{13}C values between C3 and C4) to calculate the lower, respectively the upper limit of these confidence intervals as given by:

$$\delta^{13}C_{corn,\ lower} = \overline{\delta^{13}C_{corn}} - t_{\alpha,df} \times s_{corn} \times \sqrt{1 + \frac{1}{n_{corn}}}$$

$$\delta^{13}C_{wood,\ upper} = \overline{\delta^{13}C_{wood}} + t_{\alpha,df} \times s_{wood} \times \sqrt{1 + \frac{1}{n_{wood}}}$$

$\overline{\delta^{13}C_{corn}}$	mean δ^{13}C of samples from corn origin
$\overline{\delta^{13}C_{wood}}$	mean δ^{13}C of samples from wood origin
n_{corn}	number of samples from corn origin
n_{wood}	number of samples from wood origin
s_{corn}	standard deviation of δ^{13}C values from corn samples
s_{wood}	standard deviation of δ^{13}C values from wood samples
$t_{\alpha,df}$	*t* value for a given confidence level 1-α and n-1 degrees of freedom

Setting α = 0.01 the following results were calculated:

	$\overline{\delta^{13}C}$	*s*	*n*	*df*	$t_{0.01}$	Limit of the confidence interval (‰)
Wood (C3)	-20.69	1.08	39	38	2.428	-18.03
Corn (C4)	-11.11	1.54	15	14	2.624	-15.29

The threshold values for origin assignment: If the δ^{13}C for xylitol in an unknown sample falls below -18.03 ‰ a wood origin can be assumed accepting an α of 0.01. In contrast a value of an unknown sample above -15.29 ‰ can be assumed to be of C4 plant or corn origin accepting an α error of 0.01.

Chapter 4: New concepts for the determination of oxidation efficiencies in liquid chromatography isotope ratio mass spectrometry

Daniel Köster[1], Irene M. Sanchez Villalobos[1], Maik A. Jochmann[*,1],Willi A. Brand[2], Torsten C. Schmidt[1,3]

[1]Instrumental Analytical Chemistry, University of Duisburg-Essen, Universitätsstr. 5, 45141 Essen, Germany

[2]Max Planck Institute for Biogeochemistry, Hans-Knöll-Str. 10, 07745 Jena, Germany

[3]University of Duisburg-Essen, Centre for Water and Environmental Research (ZWU) Universitätsstr. 5, 45141 Essen, Germany

Adapted with permission from: D. Köster, I.M. Sanchez Villalobos, M.A. Jochmann, W.A. Brand, T.C. Schmidt, *New Concepts for the Determination of Oxidation Efficiencies in Liquid Chromatography-Isotope Ratio Mass Spectrometry*, Analytical Chemistry, 91 (8), pp. 5067–5073, https://pubs.acs.org/doi/10.1021/acs.analchem.8b05315, further permissions related to the material excerpted should be directed to the ACS directly

4.1 Abstract

In liquid chromatography coupled to isotope ratio mass spectrometry (LC-IRMS), analytes are separated on a LC system and consecutively oxidized to CO_2 which is required for the determination of compound specific carbon isotope ratios. Oxidation is performed in an online reactor by sulfate radicals. Reaction conditions in the interface depend on the flow conditions determined by the LC method and the flow rates and concentrations of oxidation agent and phosphoric acid added in the interface. To determine accurate isotope ratios, a quantitative conversion of the carbon contained in the analyte to the CO_2 measurement gas is a prerequisite. Oxidation efficiencies are not commonly evaluated during method development, although certain analytes are known to be difficult to be oxidized by sulfate radicals. For the assessment of the oxidation efficiency of the LC-IRMS system, three different approaches were evaluated. (1) Residual organic carbon in the eluent stream of the interface was determined to calculate oxidation yields depending on the initial analyte concentration. (2) The IRMS response was calibrated to an inorganic carbon reference material to determine oxidation efficiencies with the help of the IRMS as a detector. (3) The oxidation temperature was deliberately reduced while monitoring the $\delta^{13}C$ and signal intensity. The common assumption, that a linear relation of IRMS signal to analyte concentration is an indicator for complete oxidation in LC-IRMS could be disproved. All three approaches can be applied for future method development in LC-IRMS, monitoring of existing flow-injection applications, as well as for verification of complete oxidation in established LC-IRMS methods.

4.2 Introduction

Liquid chromatography coupled to isotope ratio mass spectrometry (LC-IRMS) is a technique for the compound specific determination of carbon isotope ratios from small, polar or temperature sensitive organic molecules as well as from inorganic carbon.[73] It has found many applications mainly for food authentication[54, 56, 100], compound specific amino acid analysis from various protein sources[58, 68, 150], and the analysis of dissolved organic and inorganic carbon in water samples (DOC, DIC).[84, 151] For compound specific isotope analysis (CSIA) at natural abundance levels, the analytes have to be chromatographically separated and transformed to a measurement gas which is introduced into a specific gas-isotope ratio mass spectrometer.[152]

Different approaches for the combination of liquid chromatography (LC) and isotope ratio mass spectrometry (IRMS) have been described in the literature, where the most challenging part is the conversion of the analyte to CO_2 and the removal of the CO_2 from the liquid HPLC eluent stream. Methods employing high temperature catalytic conversion by a moving wire interface and high temperature microwave plasma have been successfully developed, but are not available in commercial instruments.[39, 41, 142, 153] Another high temperature catalytic conversion principle (based on an elemental analyzer (EA)) has recently been shown to be applicable to the flow injection analysis (FIA) for nitrogen and carbon isotope ratios, but applications for chromatographic separations of real samples are not yet available.[48] The two commercially distributed interfaces for CSIA via LC-IRMS are the IsoLink© (Thermo Fisher, Bremen, Germany) and the LiquiFace© (Elementar Analysensysteme, Hanau, Germany). Both systems use a wet chemical oxidation in the HPLC eluent stream for the analyte oxidation and a subsequent separation of the produced CO_2 via a membrane gas separation unit into a counter flow of helium which is transferred to the mass spectrometer.[36, 154] Oxidation of the analytes is achieved by the addition of peroxydisulfate salts ($M_2S_2O_8$) and phosphoric acid into the HPLC eluent. The mixture is passed through a heated oxidation reactor, where in situ generated sulfate radicals unselectively oxidize the available carbon to CO_2. The low pH of the eluent facilitates the membrane separation of CO_2 from the liquid stream into a helium carrier gas that transports the CO_2 to the mass spectrometer.

The oxidation efficiency of analytes in the LC-IRMS interface depends on several boundary conditions. The residence time in the reactor is determined by the combined flow rates of the

HPLC, the oxidation reagent, and the acid which are delivered by three independent pumps. The second factor is the relative concentration of the analyte to the oxidation agent. It has been shown that there is an upper concentration limit above which the relationship between the injected amount of carbon and the peak area response of the IRMS is not linear anymore. By reducing the amount of analyte or increasing the concentration of the oxidation agent, the linear relationship could be restored.[36] The molecular composition of the analyte can also negatively affects the mineralization efficiency, this has been shown for halogenated structures, which were analyzed in chlorinated, fluorinated, and brominated acetic acids as well as for chlorinated and brominated benzoates.[61, 155] In addition, nitrogen heteroaromatic compounds and urea were found to be oxidized incompletely.[45, 156-157] Besides the negative effect of incomplete oxidation on the sensitivity, the obtained δ^{13}C values in LC-IRMS were found to significantly deviate from reference values obtained by EA-IRMS for some analytes even after normalization.[35, 45, 157] In theory, the offset between different techniques can be compensated by identical treatment of the analyte and reference material.[23] But incomplete oxidation in LC-IRMS can lead to offsets that cannot be reliably corrected for by this technique as will be discussed later on.

In current publications, the oxidation conditions suitable for a certain combination of analytes and flow conditions in the interface are based on two approaches. The first approach is to monitor the oxygen background that is produced during the oxidation process, which is also recommended by the manufacturer.[40, 158-159] The second approach is to determine calibration functions of the injected analyte concentration compared to the signal obtained by the IRMS system. In several publications it has been suggested that a linear correlation can be used as an indicator for a complete conversion.[68, 160-161] Besides these approaches, a short review of 52 published methods for LC-IRMS and FIA-IRMS using the IsoLink© interface showed that the choice of oxidation conditions (concentration of oxidizing agent present in the reactor) is not dependent on the employed HPLC conditions **(Figure 4.1)**. Oxidation agent concentration in the reactor is often lower when higher eluent flow rates are used in the system, which additionally reduces the oxidation efficiency by a decreased residence time in the oxidation reactor. A detailed comparison of the individual methods is supplied in **Table 4.1**.

Table 4.1: Oxidation conditions published for different LC-IRMS applications

Year	Author	Method	HPLC Flow / µL min^{-1}	Flow Acid / µL min^{-1}	Flow Ox. Agent / µL min^{-1}	Conc. Ox. Agent / mol L^{-1}	Conc. Acid / mol L^{-1}	System Flow / µL min^{-1}	Conc. Ox. Agent Flow / mmol L^{-1}	Reaction Time / s	Source
2004	Krummen *et al.*	CSIA/FIA	300	60/80/100	-	-	-	-	-	-	[36]
2005	Godin *et al.*	CSIA	250	50	50	0.50	1.0	350	71.4	34	[40]
2006	Cabañero *et al.*	CSIA	400	50	50	0.50	0.5	500	50.0	24	[54]
2006	Heuer *et al.*	CSIA	300	30	30	1.26	2.2	360	105.0	33	[78]
		CSIA	500	50	70	1.26	2.2	620	142.3	19	[78]
2006	McCullagh *et al.*	CSIA	700	30	30	0.8	1.7	760	31.6	15	[68]
2007	Schierbeek *et al.*	CSIA	500	30	30	0.84	1.5	560	45.0	21	[74]
2008	Boschker *et al.*	CSIA	300	50	50	0.70	1.5	400	87.5	29	[53]
2008	Elflein & Raezke	CSIA	300	50	50	0.50	0.5	400	62.5	29	[94]
2008	Godin *et al.*	CSIA/FIA	220	50	50	0.50	1.00	320	78.1	37	[62]
2008	Godin *et al.*	CSIA/FIA	300	50	50	0.50	1.00	400	62.5	29	[160]
2008	McCullagh *et al.*	CSIA	600	-	-	0.80	1.5	-	-	-	[57]
2008	Tagami & Uchida	CSIA	400	50	50	0.84	1.5	500	84.0	24	[161]
2009	Bodé *et al.*	CSIA/FIA	400	70	40	0.40	1.5	510	31.4	23	[80]
2009	Brandes	FIA	300	50	0	0.00	1.5	350	-	34	[151]
2009	Jochmann *et al.*	FIA	300	50	50	0.80	1.5	400	100.0	29	[100]
2009	Schierbeek *et al.*	CSIA	300	50	50	0.70	1.5	400	87.5	29	[51]
2009	Schierbeek *et al.*	CSIA	500	25	25	0.84	1.5	550	38.2	21	[75]
2009	Smith *et al.*	CSIA	500	50	50	0.26	1.28	600	21.7	20	[58]
			600	50	50	0.26	1.28	700	18.6	17	[58]
2010	Cabañero *et al.*	CSIA	400	30	20	0.50	0.5	450	22.2	26	[55]
2010	Choy *et al.*	CSIA	700	-	-	-	-	-	-	-	[69]
2010	Raghavan *et al.*	CSIA	260	-	-	0.37	1.5	-	-	-	[70]
2011	Albéric	FIA	300	50	40	0.4	1.5	390	41.0	30	[84]
		FIA	300	50	35	0.4	1.5	385	36.4	31	[84]

Year	Author	Method	HPLC Flow / µL min^{-1}	Flow Acid / µL min^{-1}	Flow Ox. Agent / µL min^{-1}	Conc. Ox. Agent / mol L^{-1}	Conc. Acid / mol L^{-1}	System Flow / µL min^{-1}	Conc. Ox. Agent Flow / mmol L^{-1}	Reaction Time / s	Source
2011	Dunn *et al.*	CSIA	-	-	-	-	-	-	-	-	[67]
2011	Godin *et al.*	CSIA	350	50	50	-	-	450	-	26	[162]
2011	Lynch *et al.*	CSIA	-	-	-	0.84	1.5	-	-	-	[163]
2011	Pollard *et al.*	CSIA	-	-	-	0.37	1.5	-	-	-	[164]
2011	Zhang *et al.*	CSIA	500	50	50	0.83	1.5	600	69.2	20	[35]
2012	Kujawinski *et al.*	CSIA	500	50	50	0.84	1.5	600	70.0	20	[45]
2012	Scheibe *et al.*	CSIA	500	50	30	0.55	1.5	580	28.4	20	[85]
2013	Bai *et al.*	CSIA	400	70	40	0.40	1.5	510	31.4	23	[81]
2013	Basler & Dyckmans	CSIA	250	30	30	0.8	1.5	310	77.4	38	[159]
2013	Blyth *et al.*	FIA	300	20	20	0.13	1.28	340	7.6	35	[71]
2013	Blyth *et al.*	FIA	300	20	20	0.13	1.28	340	7.6	35	[72]
2013	Kujawinski *et al.*	CSIA	500	50	50	0.84	1.50	600	70.0	20	[165]
			300	50	50	0.84	1.5	400	105.0	29	[165]
2013	Malik & Gleixner	CSIA	500	50	30	0.55	1.5	580	28.4	20	[89]
2013	Malik *et al.*	CSIA	500	50	30	0.55	1.5	580	28.4	20	[166]
2014	Gilevska *et al.*	FIA	300	50	50	0.84	1.5	400	105.0	29	[155]
			300	100	100	0.84	1.5	500	168.0	24	[155]
			300	50	50	1.68	1.5	400	210.1	29	[155]
			200	50	50	0.84	1.5	300	140.0	39	[155]
2014	Hatton *et al.*	CSIA	400	70	40	0.40	1.5	510	31.4	23	[83]
2014	Moerdijk-Poortvliet *et al.*	CSIA	300	50	50	0.70	1.5	400	87.5	29	[167]
		CSIA	700	30	30	0.8	1.7	760	31.6	15	[167]
2014	Moerdijk-Poortvliet *et al.*	CSIA	500	50	50	0.70	1.5	600	58.3	20	[168]
2014	Zhang *et al.*	CSIA	500	50	30	0.83	1.5	580	42.9	20	[63]
2005	Grosse *et al.*	CSIA	300	50	50	0.70	1.5	400	87.5	29	[169]
		CSIA	700	30	30	0.8	1.7	760	31.6	15	[169]
2015	Moerdijk-Poortvliet *et al.*	CSIA	300	-	-	-	-	-	-	-	[170]

Year	Author	Method	HPLC Flow / µL min^{-1}	Flow Acid / µL min^{-1}	Flow Ox. Agent / µL min^{-1}	Conc. Ox. Agent / mol L^{-1}	Conc. Acid / mol L^{-1}	System Flow / µL min^{-1}	Conc. Ox. Agent Flow / mmol L^{-1}	Reaction Time / s	Source
2015	Mogusu *et al.*	CSIA	300	50	50	0.84	1.5	400	105.0	29	[33]
			300	50	50	0.42	1.5	400	52.5	29	[33]
2015	Birkigt *et al.*	CSIA	300	100	100	0.84	1.5	500	168.0	24	[171]
			500	100	100	0.84	1.5	700	120.0	17	[171]
2015	Bononi *et al.*	CSIA	300	50	30	1.5	1.5	380	118.4	31	[102]
2016	Bononi *et al.*	CSIA	300	50	30	1.5	1.5	380	118.4	31	[103]
2016	Dong *et al.*	CSIA	350	50	50	0.50	0.5	450	55.6	26	[95]
2016	Luo *et al.*	CSIA	-	-	-	0.50	0.5	-	-	-	[96]
2016	Wei *et al.*	CSIA	400	50	50	-	-	500	-	24	[60]
2017	Mora *et al.*	CSIA	-	-	-	-	-	-	-	-	[59]
2017	Powers *et al.*	FIA	-	-	-	-	-	-	-	-	[86]
2017	Powers *et al.*	FIA	350	50	-	-	1.5	400	-	29	[87]
2018	Dong *et al.*	CSIA	350	50	50	0.5	0.5	450	55.6	26	[97]
2018	Franke *et al.*	CSIA	200	75	75	0.84	1.5	350	180.0	34	[61]
2018	Köster *et al.*	CSIA	600	50	50	0.42	1.5	700	30.0	17	[56]

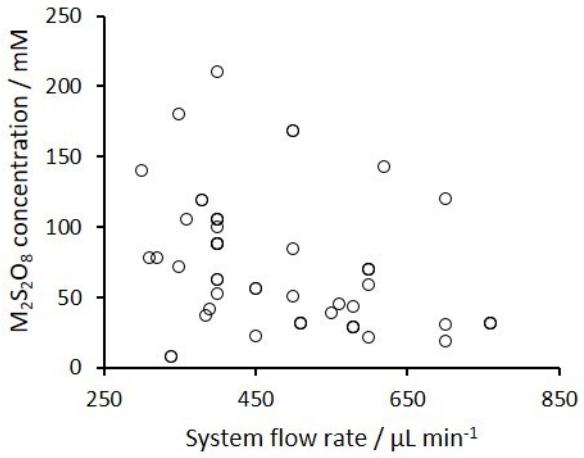

Figure 4.1: Oxidation conditions in 52 published LC-IRMS and FIA-IRMS methods for the IsoLink© interface; System flow rates are the combination of the HPLC and the two interface pumps; Concentration of the oxidation agent was based on the total flow rate in the instrument and the flow rate and concentration of the oxidation agent

High concentrations of oxidation agent are beneficial to a certain point for the oxidation efficiency, but they lead to an increased O_2 background in the ion source. This results in a decreased accuracy and precision of the $\delta^{13}C$ measurements, a reduced filament lifetime, and shorter maintenance cycles.[46, 73] To overcome this problem, Hettmann *et al.* (2007) introduced an oxygen scrubber to the LC-IRMS setup which removes excess oxygen before entering the IRMS.[46] Their copper reduction reactor setup was successfully used in several studies.[61, 85, 88, 155] The oxygen scrubber has not yet been commercialized, so the majority of users have to limit the oxygen production in the system to a reasonable level while maintaining sufficient oxidation capacity. Therefore, a series of experiments was carried out to evaluate different approaches to detect incomplete oxidation in the LC-IRMS interface. Conditions under which the concentration of oxidation agent in the system could potentially be decreased should be identified to reduce the O_2 background and increase the time period between filament replacements. The mineralization efficiency in the interface cannot easily be determined from standard LC-IRMS measurements as the instrument response depends on the gas exchange in the membrane separation unit as well as dilution in the open split system of the IRMS. To overcome this problem, three different approaches are evaluated in this work (**Figure 4.2**).

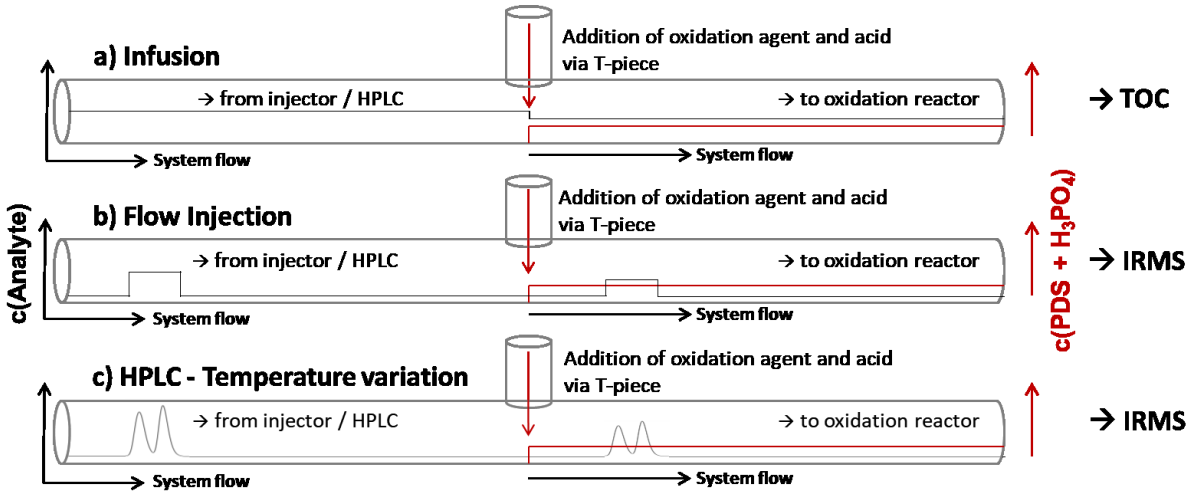

Figure 4.2: Instrumental setup for the infusion experiments with subsequent TOC measurement (a); the flow injection experiments (b); and the conventional HPLC-IRMS approach (c)

The first one is the external measurement of the remaining total organic carbon (TOC) in the aqueous effluent of the oxidation reactor in the LC-IRMS interface by a TOC analyzer. This should allow a determination of the mineralization yield independently of the IRMS as a detector. In a second approach, the response of the LC-IRMS setup is calibrated with an inorganic carbon reference material. This can be used as a reference for a complete mineralization and subsequent calibration of the IRMS response to obtain mineralization rates for other analytes. The third method is the deliberate reduction of the oxidation efficiency in the interface by a stepwise reduced oxidation temperature. Subsequently the three methods will be compared with regard to their potential to detect inefficient oxidation conditions in LC-IRMS methods and to their applicability in the method development.

4.3 Materials and Methods

4.3.1 Chemicals and Reagents

Ultrapure water for the mobile phase of the HPLC was obtained from an ELGA Purelab Ultra (Veolia Water Technologies, Ratingen, Germany) system, degassed under vacuum (Membrane pump, Vacuubrand GmbH & Co., Wertheim, Germany) and simultaneously treated by an ultrasonic bath (Sonorex RK 100, Bandelin Electronic, Berlin, Germany) for 20 min. During the LC-IMRS measurements the mobile phase and the reagents used in the LC interface were continuously sparged by a low stream of helium. (purity 5.0, Air Liquide, Oberhausen, Germany) For the oxidation, sodium peroxydisulfate (99 %, Riedel-de Haën,

Seelze, Germany) and ortho-phosphoric acid (85 %, p.a., Merck KGaA, Darmstadt, Germany) were used. Standards for TOC and dissolved inorganic carbon (DIC) were obtained from Sigma Aldrich (1000 ± 10 mg L^{-1} (C), Steinheim, Germany). Methylene blue (Merck KGaA, Darmstadt, Germany) was used for the determination of the reactor volume of the LC-IRMS interface. Chemicals used for the oxidation: Caffeine (Reagent Plus), vanillin (Reagent Plus, 99 %), D-(+)-Glucose (Purity ≥99 %) were obtained from Sigma Aldrich (Steinheim, Germany) as well as phenylalanine (Purity 99 %), and histidine (Purity 98+ %) from Alfa Aesar (Karlsruhe, Germany), methanol (UHPLC-MS Optima, Fisher Chemical, Schwerte, Germany) and xylitol from Fluka (Buchs, Switzerland).

4.3.2 Infusion Experiments

A constant stream of analyte solution at different concentrations was delivered by a Rheos Allegro HPLC pump (Flux instruments AG, Basel, Switzerland) directly to the IsoLink© interface (Thermo Fisher Scientific, Bremen, Germany). Sodium peroxydisulfate (0.84 mol L^{-1}) and phosphoric acid (1.50 mol L^{-1}) were added at a flow rate of 50 µL min^{-1} each, the oxidation was performed at 100 °C. After the oxidation reactor, the connection to the gas separation unit was replaced by a peek capillary that led to a cooled sample vessel. Approximately 10 mL of the eluate were collected for the TOC measurement. Remaining organic carbon was determined on a TOC-L analyzer (Shimadzu, Duisburg, Germany). Residual dissolved CO_2 was removed from the sample by sparging with synthetic air (80 mL min^{-1}, 3 min). 50 µL of the sample were injected into an oxidation tube filled with platinum coated ceramic particles heated to 720 °C.

4.3.3 Flow injection analysis with DIC calibration

Degassed water with a flow rate of 600 µL min^{-1} was used as the mobile phase which was delivered by a Dionex UltiMate 3000 pump and degassing unit (both Thermo Fisher Scientific, Bremen, Germany). Sample volumes of 5 µL were injected using a Dionex UltiMate 3000 autosampler unit (Thermo Fisher Scientific, Bremen, Germany). In the LC-IRMS interface, sodium peroxydisulfate (0.42 mol L^{-1}) and phosphoric acid (1.0 mol L^{-1}) were added at a flow rate of 50 µL min^{-1} each. The oxidation was performed at 100 °C. For the calibration of the amount of oxidized carbon, dilutions of a certified DIC reference standard solution were used.

4.3.4 LC-IRMS oxidation temperature variation

Experiments were performed with the LC-IRMS setup described for the flow injection experiments. Analytes were separated on a Waters XBridge C18 (3.0 × 100 mm, 3.5 µm) column (Waters, Eschborn, Germany) at 80 °C column temperature. The oxidation conditions were tested at three different concentration and flow conditions. The first one used a HPLC flow of 500 µL min^{-1} water combined with 50 µL min^{-1} of 0.84 M $Na_2S_2O_8$ solution and 50 µL min^{-1} of 1.5 M H_3PO_4. For the second set of experiments, the flow rates were kept constant, but the concentration of the oxidation agent was reduced to 0.42 M. For the third setup, the total flow rate was reduced to 300 µL min^{-1}. The HPLC flow was set to 200 µL min^{-1} and the interface pumps were set to 50 µL min^{-1} each. The concentration of the oxidation agent and the acid were reduced by a factor of two (0.21 M $Na_2S_2O_8$; 0.75 M H_3PO_4) to obtain equal concentrations of oxidation agent and acid in the reactor between setup two and three. Within these three setups, the oxidation temperature was reduced stepwise from the initially 100 °C to 75 °C in order to lower the oxidation efficiency and monitor the effect on the obtained peak areas and $\delta^{13}C$ values.

4.4 Results and Discussion

4.4.1 Choice of oxidation agent for the use in the LC-IRMS system

The oxidation agents recommended for the use in the LC-IRMS interface are the sodium, potassium, and ammonium persulfate salts.[158] Although ammonium and potassium persulfate have been used in the literature[36, 172], the sodium salt offers two main advantages. The first one being the solubility, at 20 °C the solubility of ammonium and sodium persulfate are 2.5 mol L^{-1} and 2.3 mol L^{-1} respectively, whereas the solubility of potassium persulfate is 0.17 mol L^{-1}.[173] This means, that for the potassium salt, higher flow rates have to be added to the HPLC eluent in the interface to achieve equivalent oxidation agent concentrations compared to the sodium and ammonium salt. This reduces the residence time in the oxidation reactor and therefore the oxidation efficiency. Ammonium persulfate has the disadvantage that the ammonium itself reacts with persulfate radicals to form nitrate in aqueous solutions **(see 4.6 Appendix to Chapter 4)**. This process competes for sulfate radicals with the organic carbon of the analytes. Therefore sodium persulfate offers the best potential for the application in the interface and is used in the majority of published methods.

4.4.2 Reaction time and system flow rate

To compare the influence of different instrumental conditions on the oxidation, the relation of the total flow rate and the reaction time has to be considered. Many publications compare the peak area obtained for a specific analyte under different flow conditions, e.g. an increase of the oxidation agent flow from 50 µL min^{-1} to 100 µL min^{-1}. Thereby the oxidation is improved, as the concentration of sulfate radicals will be increased, but the reaction time in the oxidation reactor and the residence time in the gas separation unit are simultaneously decreased. This interdependence of the different parameters makes it almost impossible to interpret the changes for example in the peak area obtained for the generated CO_2 which are observed. To determine the reaction time at different flow rates, a colored marker solution was manually injected via the six port valve of the interface. The connection between the oxidation reactor and the gas separation unit was opened, and the time until the marker appeared at the end of the oxidation reactor was measured. The volume of the oxidation reactor was calculated with the help of the flow rate and the residence time and was in good agreement with the volume of 196 mm^3 given by the manufacturer (the volume of the tubing from the 6-port valve to the oxidation reactor was subtracted from the result). The estimated reaction times based on common flow rate combinations used in the interface are given in **Table 4.2**.

Table 4.2: Calculation of the residence time of the analytes in the IsoLink© oxidation reactor at different interface and HPLC flow conditions based on a reactor volume of 196 mm^3

HPLC flow / µL min^{-1}	Interface pumps / µL min^{-1}	Residence time oxidation reactor / s
200	50	47
	80	42
	100	39
300	50	34
	80	31
	100	29
400	50	26
	80	25
	100	24
500	50	21
	80	20
	100	20
600	50	18
	80	17
	100	17

4.4.3 Infusion with following TOC analysis

This experimental setup offers the advantage that the oxidation in the system can be monitored without the effects of the gas separation of the interface as the TOC is determined on a separate instrument. Oxidation rates were calculated based on the initial concentration of the analyte and the individual flow rates of the HPLC pump and the two interface pumps. For this approach, the flow conditions in the interface have to be precisely known as incorrect flow rates would lead to systematic errors in the calculation. The volume delivered by each pump, as well as the combination of all three pumps were checked gravimetrically by pumping water for a defined time span and consecutive calculation of the delivered volumes. The flow rates of the interface pumps had to be adjusted slightly as the pumps delivered lower flow rates than indicated by the software. Finally, a standard with known organic carbon concentration was pumped via the HPLC system and diluted in the interface by water delivered from the two interface pumps, the eluent stream was collected after the inactive oxidation reactor and the carbon concentration was determined using the TOC analyzer. The carbon concentrations calculated based on the initial sample concentration and the dilution in the interface matched the results obtained by the TOC from the sample collected after the oxidation reactor (e.g. at 300 mg L^{-1} caffeine introduced into the interface, 296.0 ± 6.9 mg L^{-1} were recovered). With the precise knowledge of the flow conditions in the interface, analyte

solutions of different concentrations were infused by the HPLC pump at a fixed flow rate and oxidized at constant conditions regarding the $Na_2S_2O_8$ and H_3PO_4 concentrations present in the oxidation reactor. Caffeine was chosen as a model compound that contains N-heteroaromatic ring systems and has also been previously studied by LC-IRMS. The general oxidation conditions were chosen to represent those used by Zhang *et al.* (2012).[101] Caffeine concentrations were analyzed in a range from 20 to 400 mg L^{-1}. The decrease in carbon concentration due to the oxidation process was determined as the difference between the diluted initial concentration (addition of oxidation agent and acid have to be considered) and the carbon concentration measured after the oxidation by TOC analysis. This difference between the initial and the remaining carbon concentration after oxidation is equivalent to the amount of oxidized carbon which would normally be measured by the IRMS after the gas separation unit (assuming 100 % gas transfer across the membrane). In **Figure 4.3a**, the relationship between the oxidized carbon and the initial caffeine concentration is shown in the range from 20 to 400 mg L^{-1}. A linear relationship between the oxidized carbon and the initial carbon concentration was found in the range of 20 to 80 mg L^{-1} caffeine, with a correlation coefficient of 0.997. With increasing caffeine concentrations, the amount of oxidized carbon is decreasing and finally falling below the values obtained for the lower analyte concentrations. This can be explained by the decreasing ratio of oxidation agent per analyte molecule. As can be seen in **Figure 4.3b**, the percentage of oxidized carbon is almost constant if an excess of >200 mol oxidation agent per mole analyte molecules is initially present. If the ratio of oxidation agent to analyte is falling below this threshold, the oxidation is not as efficient and does not lead to CO_2 as a main mineralization product that can be separated from the liquid sample. The overall yield of carbon that was mineralized to CO_2 did not exceed 70 %. This shows that no direct conclusion from a linear correlation of the oxidized carbon (equivalent to the peak area for IRMS measurements) and the amount of introduced carbon can be drawn.

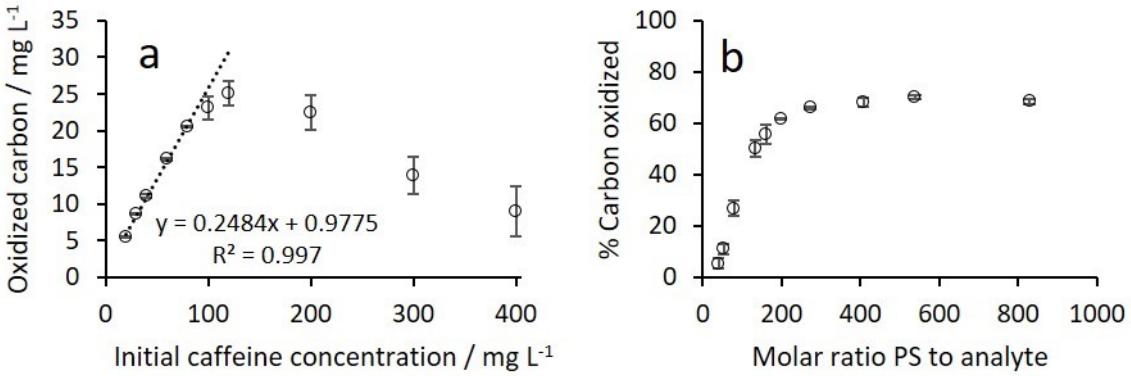

Figure 4.3: Infusion and oxidation of different concentration levels of caffeine under identical oxidation conditions with measurement of the remaining organic carbon after oxidation. a) Correlation of the oxidized carbon in relation to the initially introduced analyte concentration; b) Molar ratio of oxidation agent to the analyte concentration in relation to the oxidation efficiency; Error bars indicate 99 % confidence intervals after Gaussian error propagation for the carbon fractions

In comparison to the results obtained by Zhang *et al.* (2012), which showed a linear relationship between the IRMS peak area and the caffeine concentration up to 400 mg L^{-1} under identical oxidation conditions, the linear range observed for the infusion setup is smaller.[101] This is due to the fact that the constant introduction of the analyte by infusion is not directly comparable to the transfer of the analyte in a Gaussian peak shape concentration profile as in LC-IRMS. As a result of the diffusion and peak broadening in the HPLC and during the transfer from the column into the reactor, the ratio of oxidation agent to analyte is higher than in the infusion experiment. Therefore, the oxidation efficiency for a given experimental setup is underestimated by the infusion approach compared to LC-IRMS. To incorporate chromatographic conditions into the assessment of the oxidation efficiency, flow injection analysis with a calibration via injections of dissolved inorganic carbon (DIC) was performed. Nevertheless, the infusion setup offers the advantage that eluent of the oxidation reactor can be transferred to other analytical platforms such as ion chromatography for the monitoring of ammonium and nitrate formation as oxidation products from N-containing analytes.[174]

4.4.4 FIA with comparison to DIC standards

With the help of a calibration of the LC-IRMS response to injections of inorganic carbon standards, oxidation rates can be calculated based on the IRMS response for different organic analytes under the same conditions. As the conversion of the inorganic carbon is not

dependent on the oxidation conditions, but only on the pH in the system, the response of the DIC standard can be assumed to quantitatively represent the amount of injected carbon. The calibration for the DIC was performed in a range from 50 to 250 mg L^{-1} carbon. The linear regression showed a good correlation (R^2=0.9997) and a slope of 0.460 V s L mg^{-1}, which can be used as a measure for the sensitivity of the instrument. The linearity of the DIC measurement was checked at three different flow rates for concentrations in the rage from 100 to 900 mg L^{-1} (C) (**Figure 4.4**).

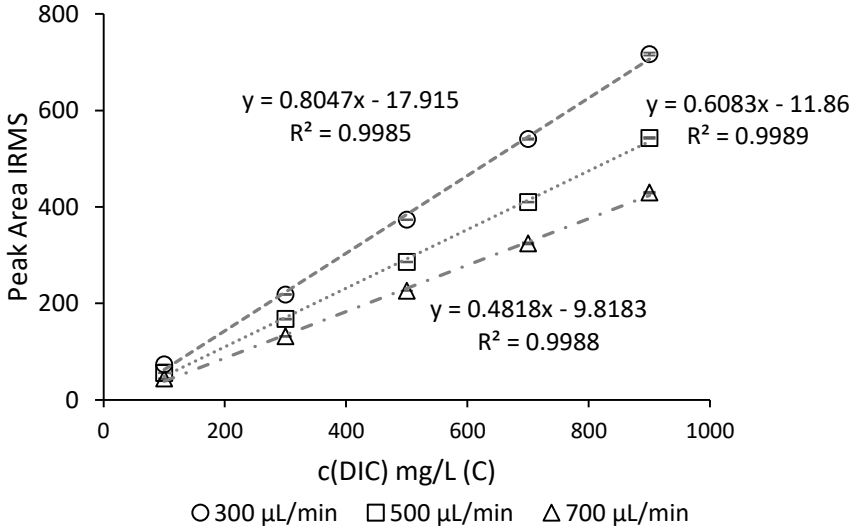

Figure 4.4: Linearity of the obtained peak areas by IRMS in relation to the injected DIC concentration. Flow injection experiments were carried out at three different system flow conditions: (system flow of 300 µL min^{-1}: 200 µL min^{-1} HPLC, 50 µL min^{-1} oxidation agent, 50 µL min^{-1} H_3PO_4), (system flow of 500 µL min^{-1}: 400 µL min^{-1} HPLC, 50 µL min^{-1} oxidation agent, 50 µL min^{-1} H_3PO_4), (system flow of 700 µL min^{-1}: 600 µL min^{-1} HPLC, 50 µL min^{-1} oxidation agent, 50 µL min^{-1} H_3PO_4)

A set of five common LC-IRMS analytes were selected and standard solutions of equal carbon concentrations were measured using flow injection at identical interface conditions. From the results presented in **Figure 4.5** it can be observed, that linear regressions with high correlation coefficients could be obtained for all analytes except for vanillin where the highest concentration level deviated from the linear trend. For vanillin, glucose, and phenylalanine oxidation rates of almost 100 % were determined for the lower analyte concentrations. For these three compounds, a slight decrease in the oxidation rates was observed with increasing concentrations. With the exception of vanillin, the decrease in oxidation efficiency did not result in a reduced correlation. For caffeine and histidine, the oxidation efficiency for the lowest concentration was 72.6 ± 1.9 % and 87.2 ± 0.4 % respectively. The percentage of

oxidized carbon dropped to 59.3 ± 0.7 % for caffeine and 81.1 ± 0.6 % for histidine with increasing concentrations. Nevertheless, the correlations between the injected amount of carbon and the IRMS peak area were completely linear over the given concentration range. The only indicator for an incomplete oxidation is the decreased slope for the obtained regression lines compared to the DIC measurements.

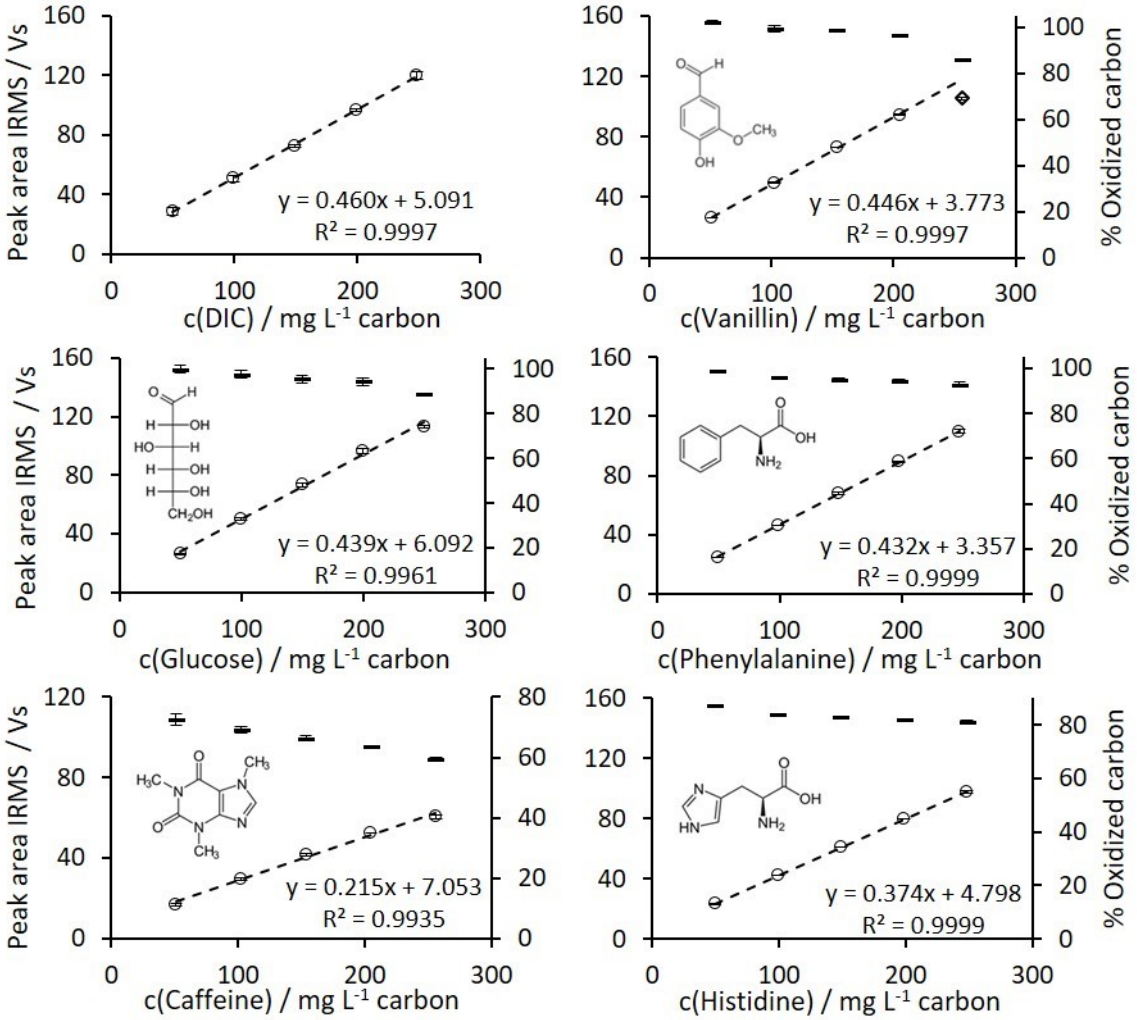

Figure 4.5: Flow injection of common LC-IRMS analytes at identical oxidation conditions and varying concentrations; circles indicate the peak area obtained by IRMS, horizontal bars correspond to the calculated oxidation efficiency compared to the DIC reference measurement. Flow rate HPLC, 600 µL min^{-1}, $Na_2S_2O_8$ (0.42 M, 50 µL min^{-1}), H_3PO_4 (1 M, 50 µL min^{-1}). Error bars might be smaller than the symbols (99 % confidence intervals)

For the easier oxidizable compounds such as vanillin, glucose, and phenylalanine, the slope of the regression line is only slightly smaller than for the DIC standard, whereas the slopes for caffeine and histidine are significantly lower. These results support the hypothesis that compounds with C-N double bonds and N-heteroaromatic systems are only partially oxidized under standard LC-IRMS conditions[156-157] which can result in systematic differences for $\delta^{13}C$ values obtained by EA-IRMS and LC-IRMS due to incomplete conversion.[45, 85, 157] The setup offers advantages over the direct infusion method, as the IRMS can be used for detection and no modifications to the instrument have to be made. The resulting $\delta^{13}C$ values obtained for each concentration level did not show a significant trend (within ± 0.5 ‰ range) although differences in the oxidation efficiency were observed (**Figure 4.6**).

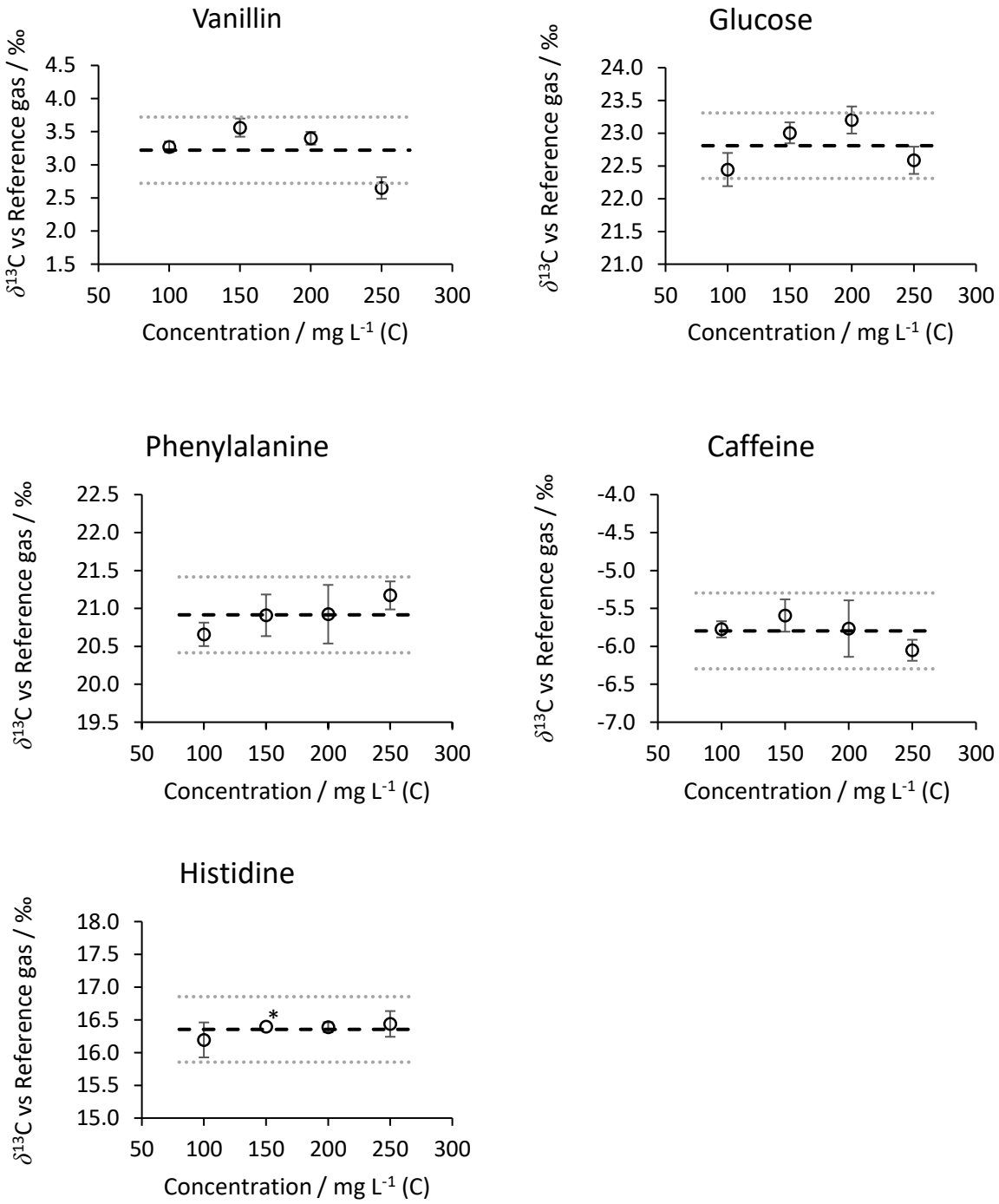

Figure 4.6: Comparison of the $\delta^{13}C$ values obtained for the compounds analyzed by flow injection. Dotted lined represent the ± 0.5 ‰ range around the mean $\delta^{13}C$ value. Error bars indicate the 99 % confidence interval. Results for the concentration level of 50 mg L^{-1} could not be obtained as the signal intensity was below the threshold of 1 V (m/z 44, 3 x 10^8 Ω). *n=2 no calculation of confidence interval possible. $\delta^{13}C$ values were calculated using CO_2 reference gas set to 0 ‰ and are not normalized to the VPDB scale as they were inteded to be used to monitor the stability of the $\delta^{13}C$ signal only and are not used for further interpreatation of the data.

Only for the highest vanillin concentration, which showed a significant decrease in the amount of oxidized carbon, a deviation of more than 0.5 ‰ from the overall vanillin mean δ^{13}C value could be observed. FIA injection with DIC calibration offers a quick and reliable way to determine the oxidation efficiency of specific analytes during the method development. If incomplete oxidation is detected at this point, the concentration of the oxidation agent could be increased to improve the oxidation. For some compounds complete oxidation might not be achievable by this procedure, so that further modifications of the flow rates in the system might be necessary to improve the oxidation. In case of complete oxidation, the oxidation agent concentrations or flow rates can be reduced to increase the lifetime of the filament and reduce instrument downtime. In LC-IMRS applications including the chromatographic separation, referencing with DIC can be difficult, as the DIC does not elute as a sharp analyte peak and can coelute with target analytes depending on the column and chromatographic conditions.[78, 161]

4.4.5 Variations of the oxidation temperature for LC-IRMS methods

To evaluate the oxidation efficiency in LC-IRMS separations, infusion and DIC referencing are often not directly applicable. In comparison to FIA, the LC column has an additional influence on the oxidation process, as column bed material is constantly washed out of the column, which increases the carbon background of LC-IRMS measurements compared to FIA.[35] For an already established LC-IRMS separation, changes in the flow rate of the eluent are not possible without affecting the chromatographic separation. A convenient way to reduce the oxidation efficiency in the LC-IRMS interface without changing any reagent concentrations or flow rates, is a reduction of the reaction temperature in the oxidation reactor. The formation of sulfate radicals from persulfate is strongly dependent on the reaction temperature.[175] A reduced reaction temperature was shown to have significant effects on the signal intensity and the obtained δ^{13}C values.[154] The results obtained for methanol and xylitol injected via an XBridge C18 column at different interface conditions are shown in **Figure 4.7**.

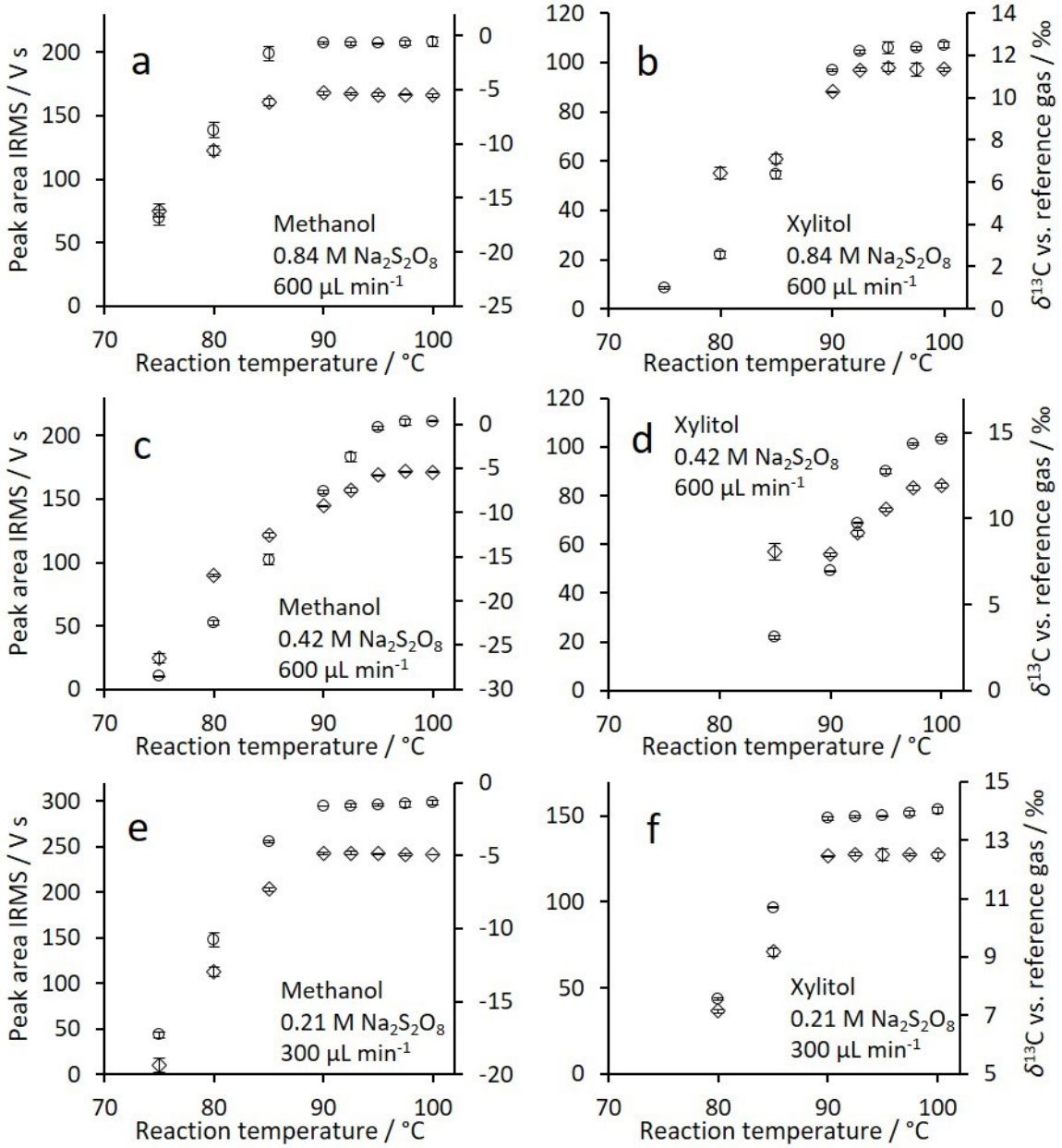

Figure 4.7: Peak areas and $\delta^{13}C$ values obtained for methanol and xylitol by LC-IRMS at different flow and oxidation conditions; circles indicate the peak area obtained by IRMS, diamonds correspond to the $\delta^{13}C$ ratio measured against the CO_2 reference gas. Instrumental parameters: (a, b: HPLC flow, 500 µL min^{-1}; H_3PO_4 1.5 M, 50 µL min^{-1}; $Na_2S_2O_8$ 0.84 M, 50 µL min^{-1}), (c, d: HPLC flow, 500 µL min^{-1}; H_3PO_4 1.5 M, 50 µL min^{-1}; $Na_2S_2O_8$ 0.42 M, 50 µL min^{-1}), (e, f: HPLC flow, 200 µL min^{-1}; H_3PO_4 0.75 M, 50 µL min^{-1}; $Na_2S_2O_8$ 0.21 M, 50 µL min^{-1}). Error bars might be smaller than the symbols (99 % confidence intervals)

For each interface condition, the temperature of the oxidation reactor was stepwise reduced from 100 to 75 °C until the amplitude of the analyte peaks (m/z 44, 3 x 10^8 Ω) dropped below 1 V (corresponds to an ion current of 3.3 x 10^{-9} A) which was set as a threshold value for the reproducible $\delta^{13}C$ determination. For the combination of high overall flow rates and high

oxidation agent concentrations, the stepwise reduction of the oxidation temperature led to significant changes in the CO_2 response and $\delta^{13}C$ values below 90 °C for methanol and 92.5 °C for xylitol **(Figure 4.7a and b)**. Above these thresholds, a constant response in the $\delta^{13}C$ value and CO_2 signal were obtained. For the measurements presented in **Figure 4.7c and d**, the concentration of the oxidation agent was decreased by 50 % while the flow rate in the interface was kept constant. The initial CO_2 response and $\delta^{13}C$ values were identical to those obtained for high oxidation agent concentrations, but a distinct plateau of the CO_2 and $\delta^{13}C$ response could not be observed with decreasing reaction temperatures. For the measurements shown in **Figure 4.7e and f**, the experimental conditions were adapted to an overall lower flow rate in the system (300 µL min^{-1}) but identical $Na_2S_2O_8$ concentrations in the oxidation reactor (reduction from 0.42 M to 0.21 M as the overall flow rate was decreased by 50 %). The stable CO_2 and $\delta^{13}C$ results in the temperature range from 90 - 100 °C indicate that stable oxidation conditions can be obtained by increased residence times in the oxidation reactor. Measurements for the caffeine under varying reaction temperatures could only be obtained for HPLC flow rates of 500 µL min^{-1}, as the long retention times at HPLC flow rates of 200 µL min^{-1} led to extreme peak broadening (results for high flow rates are shown in **Figure 4.8**).

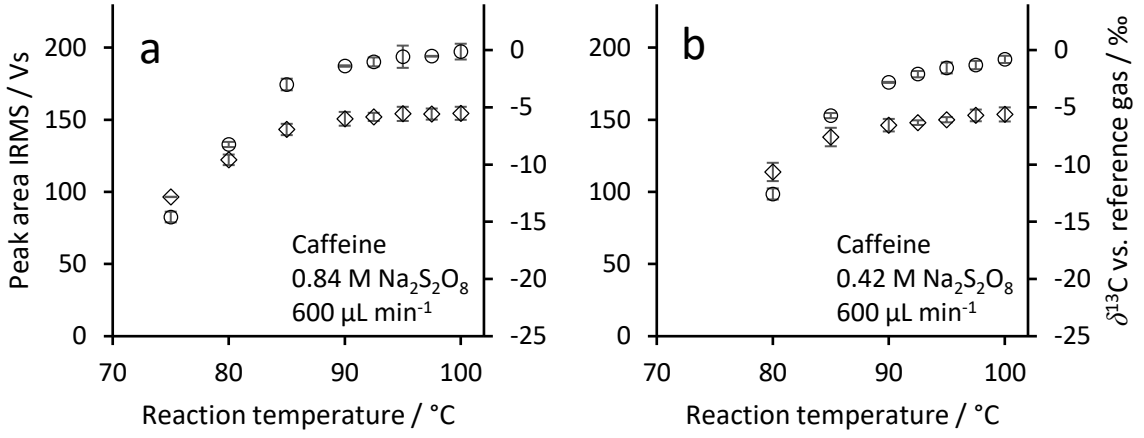

Figure 4.8: Peak areas and $\delta^{13}C$ values obtained for caffeine by LC-IRMS at different oxidation conditions; circles indicate the peak area obtained by IRMS, diamonds correspond to the $\delta^{13}C$ ratio measured against the CO_2 reference gas. Instrumental parameters: (a: HPLC flow, 500 µL min^{-1}; H_3PO_4 1.5 M, 50 µL min^{-1}; $Na_2S_2O_8$ 0.84 M, 50 µL min^{-1}), (b: HPLC flow, 500 µL min^{-1}; H_3PO_4 1.5 M, 50 µL min^{-1}; $Na_2S_2O_8$ 0.42 M, 50 µL min^{-1}). Error bars might be smaller than the symbols (99 % confidence intervals)

An additional information obtained by the measurements with decreased reactor temperature is the isotope fractionation as a result of the incomplete oxidation. For methanol, a shift of the $\delta^{13}C$ signature of more than 20 ‰ (from -5.4 ± 0.1 ‰ at 100 °C to -26.5 ± 0.6 ‰ at 75 °C) was detected. The same trend could be observed for xylitol, although the fractionation by the incomplete oxidation was lower (from 11.9 ± 0.1 ‰ at 100 °C to 8.0 ± 0.5 ‰ at 85 °C). The linearity of the system was checked by reference gas pulses and dilutions of the analytes measured at 100 °C oxidation temperature which resulted in similar peak areas obtained by the incomplete oxidation but showed $\delta^{13}C$ values unaffected by changing signal intensities (**Figure 4.9**).

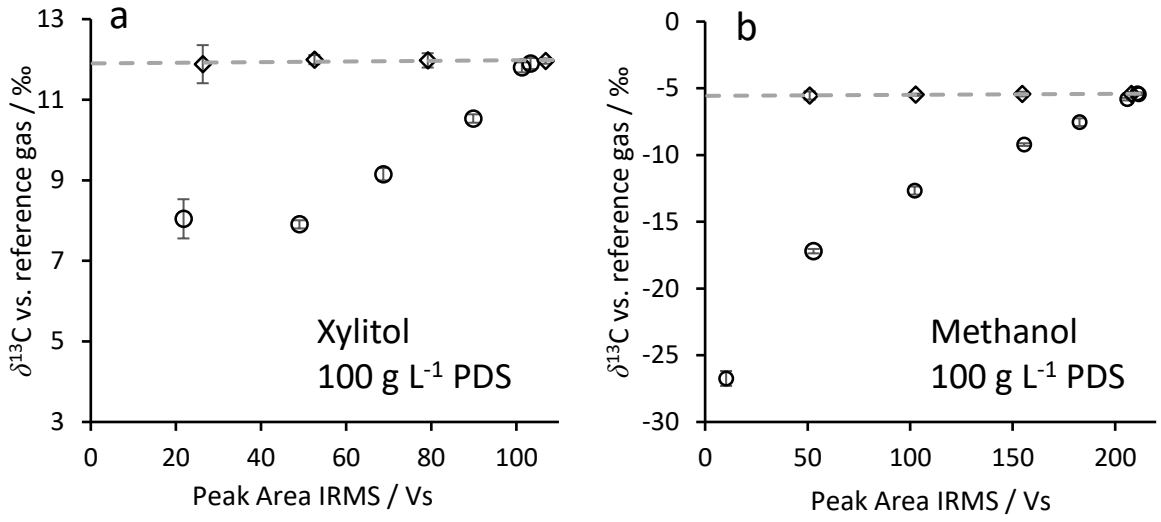

Figure 4.9: $\delta^{13}C$ values obtained for different concentrations of xylitol (a) and methanol (b) oxidized at 100 °C (diamonds) in contrast to the reduced peak areas obtained by a reduction of the oxidation temperature (circles). Error bars indicate the 99 % confidence interval and may be smaller than the symbols. $\delta^{13}C$ values were calculated using CO_2 reference gas set to 0 ‰ and are not normalized to the VPDB scale as they were intended to be used to monitor the stability of the $\delta^{13}C$ signal only and are not used for further interpretation of the data.

In contrast to the shift towards lower $\delta^{13}C$ values observed in LC-IRMS, incomplete oxidation in the field of GC-IRMS was found to result in increased peak tailing and a shift of 5 ‰ towards higher $\delta^{13}C$ values.[176] Although identical treatment of analyte and reference substances in LC-IRMS is able to compensate for possible fractionation during incomplete oxidation to a certain extent, intramolecular differences between analyte and reference substance can most probably not be compensated for with this approach. For caffeine, intramolecular differences of 7.7 ‰ were determined between the methyl groups and ring carbon in a C-N double

bond.[18] If the incomplete oxidation leads to site specific oxidation of parts of the molecule, systematic errors would be introduced if the reference and the analyte compound differ in their intramolecular isotopic composition.

4.5 Conclusion

The importance of careful evaluation of the oxidation parameters is often underestimated in the method development for LC-IRMS applications. Especially if normalization for a set of different analytes is intended by only one certified reference substance. Maintenance costs and the accuracy and precision of the results could be improved by careful evaluation of the oxidation parameters based on the flow conditions and analytes. Common strategies like monitoring the oxygen background and linear area response curves of the analytes were found to be incapable of identifying complete oxidation in the system. Previously published evaluations of the oxidation parameters often simultaneously change multiple parameters, so that a source of the observed effect (oxidation, membrane gas separation) cannot be clearly identified.[40, 61, 155] The addition of an oxygen scrubber between the LC-IRMS interface and the MS eliminates the limitation to lower oxidation agent concentration, but is not commercially available and therefore only used in few modified research-type instruments.[61, 85, 88, 155] The previously presented methods are alternatives that can be used in method development for new applications as well as for assessing the robustness of existing applications. The infusion method offers the advantage that oxidation efficiencies can be determined independently from the IRMS as a detector. The systematic reduction of the oxidation temperature was shown to be able to identify unsuitable oxidation conditions for LC-IRMS applications without changing the LC method, reagent concentrations, and flow rates in the system. Oxidation agent concentrations can thereby be adjusted to gain stable oxidation conditions and reduce the oxygen background in the ion source to reduce negative space charge effects and increase the filament lifetime.[46]

Acknowledgement

The research was funded by the German Research Foundation (DFG) under the project grant 317438550.

4.6 Appendix to Chapter 4

Oxidation of ammonium by sulfate radicals in a batch reactor experiment

The oxidation of ammonium by sulfate radicals was performed in a batch reactor setup containing a heated glass flask equipped with a reflux cooler. An ammonium sulfate solution was prepared at a concentration of 20 mg L^{-1} (N) and heated to 98 °C in the reaction vessel. After the removal of the t_0 sample, the oxidation agent ($K_2S_2O_8$) was added to the reactor to an initial concentration of 30 mmol L^{-1}. Samples were taken from the reactor at 10 time points within 30 min. The samples were immediately stored on ice until the IC analysis was performed. For the quantification of ammonium and nitrate a cation and an anion IC system were used. Both consisted of a Metrohm 883 Basic IC plus connected to a Metrohm 863 Compact autosampler (both Metrohm, Herisau, Switzerland). For the anion analysis, a Metrosep A Supp 4 (250/4.0) column (Metrohm, Herisau, Switzerland) with an eluent consisting of 1.8 mmol L^{-1} Na_2CO_3 and 1.7 mmol L^{-1} $NaHCO_3$ in a 30/70 vol.-% acetonitrile/water mixture was used. The injection volume was 10 µL and a flow rate of 1 mL min^{-1} was used. For the cation separation, a Metrosep C4 (150/4.0) column (Metrohm, Herisau, Switzerland) with an eluent consisting of 4 mmol L^{-1} HNO_3 in water with a flow rate of 0.9 mL min^{-1} was used. The injection volume was 4 µL for the cation separation. Detection on both systems was performed with a conductivity detector. The calibration was done by a dilution of stock solutions prepared from NH_4Cl and $NaNO_3$ in the presence of 30 mmol L^{-1} $K_2S_2O_8$ to obtain a comparable matrix as in the real samples from the mineralization experiments. Results of the IC analysis are shown in **Table 4.3**.

Table 4.3: Oxidation of ammonium to nitrate by sulfate radicals in a batch reactor experiment

Batch reactor reaction time / min	c(Ammonium) / mg L^{-1} (N)	CI 99 % c(Ammonium) / mg L^{-1} (N)	c(Nitrate) / mg L^{-1} (N)	CI 99 % c(Nitrate) / mg L^{-1} (N)
0	20.37	0.09	-	-
1	19.63	0.28	1.18	0.00
2	20.49	0.07	1.33	0.03
3	20.62	0.17	1.40	0.01
4	20.39	0.55	1.47	0.02
5	20.11	0.53	1.59	0.01
7.5	20.09	0.08	1.68	0.01
10	19.60	1.01	1.89	0.01
15	18.91	0.38	2.16	0.11
20	18.56	0.40	2.37	0.06
30	18.13	0.48	2.60	0.10

Chapter 5: Monitoring of the total carbon and nitrogen balance during the mineralization of nitrogen containing compounds by heat activated persulfate

Köster, Daniel[1], Jochmann, Maik A.[1,2,], Lutze, Holger V.[1,2,3], Schmidt, Torsten C.[1,2,3]

[1] Instrumental Analytical Chemistry, University of Duisburg-Essen, Universitätsstr. 5, 45141 Essen, Germany

[2] University of Duisburg-Essen, Centre for Water and Environmental Research (ZWU) Universitätsstr. 5, 45141 Essen, Germany

[3]IWW Water Centre, Moritzstraße 26, 45476 Mülheim an der Ruhr, Germany

Adapted with permission from: D. Köster, M.A. Jochmann, H.V. Lutze, T.C. Schmidt, *Monitoring of the total carbon and nitrogen balance during the mineralization of nitrogen containing compounds by heat activated persulfate,* Chemical Engineering Journal, 367, pp. 160-168, DOI: https://doi.org/10.1016/j.cej.2019.02.115

5.1 Abstract

Peroxydisulfate ($S_2O_8^{2-}$) is widely applied in environmental remediation and water treatment as an agent for the unselective oxidation of organic contaminants. $S_2O_8^{2-}$ itself is a strong oxidation agent but activation by heat, UV radiation, or metal catalysts forms sulfate radicals ($SO_4^{\bullet-}$), which offer a higher oxidation potential and faster reaction kinetics. The mechanism of degradation for many organic contaminants by sulfate radicals is well studied, but the final mineralization products are not commonly evaluated. Nitrogen containing compounds are known to produce different mineralization products depending on their structure and the reaction conditions. For the identification of the main mineralization products, two approaches for the determination of nitrogen mass balances were evaluated. The first approach was based on a combination of total organic carbon (TOC), and total nitrogen bound (TNb). The second approach used a combination of TOC and ion chromatography (IC). The evaluation based on the TOC and TNb by high temperature combustion was found to be significantly biased as measured ammonium concentrations were underestimated by the TNb measurements in the presence of peroxydisulfate. With the TOC/TNb method, 83.2 ± 1.1 % of the initial nitrogen could be recovered after the oxidation. The TOC/IC based approach led to an overall recovery of 91.1 ± 1.4 %, where NO_3^- and NH_4^+ were identified as the main products. Based on the fraction of ammonium provided by the IC measurements, the TOC/TNb based results could be corrected for the underestimation of ammonium which led to a recovery of 95.9 ± 3.1 %. The presented methods are applicable for the determination of nitrogen mass balances in lab-scale studies, as well as for the monitoring of mineralization products in field applications.

5.2 Introduction

Peroxydisulfate ($S_2O_8^{2-}$, PDS) is a strong oxidizing agent that is used in technical scale applications such as the remediation of soil and groundwater as well as in drinking and wastewater treatment.[177-179] Reaction mechanisms for the oxidation of environmentally relevant contaminants such as atrazine herbicides [180-181], antibiotics [182-183], persistent surfactants [184], and azo dyes [185] have been elucidated. PDS is also widely applied for the mineralization of organic molecules in applications for analytical chemistry. Sum parameters in the field of water analysis like the total organic carbon (TOC) depend on the complete mineralization of organic constituents regardless of their molecular structure.[186-187] In addition, PDS is used for the combination of liquid chromatography and isotope ratio mass spectrometry in compound specific isotope analysis where organic analytes are converted to CO_2 by heat activated PDS after chromatographic separation. The produced CO_2 carries the isotopic information of the original compound and can be determined.[36]

PDS ($S_2O_8^{2-}$) itself is a strong oxidant (E°=2.1 V), but it has an overall slow reaction kinetic. However, PDS can be used to form highly reactive, sulfate radicals ($SO_4^{\bullet-}$) with an oxidation potential of E°=2.6 V.[177] The radical formation can be initiated by heat, UV light, and transition metals as well as by different combinations of the aforementioned methods.[188] **(Equation 5.1 and 5.2)**

$$S_2O_8^{2-} \xrightarrow{Heat,\ UV} 2\ SO_4^{\bullet-} \qquad \textbf{(5.1)}$$

$$S_2O_8^{2-} + M^{n+} \rightarrow SO_4^{\bullet-} + SO_4^{2-} + M^{(n+1)+} \qquad \textbf{(5.2)}$$

In the case of thermal activation of PDS high reaction temperatures generally lead to increased radical formation and faster reaction rates.[187-189] The effect of metal catalysts (e.g. Fe^{2+}, Ag^{+}, Mn^{2+}) strongly depends on the individual system, as the metal species are involved in the formation of sulfate radicals as well as in the scavenging process according to **Equation 5.3** at the same time. [177, 179, 190]

$$SO_4^{\bullet-} + M^{n+} \rightarrow SO_4^{2-} + M^{n+1} \qquad \textbf{(5.3)}$$

The effect of the pH on the oxidation of organic compounds is still not completely elucidated. For strongly acidic conditions, a reduced formation of sulfate radicals was observed.[175, 191] Under alkaline conditions, reactions according to **Equation 5.4** can occur.[187]

$$SO_4^{\bullet -} + OH^- \rightarrow HO^{\bullet} + SO_4^{2-} \quad \textbf{(5.4)}$$

This leads to the formation of hydroxyl radicals and a change in the oxidation mechanism from the production of organic radical cations by electron transfer via sulfate radicals to H abstraction and addition reactions of hydroxyl radicals.[192] The oxidation can also significantly be affected by other matrix components such as chloride, carbonate or phosphate which can form secondary radicals that react with the analyte or lead to the generation of hydroxyl radicals.[193] In lab-scale experiments, this can partly be avoided if the system is deliberately chosen to be free from species that can participate in secondary reactions. This could be problematic if pH control during the reaction is required as many buffer systems will react with sulfate radicals and form reactive by-products that can affect the oxidation of the target analyte.

In the determination of sum parameters such as total carbon (TC) and total nitrogen bound (TNb), different mineralization approaches based on heat activated persulfate have been applied and are used in commercially available instruments.[43, 194] With the exception of recalcitrant halogenated organic chemicals, most analytes could be completely transformed and measured as a single species (CO_2 in the case of TC, NO_2^- in the case of alkaline PDS for TNb).[119] In contrast to heteroatoms such as phosphorus, which produces a single mineralization product, organic nitrogen compounds led to different inorganic species dependent on the molecular structure of the analyte and the oxidation conditions.[119, 195] Studies on the photochemical degradation of nitrogen-containing compounds with the help of titanium dioxide suggest similar results.[196] Recent studies focussing on the degradation of nitrogen-containing environmental contaminants mainly monitor the decreasing concentration of the target molecule and possible transformation products, but the final mineralization products are not commonly monitored.[181-183, 197] TOC measurements have successfully been applied to monitor the mineralization of Diuron by activated persulfate, but monitoring of the TNb or inorganic nitrogen species by IC have not been performed.[198]

In this study, the reaction products of the heat activated persulfate based mineralization of nitrogen-containing organic molecules at initially neutral, unbuffered pH conditions were studied. A batch reactor experiment for the controlled mineralization and time dependent sampling was developed. With this setup, the degree of mineralization as well as the resulting reaction products have been monitored. To quantify the amount of remaining organic carbon

at each time point during the oxidation, a TOC based high temperature conversion measurement was employed. At the same time, nitrogen species were monitored by two different approaches. The first one used the TNb as a sum parameter for the present nitrogen species, the second approach was based on a mass balance obtained by the measurement of individual inorganic nitrogen species by ion chromatography. For the interpretation of the results, a Gaussian error propagation approach was used to combine the uncertainties of analytical results obtained from different instruments in a single nitrogen mass balance.

5.3 Materials and Methods

5.3.1 Chemicals and Reagents

For the mineralization experiment, caffeine (p.a. 99.9 % Sigma-Aldrich, Steinheim, Germany) was used. The calibration of the TOC and the TNb measurements was performed using a 1000 mg L^{-1} TOC reference standard (Sigma-Aldrich, Steinheim, Germany) as well as glycine (ReagentPlus, ≥99 %, Sigma-Aldrich, Steinheim, Germany). For the mineralization and the method development, potassium and sodium peroxydisulfate (both puriss. p.a., >99 %, Sigma-Aldrich, Steinheim, Germany) were used. Recovery rates for the TNb method were determined using potassium sulfate (p.a., AppliChem, Darmstadt, Germany), and sodium chloride (p.a. 99.5 %, Bernd Kraft, Duisburg, Germany). Mobile phases for the IC systems were prepared from ultrapure water obtained from an ELGA Purelab Ultra system (Veolia Water Technologies, Ratingen, Germany). A 1 M nitric acid solution from Fluka Analytical (Seelze, Germany) was used for the mobile phase of the cation chromatography system. For the anion chromatography, the mobile phase was prepared from sodium carbonate and sodium bicarbonate (both puriss. p.a.) obtained from Riedel-de Haën (Seelze, Germany) and acetonitrile (HPLC gradient grade) from Fisher Scientific (Loughborough, United Kingdom).

5.3.2 Mineralization Experiments

The mineralization of the analytes was performed in an experimental batch reactor setup containing a triple-necked glass flask, heated by a heating plate with automatic temperature control via a thermometer that was immersed in the reaction vessel (C-MAG HS7, ETS-D5 both IKA-Werke GmbH & Co. KG, Staufen, Germany). To avoid evaporation of water during the

experiment, the flask was equipped with a reflux cooler. The third neck was used to sample aliquots from the reactor. A stainless steel capillary was connected to a three-port valve, leading to a 50 mL syringe and a cooling loop made of a stainless steel capillary immersed in crushed ice. With the help of the syringe, samples were taken from the reactor and transported through the cooling loop after changing the position of the three-port valve. The reaction vessel was constantly agitated using a magnetic stir bar. A schematic view of the setup is presented in **Figure 5.1**.

Figure 5.1: Setup for the mineralization experiments: triple-necked glass flask with reflux cooler, heating plate with automatic temperature control, manual three-port valve, and crushed ice cooling system

Initially the glass flask contained 1490 mL of water, to which 10 mL of stock solution of the analyte was pipetted to obtain an initial carbon mass concentration of 50 mg L^{-1} (C). The solution was heated to 100 °C and the first sample at t_0 was taken without the addition of PDS. In the next step, solid PDS and 50 mL of water were added to obtain a total volume of 1.5 L with a PDS concentration of 30 mmol L^{-1}. $K_2S_2O_8$ had to be added in solid form due to its low water solubility (46.0 g L^{-1} at 20 °C) [173], the addition in dissolved form as a stock solution would require 264 mL concentrated $K_2S_2O_8$ solution which would lead to a significant temperature drop in the reactor. The dilution by the addition of water together with the PDS was taken into account during the evaluation of the results. By the addition of 50 mL water and solid PDS, the temperature dropped to 96 to 98 °C and was kept constant at that level for the course of the

experiment. At each following time point 50 mL samples were taken from the system without replacing the volume. Of the 50 mL sample, 10 mL were discarded and used to purge the cooling loop, the following 40 mL were collected for further analysis. From the obtained 40 mL, aliquots of 10 mL were separated for the cation and anion chromatography. For ion chromatography, 1 mL of methanol was added to each sample aliquot. For the TOC and TNb measurement the remaining 20 mL of the sample were used. The individual subsamples were stored on ice until the analysis was performed.

5.3.3 Analysis of the Non-purgeable Organic Carbon and Total Nitrogen bound

The analysis was performed on a TOC-L total organic carbon analyzer (Shimadzu, Duisburg, Germany). For the determination of the non-purgeable organic carbon, 20 mL of the sample from each time point of the mineralization experiment were transferred into open glass vials for the TOC-L autosampler (Shimadzu, Duisburg, Germany). Prior to the measurement, the whole system was washed twice with the sample to avoid carry over between the individual samples. For the determination of the non-purgeable organic carbon (NPOC), the sample was purged with synthetic air (80 mL min^{-1}) inside the needle body of the autosampler unit. After 3 min of purging, 50 µL of the sample were injected into an oxidation tube filled with platinum coated ceramic particles at 720 °C. The CO_2 formed during the oxidation was measured by infrared spectroscopy. A calibration was performed with dilutions prepared from a certified TOC reference standard (Sigma Aldrich, 1000 ± 10 mg L^{-1} TOC). For the measurement of the TNb in the samples, 50 µL of the sample were injected analogue to the TOC determination, but the measurement was performed by a chemiluminescence detection after the reaction of NO with ozone. The TNb measurements were calibrated with a standard solution prepared from glycine as a reference compound.

5.3.4 Ion Chromatography

For the measurement of nitrate, nitrite, and ammonium, two different IC systems were used. Both consisted of a Metrohm 883 Basic IC plus connected to a Metrohm 863 Compact autosampler (both Metrohm, Herisau, Switzerland). For the analysis of the anions, a Metrosep A Supp 4 (250 mm x 4.0 mm) column (Metrohm, Herisau, Switzerland) with an eluent consisting of 1.8 mmol L^{-1} Na_2CO_3 and 1.7 mmol L^{-1} $NaHCO_3$ in a 30/70 vol.-% acetonitrile/water mixture was used. The injection volume was 10 µL and a flow rate of

1 mL min^{-1} was used for the anion separation. An ion suppression module (MSM, Metrohm, Herisau, Switzerland) was used for the anion chromatography to reduce the background conductivity of the eluent and increase the sensitivity. For the separation of the cations, a Metrosep C4 (150 mm x 4.0 mm) column (Metrohm, Herisau, Switzerland) with an eluent consisting of 4 mmol L^{-1} HNO_3 in water with a flow rate of 0.9 mL min^{-1} was used. The injection volume was 4 µL for the cation separation. Detection on both systems was performed with a conductivity detector. The calibration was done by a dilution of stock solutions prepared from NH_4Cl and $NaNO_3$ in the presence of 30 mmol L^{-1} PDS to obtain a comparable matrix as in the real samples from the mineralization experiments.

5.4 Results and Discussion

5.4.1 Cation-Exchange Chromatography for the Ammonium Analysis

For the determination of ammonium concentrations during the mineralization of organic compounds, ion chromatography with a Metrosep C 4 (150 mm x 4.0 mm) column was chosen. This type of column is used as a standard column in cation analysis in water samples with a high separation efficiency and short analysis times. For the method development, calibrations for ammonium in the presence and absence of PDS were performed. Literature indicated that the quantification of ammonium in high excess of sodium is difficult as the selectivity for the two ions is very similar on cation-exchange columns based on carboxyl and sulfonyl groups [199]. The quantification of ammonium was not possible under the conditions that would be expected for the samples provided by the mineralization experiments. The initial concentration of 30 mmol L^{-1} of $Na_2S_2O_8$ results in concentration of 1379 mg L^{-1} of Na^+ in the samples. This is way above the concentrations of NH_4^+ expected in the mineralization experiments (0 to 30 mg L^{-1}). As an alternative to $Na_2S_2O_8$, the potassium salt was used, as potassium and ammonium can be base-line separated even with a high excess of potassium. In **Figure 5.2** a chromatogram for solutions containing 30 mmol L^{-1} $Na_2S_2O_8$, 30 mmol L^{-1} $K_2S_2O_8$, and 50 mg L^{-1} (N) of NH_4^+ are shown, respectively.

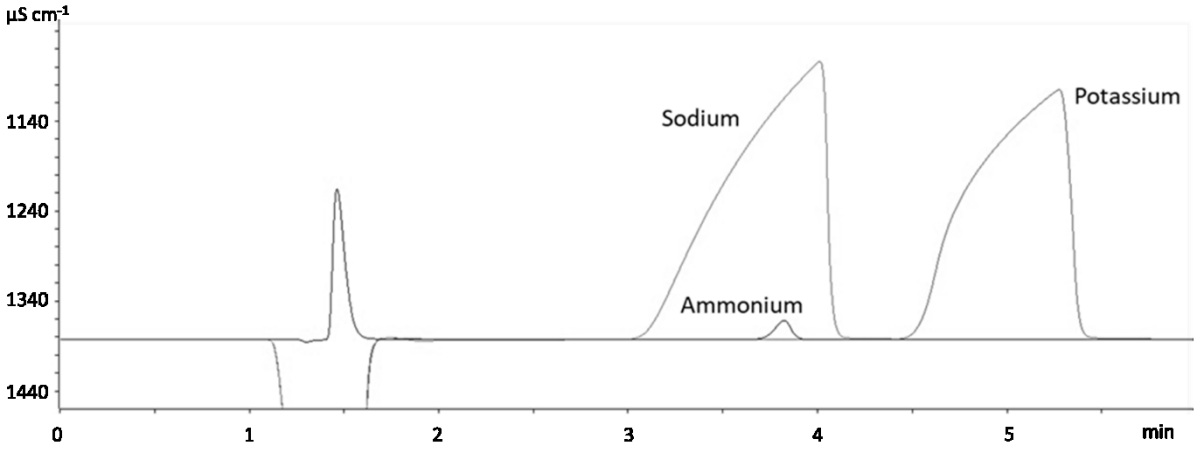

Figure 5.2: Cation chromatogram of solutions containing $Na_2S_2O_8$ (30 mmol L^{-1}), $K_2S_2O_8$ (30 mmol L^{-1}), and NH_4Cl (50 mg L^{-1} (N))

In final applications for the PDS oxidation, $Na_2S_2O_8$ is commonly used as it possesses a significantly higher solubility in water than $K_2S_2O_8$ (2.3 mol L^{-1}; 547.5 g L^{-1} for $Na_2S_2O_8$ in contrast to 0.17 mol L^{-1}; 46.0 g L^{-1} for $K_2S_2O_8$ at 20 °C) [173]. As a result of the high potassium concentration, the injection volume for the method also had to be optimized. High injection volumes can improve the quantification limit of ammonium. However, they also result in large on-column potassium concentrations which deteriorate the peak shape of ammonium. **Figure 5.3** shows the differences in peak shape obtained for ammonium at different concentrations in the presence of 2.35 g L^{-1} (60 mmol L^{-1}) potassium, measured with injection volumes of 4 and 10 µL.

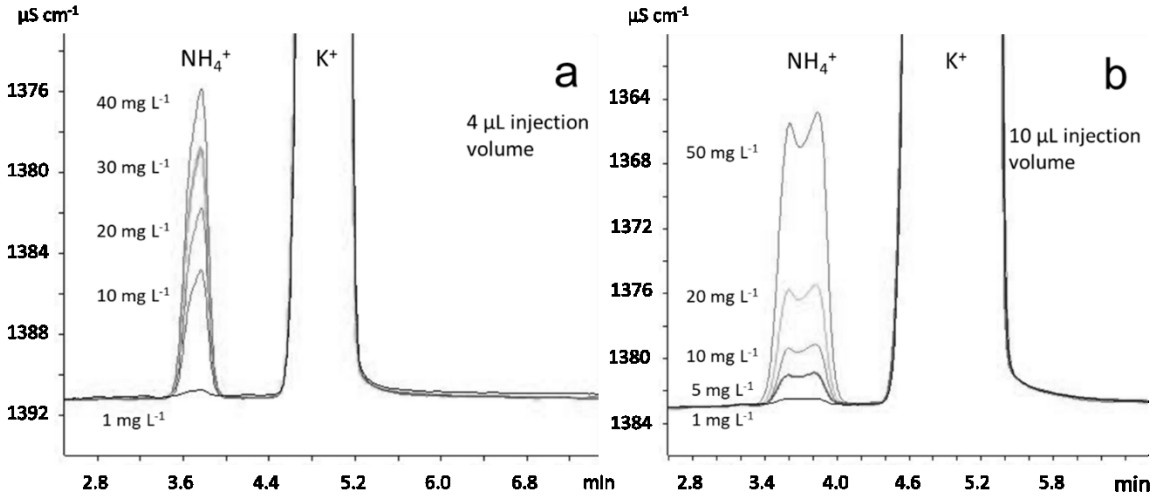

Figure 5.3: Effect of the injection volume on the chromatographic separation of ammonium and potassium by cation chromatography ($c(K^+)$=60 mmol L^{-1}) a) injection volume of 4 µL b) injection volume of 10 µL

For the higher injection volumes, a split peak was obtained for ammonium, which could be the result of the column being overloaded with analytes due to the high potassium concentrations in the samples. To reduce this effect, different injection volumes were compared, where 4 µL was found to produce an acceptable Gaussian peak shape and reproducible signals to quantify ammonium formed during the experiments. From an equidistant ten point calibration for NH_4^+ in a nitrogen mass concentration range from 1 to 10 mg L^{-1} (N) in the presence of 30 mmol L^{-1} PDS a limit of quantification of 0.5 mg L^{-1} was obtained according to the method described in DIN 32645 (*α=0.05)*.[200]

5.4.2 Anion Chromatography for the Nitrate and Nitrite Analysis

For the analysis of NO_3^- and NO_2^-, a method proposed by Lutze *et al.* for the quantification of chloride in the presence of sulfate and PDS ions was further evaluated.[180] Both species could be separated and quantified with a detection limit of 0.2 mg L^{-1} for nitrate in the presence of 30 mmol L^{-1} PDS. Although nitrite could be separated in synthetic samples containing nitrate and $K_2S_2O_8$, the real samples obtained from the mineralization experiments were found to contain no detectable amounts of nitrite under the given conditions. In fact, nitrite reacts very fast with sulfate radicals in solution with rate constants of 9.8 x 10^8 M^{-1} s^{-1} to 8.8 x 10^8 M^{-1} s^{-1}.[201-202] Thus, the initially formed nitrite was instantaneously converted to nitrate, which could be quantified with the presented method. PDS is strongly retained on the Metrosep A Supp 4 column and elutes with a retention time of 20 min and a peak width of almost 16 min. Hence, 10 minutes of reconditioning time was required. The long individual run times result in long time periods prior to the measurement in which the samples are kept at the autosampler (up to 12 h). As the samples in the autosampler for the IC cannot be cooled, precautions have to be taken to avoid reactions of the sulfate radicals formed at room temperature by thermal activation of PDS. Therefore, 10 vol.-% methanol was added to the sample as a radical scavenger. Methanol reacts fast with sulfate radicals (rate constant 1.0 x 10^7 M^{-1} s^{-1}) and does not interfere in the ion chromatography.[180, 203] The resulting dilution of the sample was taken into account later on in the mass balance calculation.

5.4.3 TOC and TNb analysis

In contrast to the TOC measurement with high temperature combustion, which is known to be relatively robust against changes in the matrix composition as for example increased salt

concentrations in the sample, the TNb has been reported to be affected by varying matrix conditions in the sample.[204] So far, high temperature conversion of nitrogen containing organic compounds for TOC and TNb measurement in the presence of high sulfate and PDS concentrations have not been reported. To test the influence of sulfate and PDS, recovery rates for TOC and TNb from glycine, as well as TNb from NH_4Cl, and $NaNO_3$ were analysed at different $K_2S_2O_8$ concentrations and the recovery was compared as shown in **Figure 5.4**.

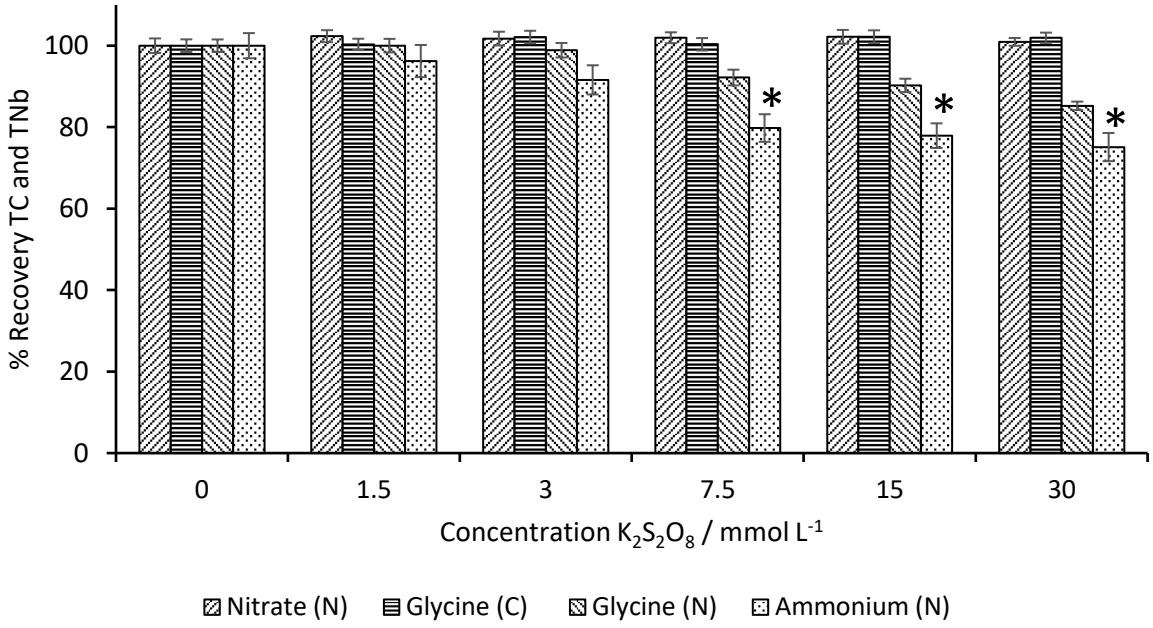

Figure 5.4: Recovery rates obtained for the determination of TOC and TNb from glycine, NH_4Cl, and $NaNO_3$ at different $K_2S_2O_8$ concentration in the sample matrix. Error bars indicate the 95 % confidence interval after error propagation of the individual measurement uncertainties. *used to calculate the correction factor in section 5.6.4

For the determination of the TOC from glycine in the presence of peroxydisulfate, as well as TNb from nitrate, no effect of the $K_2S_2O_8$ concentration in the range from 1.5 to 30 mmol L^{-1} could be observed. In contrast, the recoveries obtained for the TNb from glycine dropped significantly below 100 % for PDS concentrations higher than 3 mmol L^{-1}. The recovery of TNb from ammonium decreased to around 80 % for PDS concentrations between 7.5 and 30 mmol L^{-1}. To assess whether the effect of the PDS on the recoveries of the TNb from organic nitrogen and ammonium were a PDS specific result, samples containing NaCl and K_2SO_4 at the same ionic strength as the PDS samples were prepared and the recoveries of TOC and TNb for the different species were determined. The results in the presence of NaCl and K_2SO_4 are shown in **Figure 5.5**.

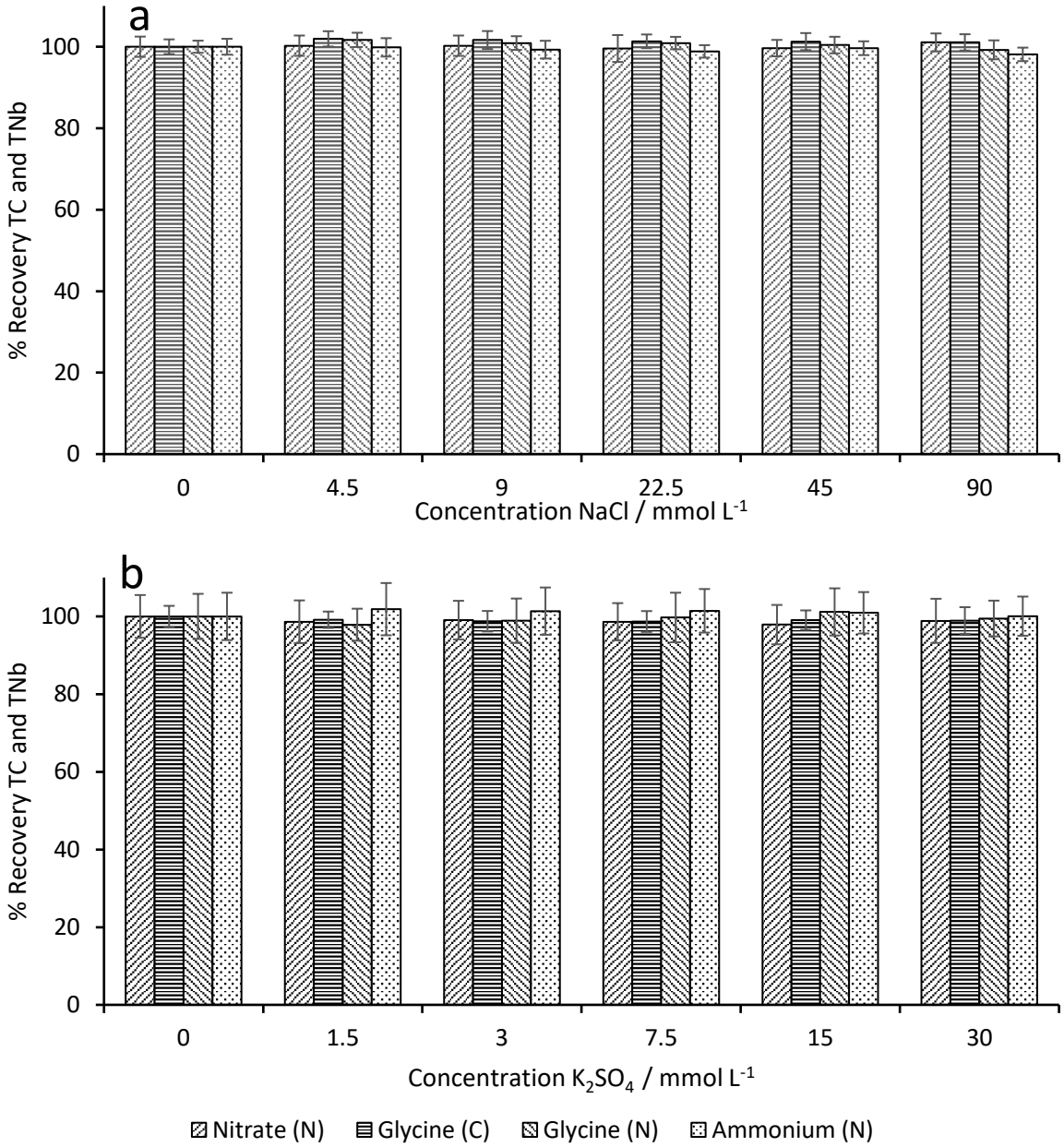

Figure 5.5: Recovery rates obtained for the determination of TOC and TNb from glycine, NH_4Cl, and $NaNO_3$ at different NaCl (a) and K_2SO_4 (b) concentration in the sample matrix. Error bars indicate the 95 % confidence interval after error propagation of the individual measurement uncertainties

Taking the uncertainty of the individual measurements into account, there was no significant effect of the amount of chloride, sulfate, and potassium in the sample on the recovery of the TOC and the TNb for the tested compounds. This indicates, that the negative effect of PDS on the recoveries is a result of the high concentration of PDS ions rather than the high salt load or an effect caused by the potassium as a counterion.

These results are important in the interpretation of the TNb values measured during mineralization experiments, as the concentration of PDS is decreasing throughout the course of the experiment while the distribution of nitrogen between the organic and inorganic fractions changes with time. In **Figure 5.6**, the concentration of PDS over a reaction time of 30 min is shown. PDS concentrations were determined by ion chromatography during the nitrate analysis. From the decrease in PDS concentration over time, the first order reaction rate constant can be determined. The obtained k_1 from the batch experiment was 0.74 x 10^{-3} s^{-1} which is comparable to the rate constants obtained in deionized water at 100 °C by Peyton and Goulden and Anthony (1.0 x 10^{-3} s^{-1} and 1.12 x 10^{-3} s^{-1} respectively).[187, 205] The higher reaction rates described in the literature can be explained by the reaction conditions during the batch experiment, as the temperature was fluctuating between 96 and 98 °C. Lower reaction temperatures have a strong influence on the PDS decomposition as can be seen from the reaction rate observed at 90 °C of 0.35 x 10^{-3} s^{-1}.[205]

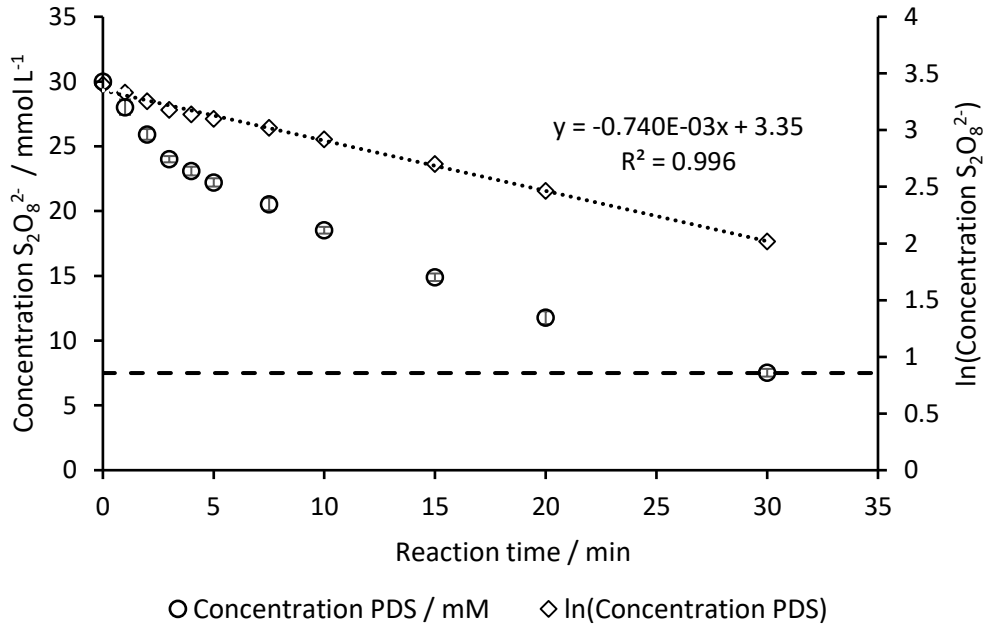

Figure 5.6: PDS concentration during the mineralization of organic compounds as a result of the heat induced decomposition and further transformation to sulfate. The dashed line indicates the 7.5 mmol L^{-1} threshold above which a constant effect of the PDS on the TNb measurements was observed. k_1 (batch experiment 96-98 °C) = 0.74 x 10^{-3} s^{-1}

From the course of the PDS concentration over time it can be concluded, that the concentration will be above 7.5 mmol L^{-1} in the samples obtained between 0 and 30 min, which results in an underestimation of roughly 20 % for ammonium and between 10 to 15 % for nitrogen from organic compounds (see **Figure 5.4**). From the TNb recovery rates obtained in the presence of 7.5, 15, and 30 mmol L^{-1} PDS (indicated with an asterisk in **Figure 5.4**) a correction factor for the measured ammonium concentrations was calculated to later on account for the underestimation of ammonium within the TNb based mass balance. Based on the results of Ammann *et al.*, and as recommended by the manufacturer of the TOC/TNb analyzer, a thin layer of ceramic fibers was placed on top of the catalysts coated ceramic spheres in the oxidation reactor to achieve a better conversion of the N-species to NO.[204] Nevertheless, in the presence of PDS this procedure did not result in a complete conversion. One explanation could be that different gaseous nitrogen species are formed in the oxidation reaction. The oxidation of ammonium in the presence of a platinum catalyst as in the TOC instrument should normally lead to NO as the main reaction product according to **Equation 5.5**.[206]

$$4\,NH_3 + 5\,O_2 \rightarrow 4\,NO + 6\,H_2O \qquad \textbf{(5.5)}$$

For the uncatalyzed reaction, molecular nitrogen would be the only reaction product according to **Equation 5.6**. Only by the influence of the catalyst and suitable reaction conditions, up to 98 % of NO can be obtained under optimal conditions as a result of the different kinetics of the reactions.[206]

$$4\,NH_3 + 3\,O_2 \rightarrow 2\,N_2 + 6\,H_2O \qquad \textbf{(5.6)}$$

$$4\,NH_3 + 4\,O_2 \rightarrow 2\,N_2O + 6\,H_2O \qquad \textbf{(5.7)}$$

$$2\,NO \rightarrow N_2 + O_2 \qquad \textbf{(5.8)}$$

If the reaction pathways according to **Equation 5.6** to **Equation 5.8** are affected by the presence of excess PDS in the reactor, they would lead to gaseous nitrogen species that will not be detectable by the chemiluminescence detector (N_2O and N_2 will not react with ozone and produce a detectable chemiluminescence). This would explain the reduced recoveries for the high PDS concentration, but comparable results or experimental setups to study the behaviour of PDS at the present temperature in the gas phase are not available in the

literature. Nevertheless, the effect of PDS on the TNb recovery rates for ammonium and organic nitrogen can be important in the monitoring of the TNb at environmental remediation sites where high PDS concentrations could be present.

5.4.4 Mineralization of Caffeine as a Model Compound

To monitor the carbon and nitrogen balance during the mineralization of a model compound, a combination of the four analytical methods was used. The intially measured carbon concentration (TOC) was used to calculate the initial nitrogen concentration based on the elemental composition of the analyte. The obained initial N concentration was set to 100 % and the results obtained for the later time points of the experiment were calculated relative to these values. The fraction of remaining TOC indicates the degree of mineralization, as the final product, CO_2 is removed during the sparging step in the NPOC analysis. Ammonium and nitrate concentrations were transformed to mass concentration of nitrogen for comparability. The sum of both inorganic nitrogen species as well as the individual concentrations were related to the initial amount of nitrogen present to obtain relative values for comparison. In **Figure 5.7**, the results for the mineralization of caffeine by heat activated persulfate are shown. Control experiments with caffeine were performed without the addition of PDS as an oxidation agent as well as with the addition of PDS but without heat activation (30 min at 21 °C). By NPOC measurement, no mineralization of caffeine could be detected, which indicates, that caffeine is hydrolysis-resistant and thermally stable under the experimental conditions. Experimental results are supplied in the appendix to this chapter.

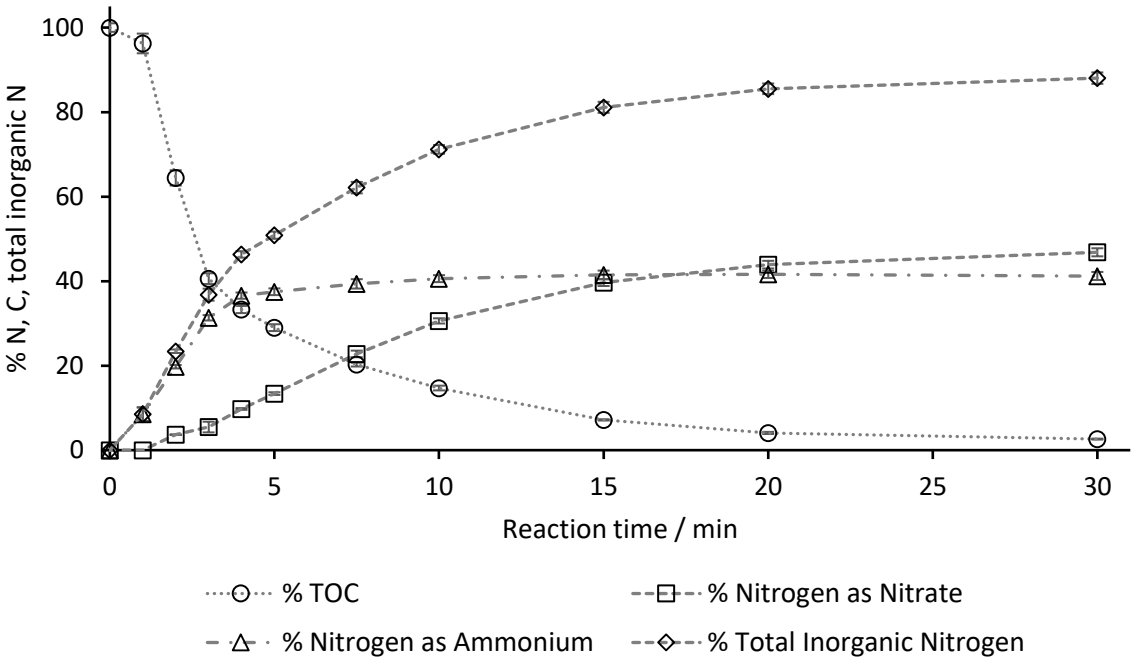

Figure 5.7: Mineralization of caffeine by heat activated PDS (initially 50 mg L^{-1} (C), 30 mmol $K_2S_2O_8$, temperature 96-98 °C), error bars indicate the 95 % confidence intervals obtained by Gaussian error propagation of the uncertainties of the individual measurements

From the TOC results, a fast decrease of the remaining carbon can be observed in the first 3 min, after which the mineralization rate steadily decreases. In the final sample after 30 min reaction time, 2.6 % of the initial carbon content could still be measured as TOC. From the cation chromatography data, a production of ammonium within the first 5 min of the experiment could be observed. For the remaining 25 min, the ammonium concentration was almost constant. The nitrate concentration in contrast steadily increased over the whole course of the experiment, while the majority was produced in the first 15 min. Similar results were found for the photocatalytic oxidation of nitrogen containing organic compounds, where the production of ammonium was initially high, and the formation of nitrate was observed with a later onset.[196] After 30 min, the total inorganic nitrogen reached a final value of 91.1 ± 1.4 % of the initial organic nitrogen present at the beginning of the mineralization. In **Figure 5.8**, the TNb values obtained for each time point during the caffeine mineralization experiment are shown. The initial concentration obtained before the PDS was added to the system is in agreement with the calculated initial nitrogen concentration based on the TOC concentration at t_0. The initial carbon concentration was 48.6 ± 1.0 mg L^{-1} (C) which results in a calculated nitrogen concentration of 28.3 ± 0.6 mg L^{-1} (N) (molecular composition of caffeine

can be used at t_0), the nitrogen concentration measured as TNb was 28.2 ± 0.8 mg L^{-1} (N). These values are in good agreement and show that the two independent calibrations for TOC and TNb are in accordance with each other.

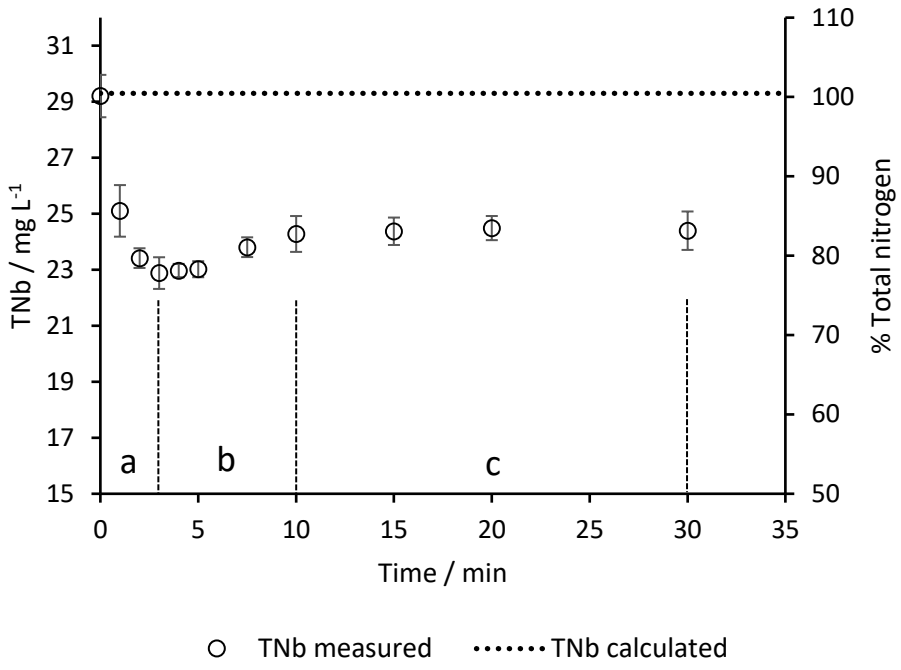

Figure 5.8: TNb measured during the mineralization of caffeine with heat activated PDS (Initial caffeine concentration 50 mg L^{-1} (C), initial PDS concentration 30 mmol L^{-1}, mineralization at 96-98 °C). Expected TNb was calculated based on the initially measured TOC, error bars indicate the 95 % confidence interval

After the addition of the PDS to the system, the measured TNb values decrease to around 80 % after 3 min. This is a result of the varying TNb recoveries observed for different nitrogen containing species. As mentioned above, the PDS concentration has an influence on the recoveries of the measured TNb for organic molecules and ammonium (**Figure 5.4**). As presented in **Figure 5.8** section (a), during the first 3 min, the ammonium concentration as well as the high caffeine concentrations in the system are influencing the measured TNb. These species lead to an underestimation of the TNb in the presence of PDS, which results in an apparent minimum of the measured TNb around 3 min. After 3 min the formation of ammonium is very small, and the remaining organically bound nitrogen is mainly converted to nitrate directly (see **Figure 5.7**). As TNb from nitrate is less affected by the presence of PDS, the measured TNb values apparently increase after 3 min (section (b) **Figure 5.8**). In section (c) in **Figure 5.8** the apparent TNb results remain almost constant, as only small amounts of

remaining organic nitrogen are transformed to nitrate. At the end of the experiment, 83.2 ± 1.1 % of the initial nitrogen were determined by TNb. This value represents the nitrate fraction of the mineralization products which can be correctly determined by the TNb method as well as the ammonium fraction, which is affected by the present PDS concentrations and has to be corrected for further comparison to the ion chromatography based mass balance approach.

For a correction of the TNb result, the fraction of ammonium, nitrate, and organically bound nitrogen have to be known precisely as every fraction is affected to a different extent. This is only possible at the end of the mineralization experiment when the remaining carbon is almost completely mineralized. In case of incomplete mineralization, the nitrogen bound in the organic fraction cannot be derived from the TOC result, as the elemental composition of the remaining organic substances is not defined. After 30 min, the amount of remaining organic compounds can be almost neglected, and the fraction of ammonium and nitrate are known from the IC measurements. With the help of the concentrations of ammonium and nitrate at 30 min measured by IC and the correction factor of 0.776 derived from the TNb measurements of ammonium in the presence of 7.5 to 30 mmol L^{-1} PDS (**Figure 5.4**), a final corrected TNb value of 95.9 ± 3.1 % can be obtained. Mineralization experiments under the same conditions were carried out for the amino acid histidine and the aliphatic N-heterocycle piperidine. The underestimation of the ammonium fraction by the TNb measurement could be proven for the two additional compounds. In addition, the correction of the TNb mass balance was applied, and nitrogen recovery rates close to 100 % could be obtained for all three compounds analysed. The additional experimental results and the detailed calculation of the correction applied to the TNb measurements are shown in the appendix to this chapter.

5.4.5 Comparison of the two Nitrogen Mass Balance Approaches

Both presented methods for the determination of nitrogen mass balances led to conclusive results. Considering, that the determination of total inorganic nitrogen does not include the amounts of nitrogen contributed by residual organic compounds (2.6 % TOC remaining), a recovery of 91.1 ± 1.4 % is a good indication that the majority of organic nitrogen could be recovered in the produced ammonium and nitrate after complete mineralization. In contrast to the IC based method, the TNb approach is capable of determining remaining organic and inorganic nitrogen. However, this method is biased by the presence of PDS, which leads to an

underestimation of ammonium and organic nitrogen. The presented correction of the TNb is only applicable if in addition, IC experiments are carried out to determine the fraction of different inorganic nitrogen species. This leads to the conclusion that the TNb can only be used to additionally check whether a complete conversion was obtained at the end of the experiment when distinct IC results for each species are available. But, as a single parameter, the TNb cannot be used in the presence of PDS if a similar high temperature conversion method is used. The mass balance approach taking the IC and TOC measurements into account can be used for a nitrogen mass balance, when the reaction times are chosen long enough, so that the organically bound nitrogen is completely mineralized. From the final results of the two mass balances, the recovery after the mineralization is between 91.1 ± 1.4 % and 95.9 ± 3.1 %. This indicates, that gaseous nitrogen oxidation products, if present at all, only account for a very small fraction of the overall mineralization products as the obtained mass balances are almost closed, given the uncertainty of the final recoveries and the fact, that the mineralization was not 100 % complete. For the oxidation experiments of N-containing analytes by photo oxidation, a mass balance of the final mineralization products was not carried out, but N-recoveries obtained for the alkaline PDS oxidation of caffeine were found to be in the range of 86.7 to 88.0 %.[120, 196]

5.5 Conclusion

The mineralization products of the oxidation of organic nitrogen containing compounds by PDS are important factors that have to be identified in the field of environmental remediation as well as for analytical chemistry applications. With the help of the presented TOC/IC based mass balance approach, the oxidation of target compounds can be studied in a batch setup. More than 90 % of the initially present nitrogen could be recovered after 30 min of oxidation in the form of ammonium and nitrate. In contrast to the TOC/TNb based mass balance, residual organic nitrogen will not be included in the mass balance. The use of the TNb by high temperature combustion for nitrogen mass balances in the presence of peroxydisulfate was shown to be significantly biased by the underestimation of ammonium which could only be corrected with the help of species specific information by IC. The presented combined error propagation of the TOC and IC results is necessary for the interpretation of the mass balance, as the individual uncertainties of each measurement can have significant effects on the overall recovery.

Acknowledgement

We would like to thank Willi A. Brand from Max-Planck-Institute for Biogeochemistry for the fruitful discussions about the subject and comments. The research was funded by the German Research Foundation (DFG) under the project grant 317438550.

5.6 Appendix to Chapter 5

5.6.1 Control Experiments for the Caffeine Stability under the Experimental Conditions

Caffeine standard solutions (50 mg L^{-1} (C)) were tested on their stability in aqueous solution at room temperature (21 °C), experimental conditions during the mineralization experiment (96-98 °C) without addition of PDS, and at 21 °C with the addition of PDS (30 mmol L^{-1}) without additional heat activation. NPOC analysis was performed as described in the material and methods section for the mineralization experiments. The results are presented in **Table 5.1**.

Table 5.1: Caffeine stability measurements

	NPOC (mg L^{-1} (C))	95 % CI	Recovery %
21 °C without PDS	49.8	0.6	99.6
21 °C with PDS	50.2	0.6	100.4
96-98 °C without PDS	50.4	0.5	100.8

The results obtained by the NPOC measurement show, that no significant mineralization of the target compound occurs at room temperature with or without addition of the oxidation agent. In addition, no significant mineralization could be observed due to hydrolysis of caffeine at the experimental conditions of 96 to 98 °C within 30 min.

5.6.2 Error Propagation for the Statistical Evaluation of the Mass Balance

For the mass balance, analytical results from different measurements and instruments have to be combined. Measurements for the TOC, TNb, the nitrate and the ammonium concentration at each time point were at least performed in triplicates, so that individual standard deviations for each measurement can be calculated. The error propagation was calculated based on a Gaussian error propagation model according to **Equation 5.9 to 5.11**.

$$Z = f(X; Y) \quad \textbf{(5.9)}$$

$$Z = X + Y \qquad \Delta z = \sqrt{(\Delta x)^2 + (\Delta y)^2} \qquad \textbf{(5.10)}$$

$$Z = k \times \frac{X}{Y} \qquad \Delta z = \sqrt{\left|\frac{\Delta x}{\bar{x}}\right|^2 + \left|\frac{\Delta y}{\bar{y}}\right|^2} \times |\bar{z}| \qquad \textbf{(5.11)}$$

To monitor the degree of mineralization, the percentage of remaining carbon at each time point was related to the initial carbon concentration according to **Equation 5.12**. The standard deviations for the TOC measurements were combined according to **Equation 5.13** to obtain standard deviations for the percentage of remaining carbon.

$$\%C_t = \frac{\beta_{C,t}}{\beta_{C,0}} \times 100\ \% \qquad \textbf{(5.12)}$$

$\%C_t$ % remaining carbon at time t

$\beta_{C,0}$ Initial mass concentration carbon at time 0

$\beta_{C,t}$ Mass concentration carbon at time t

$$s_{\%C,t} = \sqrt{\left|\frac{s_{\beta_{C,t}}}{\overline{\beta_{C,t}}}\right|^2 + \left|\frac{s_{\beta_{C,0}}}{\overline{\beta_{C,0}}}\right|^2} \times |\overline{\%C_t}| \qquad \textbf{(5.13)}$$

$s_{\%C,t}$ Standard deviation of the % remaining carbon at time t

$s_{\beta_{C,t}}$ Standard deviation of the mass concentration of carbon at the time t

$\overline{\beta_{C,t}}$ Mean carbon mass concentration at time point t

$s_{\beta_{C,0}}$ Standard deviation of the initial mass concentration of carbon

$\overline{\beta_{C,0}}$ Initial mean carbon mass concentration

$\overline{\%C_t}$ Mean % of remaining carbon at time t

On the basis of the initial carbon concentration, the initial nitrogen concentration was calculated according to **Equation 5.14**.

$$\beta_N = \beta_C \times \frac{\#N_x \times M_N}{\#C_x \times M_C} \qquad \textbf{(5.14)}$$

β_N Mass concentration of nitrogen

β_C Mass concentration of carbon

$\#N_x$ Number of nitrogen atoms in the molecule

$\#C_x$ Number of carbon atoms in the molecule

M_N Molecular mass of nitrogen

M_C Molecular mass of carbon

The corresponding standard deviation of the initial nitrogen concentration can be calculated according to **Equation 5.15**.

$$s_{\beta_N} = s_{\beta_C} \times \frac{\#N_x \times M_N}{\#C_x \times M_C} \quad \textbf{(5.15)}$$

s_{β_N} Standard deviation of the initial nitrogen mass concentration

s_{β_C} Standard deviation of the initial carbon mass concentration

With the help of the initial nitrogen mass concentration and the mass concentrations of the individual inorganic nitrogen species at each time point, corresponding percentages of the total initial nitrogen can be calculated. The corresponding standard deviations of these percentages can be calculated according to **Equation 5.16**.

$$s_{\%Nx,t} = \sqrt{\left|\frac{s_{\beta_{Nx,t}}}{\overline{\beta_{Nx,t}}}\right|^2 + \left|\frac{s_{\beta_{Nx,0}}}{\overline{\beta_{Nx,0}}}\right|^2} \times \left|\overline{\%N_{x,t}}\right| \quad \textbf{(5.16)}$$

$s_{\%Nx,t}$ Standard deviation of the percentage of initial nitrogen present as the species *x* at the time point *t*

$s_{\beta_{Nx,t}}$ Standard deviation of the mass concentration of the nitrogen species *x* at the time point *t*

$\overline{\beta_{Nx,t}}$ Mean nitrogen mass concentration of the species *x* at the time point *t*

$s_{\beta_{Nx,0}}$ Initial standard deviation of the mass concentration of the nitrogen species *x*

$\overline{\beta_{Nx,0}}$ Initial nitrogen mass concentration of the species *x*

$\overline{\%N_{x,t}}$ Mean % of remaining nitrogen species x at time t

The relative amount of inorganic nitrogen formed in comparison to the initially determined organic nitrogen content can be calculated according to **Equation 5.17.** Therefore the standard deviations of the ammonium and nitrate measurements have to be combined according to **Equation 5.18**.

$$\%N_t = \frac{\beta_{N,t}}{\beta_{N,0}} \times 100\% \quad \textbf{(5.17)}$$

$\%N_t$ % sum of inorganic nitrogen at time t

$\beta_{N,0}$ Initial mass concentration of organic nitrogen at time 0

$\beta_{N,t}$ Mass concentration of inorganic nitrogen at time t

$$s_{\%Ntot,t} = \sqrt{\left(s_{\%NH_4^+,t}\right)^2 + \left(s_{\%NO_3^-,t}\right)^2} \quad \textbf{(5.18)}$$

From the final standard deviations, two-sided confidence intervals based on the t-distribution with α=0.05 were calculates according to **Equation 5.20** was used

$$\bar{x} \pm t_{1-\alpha} \times \left(\frac{s_x}{\sqrt{n}}\right) \quad \textbf{(5.20)}$$

5.6.3 Mineralization of Histidine and Piperidine

Besides caffeine as a model compound for environmentally relevant contaminants, the amino acid histidine and the aliphatic N-heterocyclic compound piperidine were mineralized in the batch-reactor setup. The mineralization was monitored by TOC measurements as well as nitrate and ammonium measurements by ion chromatography. The results obtained over the course of the 30 min mineralization experiment are shown in **Figure 5.9**. In contrast to the results obtained for caffeine, a significant amount of organic oxidation products (5 % of the initial TOC) could not be oxidized over 30 min for histidine.

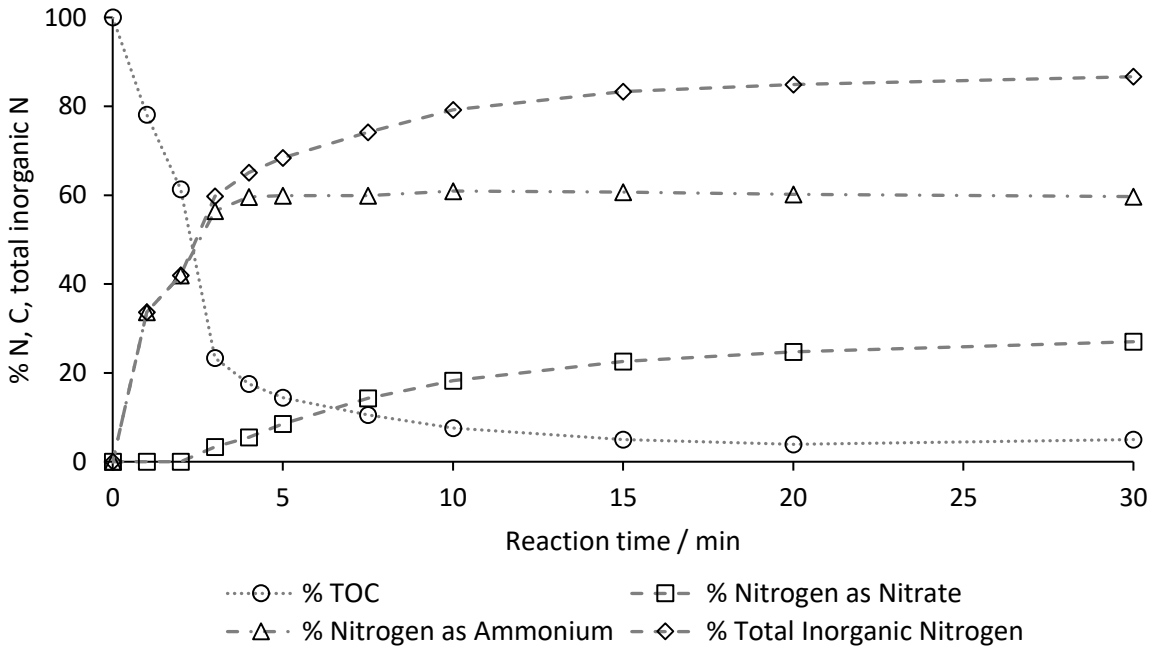

Figure 5.9: Mineralization of histidine by thermally activated PDS (initially 50 mg L^{-1} (C), 30 mmol L^{-1} $K_2S_2O_8$, temperature 96-98 °C)

The TNb was monitored as described in the material and methods section. The systematic underestimation of the TNb by the experimentally obtained results is shown in **Figure 5.10**.

The observed trend for the TNb results is comparable to the results obtained for caffeine, although relatively lower amounts of nitrate are formed in comparison to ammonium.

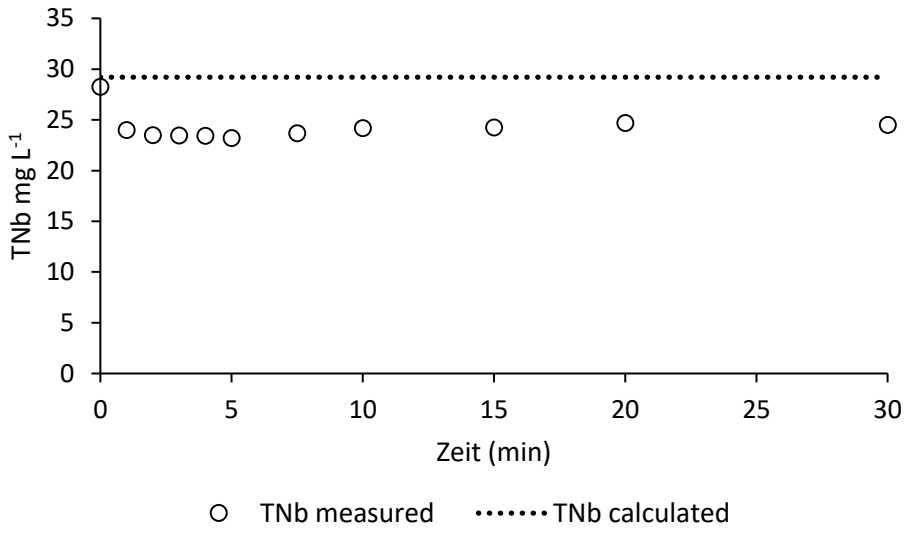

Figure 5.10: TNb measured during the mineralization of histidine with thermally activated PDS (Initial histidine concentration 50 mg L^{-1} (C), initial PDS concentration 30 mmol L^{-1}, mineralization at 96-98 °C). Expected TNb was calculated based on the initially measured TOC

For the mineralization of piperidine, similar ratios of nitrate to ammonium were obtained as for histidine as shown in **Figure 5.11**. In comparison to histidine and caffeine, the formation of nitrate and ammonium was delayed, although significant mineralization could be observed by the loss of organic carbon from the system.

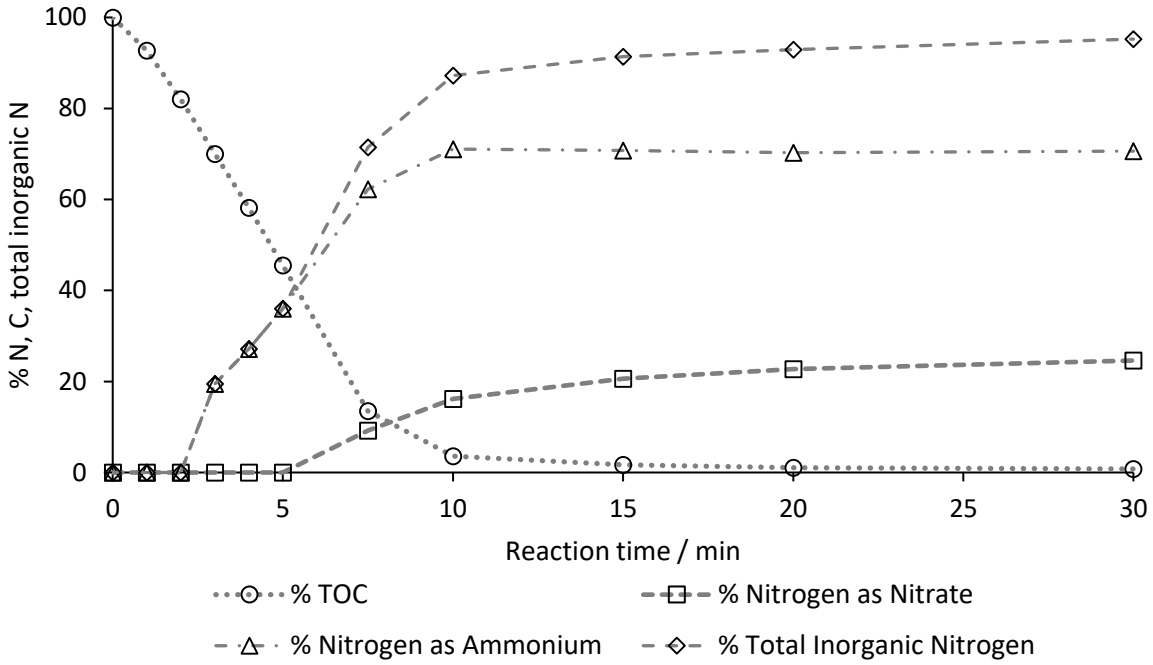

Figure 5.11: Mineralization of piperidine by thermally activated PDS (initially 50 mg L^{-1} (C), 30 mmol L^{-1} $K_2S_2O_8$, temperature 96-98 °C)

The TNb measurements during the mineralization of piperidine as presented in **Figure 5.12,** show the same trend as already observed for the measurements of caffeine and histidine. For histidine and piperidine, evaluation of the different mass balance approaches was carried out as described for caffeine. The recovery of the TNb in the system is compared in **Table 5.2**.

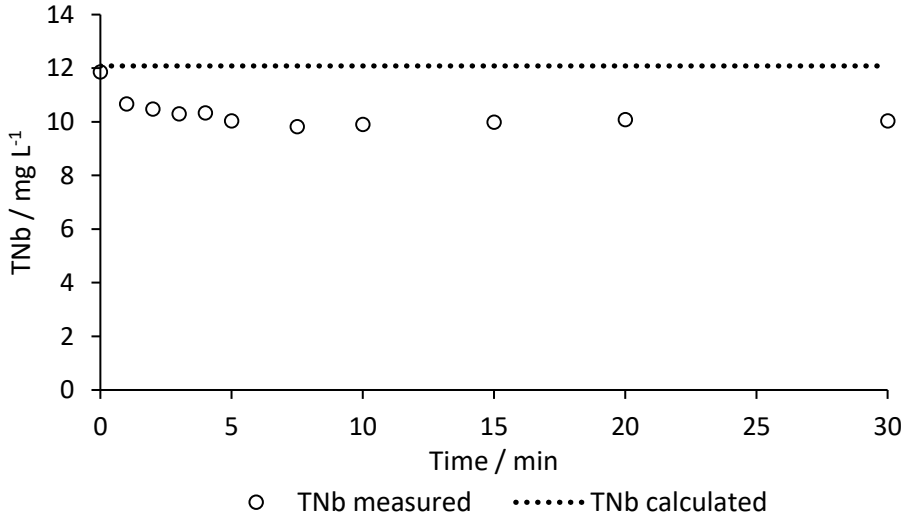

Figure 5.12: TNb measured during the mineralization of piperidine with thermally activated PDS (Initial piperidine concentration 50 mg L^{-1} (C), initial PDS concentration 30 mmol L^{-1}, mineralization at 96-98 °C). Expected TNb was calculated based on the initially measured TOC

Table 5.2: Comparison of the nitrogen recovery rates based on the three different mass balance approaches by ion chromatography, TNb, and the corrected TNb

	% Nitrogen Recovery		
	IC (NO_3^- + NH_4^+)	**TNb**	**TNb corrected**
Caffeine	91.1	83.2	95.9
Piperidine	95.3	83.1	99.7
Histidine	86.7	83.9	102.5

The mass balance obtained by the combination of IC measurements for ammonium and nitrated for caffeine and piperidine was comparable. For histidine, significant amounts of organic carbon was still present after 30 min of oxidation. Although the structure of the remaining organic oxidation products was not evaluated, it can be concluded, that a fraction of the total nitrogen is still bound in the organic residue as indicated by the lower recovery for the IC mass balance for histidine. The TNb measurements obtained without correction are comparable for the three model compounds and prove the constant underestimation of the ammonium fraction. If the proposed correction of the ammonium fraction is performed, the TNb mass balance for all three compounds can be improved to obtain recoveries close to 100 %.

5.6.4 Correction of the TNb Results

Calculated underestimation of ammonium in the presence of 7.5 to 30 mmol L^{-1} $K_2S_2O_8$ by a factor of 0.776 (Mean value calculated from the results shown in Figure 5.4 for the TNb determination of an ammonium solution n=23; s=0.044) according to **Equation 5.21**.

$$F_{corr} = \frac{\bar{x}_{c0}}{\bar{x}_{c7.5-30}} \qquad \textbf{(5.21)}$$

F_{corr} Correction factor for ammonium

$\bar{x}_{c0}$ Mean concentration of ammonium without $K_2S_2O_8$

$\bar{x}_{c7.5-30}$ Mean concentration measured for ammonium at 7.5, 15, and 30 mmol L^{-1} $K_2S_2O_8$

From the results obtained from the IC measurements after 30 min oxidation, the fraction of ammonium and nitrate of the inorganic nitrogen can be calculated. With the known composition of the inorganic species and under the assumption that the remaining organic N

can be neglected, **Equation 5.22 and 5.23** can be combined to calculate the corrected TNb after 30 min of mineralization.

$$R_{NO_3^-/NH_4^+} = \frac{c(NO_{3\ IC,30\ min}^-)}{c(NH_{4\ IC,30\ min}^+)} \quad \textbf{(5.22)}$$

$$TNb_{measured,30\ min} = c(NO_3^-) + F_{corr} \times c(NH_4^+)_{corr} \quad \textbf{(5.23}$$

The corrected TNb was obtained as the sum of the calculated nitrate fraction of the TNb and the corrected ammonium fraction. To obtain the recovery, the corrected TNb after 30 min of oxidation was divided by the initial TNb before oxidation **(Equation 5.24)**.

$$\%N = \frac{c(NO_3^-)_{30\ min} + c(NH_4^+)_{corr,\ 30\ min}}{TNb_{initial}} \times 100\% \quad \textbf{(5.24)}$$

F_{corr}		**0.776**	
$\bar{x}_{c0}$		29.70	mg/L (N)
$\bar{x}_{c7.5-30}$		23.05	mg/L (N)
$R_{NO_3^-/NH_4^+}$		1.137	
$TNb_{measured,30\ min}$		24.39	mg/L (N)
$c(NO_3^-)$		14.45	mg/L (N)
$c(NH_4^+)_{corr}$		12.71	mg/L (N)
$TNb_{initial}$		28.32	mg/L (N)
$\%N$		95.90	%

Chapter 6: Alkaline persulfate oxidation for the development of a wet chemical oxidation interface for compound specific δ^{15}N analysis by LC-IRMS

Köster, Daniel[1], Hesse, Tobias[1], Jochmann, Maik A.[1], Schmidt, Torsten C. [1,2]

[1] Instrumental Analytical Chemistry, University of Duisburg-Essen, Universitätsstr. 5, 45141 Essen, Germany

[2] University of Duisburg-Essen, Centre for Water and Environmental Research (ZWU) Universitätsstr. 5, 45141 Essen, Germany

6.1 Abstract

In order to realize an online determination of compound specific nitrogen isotope ratios by LC-IRMS with a wet chemical oxidation interface, the transformation of the nitrogen containing analytes into a single nitrogen containing species for further reaction pathways towards the measurement gas for IRMS has been developed. A detailed comparison of the mineralization products formed during the oxidation of nitrogen containing analytes by heat activated persulfate at acidic and alkaline conditions was performed. With the help of TOC and IC measurements, the remaining organic carbon fraction as well as the inorganic nitrogen species nitrate, nitrite, and ammonium were monitored in batch reactor experiments. From the results obtained in the batch experiments, the alkaline oxidation environment was identified to be favourable for the δ^{15}N LC-IRMS application, as it can lead to nitrate as a single oxidation product. The alkaline oxidation conditions from the batch reactor experiments were successfully transferred to the flow-through oxidation reactor of the LC-IMRS interface. In infusion experiments with different model compounds, 62.5 % to 99.8 % of the initially present nitrogen could be transformed to nitrate within 43 s residence time in the on-line reactor. The reaction time and oxidation agent concentration in the interface were identified as the main parameter for optimization of the nitrate recovery.

6.2 Introduction

Liquid chromatography coupled to isotope ratio mass spectrometry (LC-IRMS), is a technique which is routinely applied to perform compound specific isotope analysis (CSIA) in order to obtain carbon isotope ratios of individual compounds.[73, 152] Analytes are separated by liquid chromatography and introduced into the LC-IRMS interface, where they are oxidized by heat activated persulfate in a wet chemical flow-through reactor. The resulting CO_2 is separated from the liquid mobile phase by a membrane system and transferred to the IRMS for isotope measurement.[36] In contrast to gas chromatography coupled to isotope ratio mass spectrometry (GC-IRMS) the LC-IRMS system is suitable for the determination of isotope ratios in polar small molecules which are not directly amenable for GC measurement without derivatization.[32, 40] In GC-IRMS, stable isotope ratios of hydrogen, nitrogen and carbon are routinely measured, whereas LC-IRMS is currently limited to the measurement of $\delta^{13}C$ isotope ratios. For the measurement of dual-isotope data ($\delta^{13}C$ and $\delta^{15}N$) of polar target molecules, such as the herbicides glyphosate and chloridazon, LC-IRMS is utilized for the $\delta^{13}C$ measurement in addition to $\delta^{15}N$ measurement after derivatization by GC-IRMS.[33, 123] For the assessment of transformation mechanisms of environmental contaminants, the application of dual element analysis has been shown to provide information not accessible by single isotope monitoring e.g. $\delta^{13}C$ analysis alone.[124-125] Bulk nitrogen stable isotope analysis plays an important role in the study of food web structures in various eco systems, as the heavier ^{15}N isotope is enriched by 3 to 5 ‰ by each trophic cycle in the organism compared to isotope ratios in the food sources.[207-208] Especially in very complex trophic interactions such as host parasite systems, stable isotope analysis could be applied to elucidate the feeding behaviour of fish parasites.[209-210] In contrast to bulk stable isotope measurements, CSIA could lead to valuable additional information in these fields by the monitoring of specific nitrogen containing marker compounds rather than the analysis of the whole nitrogen content by EA-IRMS systems. With the help of CSIA, it is possible to differentiate the individual isotopic signature of essential and non-essential amino acids. It has been shown, that essential amino acids such as phenylalanine show a small fractionation of <0.5 ‰ per trophic transfer, whereas non-essential amino acids such as glutamic acid showed significant fractionation in their nitrogen isotope ratio of about 6-8 ‰.[211] Many published applications for $\delta^{13}C$ analysis by LC-IRMS focussing on amino sugar analysis, authenticity of caffeine containing drinks, analysis

of pharmaceuticals, and amino acids could benefit from the additional δ^{15}N information which is not directly accessible by LC-IRMS alone.[45, 57, 81-82, 101]

Currently, the determination of δ^{15}N isotopic signatures in addition to δ^{13}C information of polar compounds that are not directly GC measurable, is mostly performed on two parallel analytical platforms.[123, 212] Carbon isotope ratios can also be determined by GC after derivatization, but the introduction of carbon containing groups into the molecule will alter the isotopic signature of the analyte which has to be corrected afterwards.[213] In addition, the derivatization process has to be very well understood and controlled, so that incomplete derivatization does not introduce isotopic shifts into the results. A combination of preparative LC separation and isotope measurement of nitrogen containing analytes such as amino acids by elemental analyzer IRMS (EA-IRMS) has been demonstrated and showed increased precision of the δ^{15}N results compared to GC-IRMS after derivatization.[214] The main drawback of this technique is that it cannot be combined into an online-system and that the experimental effort drastically increases with multi component LC separations. An online combination of LC separation and EA-IRMS measurement has been developed by Federherr *et al.*, which combines LC with high temperature catalytic conversion of the analytes for δ^{15}N measurments.[48-49] The system has successfully been tested for the measurement of compound specific carbon and nitrogen isotope ratios, but problems due to the introduction of large amounts of liquid mobile phase into the EA oxidation reactor and deactivation of the catalyst by mobile phase additives have restricted the further application so far. To overcome these drawbacks, an instrumental solution based on the already well established δ^{13}C LC-IRMS interface architecture commercialized by Thermo Fisher and Elementar Analysensysteme (IsoLink® and Liquiface®, respectively) using online wet chemical oxidation and separation of the analyte gas by a membrane system would be preferable.

The oxidation of nitrogen containing analytes for δ^{13}C measurements in the LC-IRMS system has been shown to require special optimization of the reaction conditions, as especially nitrogen containing heterocyclic ring systems were found to be oxidized comparably slower than simple non-heterocyclic analytes or amino acids.[45, 156, 215] Nevertheless, under the standard LC-IRMS measurement conditions for carbon isotope ratios, nitrogen containing oxidation products of the wet chemical oxidation cannot be monitored directly. For the analysis of the nitrogen containing reaction products, additional ion chromatography methods were developed that are able to determine nitrate, nitrite, and ammonium in the presence of

large excess of persulfate, sulfate and potassium or sodium present in the oxidation reactor of the LC-IRMS interface.[174]

Outside of the LC-IRMS context, the oxidation products formed by the reaction of nitrogen containing species with heat activated persulfate were evaluated for the determination of total nitrogen analysis in water samples.[119] The oxidation was performed in a batch process in 50-mL glass vessels, which were autoclaved at 100-110 °C for more than 30 min. The determination of specific oxidation products, and a recovery calculation based on the amount of initially introduced nitrogen in comparison to the measured species after oxidation was only performed at the end of the batch oxidation process.[119, 216] As the oxidation reaction in the IsoLink® LC-IRMS interface has to take place in a much shorter time interval of < 1 min based on the flow condition and dimensions of the oxidation reactor, intermediate species formed during the initial phase of the oxidation reaction are of great importance in this context. The results obtained from the batch experiments could be used to identify suitable reaction conditions for the application in the development of an online oxidation process for the compound specific δ^{15}N isotope analysis.

In the present chapter, a direct comparison of the oxidation of model compounds at acidic and initially alkaline oxidation conditions should be performed. Speciation of the nitrogen containing reaction products over the course of the oxidation reaction should give insight into primary and secondary oxidation reactions taking place. The results obtained by the alkaline batch oxidation will be transferred to the LC-IRMS system to evaluate the applicability of the alkaline oxidation conditions for further steps in the development of an instrumental setup for compound specific δ^{15}N LC-IRMS measurements.

6.3 Materials and Methods

6.3.1 Chemicals and Reagents

For the batch reactor mineralization experiment, caffeine (p.a. 99.9 % Sigma-Aldrich, Steinheim, Germany) and glycine (ReagentPlus, ≥99 %, Sigma-Aldrich, Steinheim, Germany) were used. For the mineralization experiments in the LC-IMRS interface, the aforementioned glycine and caffeine as well as potassium nitrate (Fluka Chemika, >99.0 %, Seelze, Germany), ammonium sulfate (ReagentPlus, ≥99 %, Sigma-Aldrich, Steinheim, Germany), urea (puris p.a., ≥99 %, Sigma-Aldrich, Steinheim, Germany), and acetonitrile (HPLC gradient grade, Fisher Scientific, Loughborough, United Kingdom) were used. The calibration for the TOC analysis was performed with a 1000 mg L^{-1} TOC reference standard (Sigma-Aldrich, Steinheim, Germany). For the oxidation reactions, potassium peroxydisulfate (puriss. p.a., >99 %, Sigma-Aldrich, Steinheim, Germany) and sodium peroxydisulfate (99 %, Riedel-de Haën, Seelze, Germany) were used. Mobile phases for the IC systems were prepared from ultrapure water obtained from an ELGA Purelab Ultra system (Veolia Water Technologies, Ratingen, Germany). A 1 M nitric acid solution from Fluka Analytical (Seelze, Germany) was used for the mobile phase of the cation chromatography system. For the anion chromatography, the mobile phase was prepared from sodium carbonate and sodium bicarbonate (both puriss. p.a.) obtained from Riedel-de Haën (Seelze, Germany) and acetonitrile (HPLC gradient grade) from Fisher Scientific (Loughborough, United Kingdom).

6.3.2 Batch Reactor Mineralization Experiments

The mineralization of the analytes was investigated in a batch reactor setup as described in **Chapter 5**. A schematic view of the setup also used for the oxidation at neutral pH conditions is presented in **Figure 5.1**. Initially the reactor contained 1490 mL of water adjusted to the desired pH level by the addition of sulfuric acid or potassium hydroxide. After the reaction temperature of 96-98 °C was reached, 10 mL of stock solution of the analyte was pipetted to obtain an initial carbon mass concentration of 50 mg L^{-1} (C). The first sample at t_0 was withdrawn without the addition of $K_2S_2O_8$. After the collection of the first sample, solid $K_2S_2O_8$ and 50 mL water were added to obtain a volume of 1.5 L with a $K_2S_2O_8$ concentration of 30 mmol L^{-1}. At each following time point 60 mL samples were withdrawn from the system without replacing the volume. Of the 60 mL sample, 10 mL were discarded and used to purge

the cooling loop, the following 50 mL were collected for further analysis. From the obtained 50 mL, aliquots of 10 mL were separated for the cation and anion chromatography. For the ion chromatography 1 mL of methanol was added to each sample aliquot. The pH of the subsamples used for the cation chromatography was adjusted by the addition of 0.5 mL of 1 M HCl for the alkaline oxidation experiments. For the TOC measurement the remaining 20 mL of the sample were used, in the case of the alkaline oxidation conditions, 2 mL of 1 M HCl were added to the subsample for the NPOC analysis. The individual samples were stored on ice until the analysis was performed. The remaining sample material from each time point was used for the pH measurement (Metrohm 827 pH lab, Metrohm, Herisau, Switzerland).

6.3.3 LC-IRMS Interface Mineralization Experiments

For the mineralization of analytes in the LC-IRMS system, modifications were made to the system, so that a constant stream of analyte solution at different concentrations was delivered directly to the oxidation reactor in the LC-IRMS interface (LC-IsoLink, Thermo Fisher Scientific, Bremen, Germany) by a Rheos Allegro HPLC pump (Flux instruments AG, Basel, Switzerland). The setup of the system in comparison to the regular LC-IRMS system is shown in **Figure 6.1**.

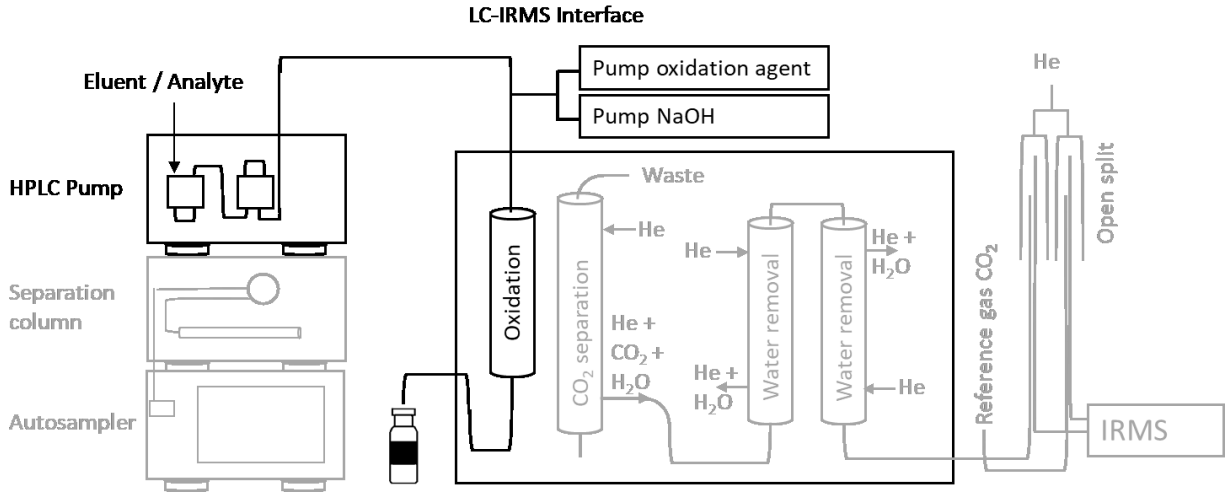

Figure 6.1: Modification of the LC-IRMS interface for the mineralization experiments

In the interface, sodium peroxydisulfate (100 g L^{-1} or 200 g L^{-1}) and sodium hydroxide (1.25 mol L^{-1}) were added at a flow of 50 µL min^{-1} or 25 µL min^{-1} each depending on the specific experimental conditions. The oxidation in the LC-IRMS interface flow-through reactor was performed at 100 °C. After the oxidation reactor, the connection to the gas separation unit was replaced by a PEEK capillary that led to an ice cooled sample vessel outside of the interface. The analyte solution as well as the oxidation reagent and NaOH solution were continuously introduced into the instrument for at least 30 min to equilibrate and flush the system between different analytes or flow conditions. After equilibration, approximately 20 mL of sample were collected. The nitrate measurement by IC was performed directly after the sample collection.

6.3.4 Analysis of the Non-purgeable Organic Carbon

The measurement of the NPOC was performed on a TOC-L total organic carbon analyser (Shimadzu, Duisburg, Germany) as described in **Chapter 5**. In brief, 20 mL of the sample from each time point of the mineralization experiment were transferred to the TOC-L autosampler, the already manually pH adjusted samples were additionally acidified by the instrument using 1 M HCl and purged with synthetic air (80 mL min^{-1}) to remove dissolved inorganic carbon. After 3 min of purging, 50 µL of the sample were injected. The CO_2 formed during the oxidation was measured by infrared spectroscopy. A calibration was performed with dilutions prepared from a certified TOC reference standard (Sigma Aldrich, 1000 ± 10 mg L^{-1} TOC).

6.3.5 Ion Chromatography

Two different IC systems were used for the measurement of nitrate, nitrite, and ammonium. Both consisted of a Metrohm 883 Basic IC plus connected to a Metrohm 863 Compact autosampler (both Metrohm, Herisau, Switzerland). For the analysis of the anions, a Metrosep A Supp 4 (250 mm x 4.0 mm) column (Metrohm, Herisau, Switzerland) with an eluent consisting of 1.8 mmol L^{-1} Na_2CO_3 and 1.7 mmol L^{-1} $NaHCO_3$ in a 30/70 vol.-% acetonitrile/water mixture was used. The injection volume was 10 µL and a flow of 1 mL min^{-1} was used for the anion separation. An ion suppression module (MSM, Metrohm, Herisau, Switzerland) was used for the anion chromatography to reduce the background conductivity of the eluent and increase the sensitivity. For the separation of the cations, a Metrosep C4 (150 mm x 4.0 mm) column (Metrohm, Herisau, Switzerland) with an eluent consisting of 4 mmol L^{-1} HNO_3 in water with a flow of 0.9 mL min^{-1} was used. The injection volume was 4 µL for the cation separation. Detection on both systems was performed with a conductivity detector. The calibration was done by a dilution of stock solutions prepared from NH_4Cl and $NaNO_3$ in the presence of 30 mmol L^{-1} $Na_2S_2O_8$ to obtain a comparable matrix as in the real samples from the mineralization experiments.

6.4 Results and Discussion

6.4.1 Influence of the pH on the oxidation of reference substances in a batch reactor system

In order to evaluate the influence of the initial pH in the oxidation of nitrogen containing organic molecules by heat activated persulfate, batch rector experiments with two reference substance (caffeine and glycine) were conducted. The initial pH of the system was chosen at pH 2 for the oxidation at acidic conditions and pH 12 for the alkaline oxidation experiments. The overall oxidation of the analyte was monitored by the amount of total organic carbon present at each time point during the oxidation. Dissolved inorganic carbon as an oxidation product during the alkaline oxidation was eliminated during the TOC analysis by acidification and sparging of the sample. The inorganic nitrogen species nitrite, nitrate and ammonium were monitored by IC measurements at each time point. For glycine, the results obtained for the oxidation under acidic conditions are shown in **Figure 6.2.**

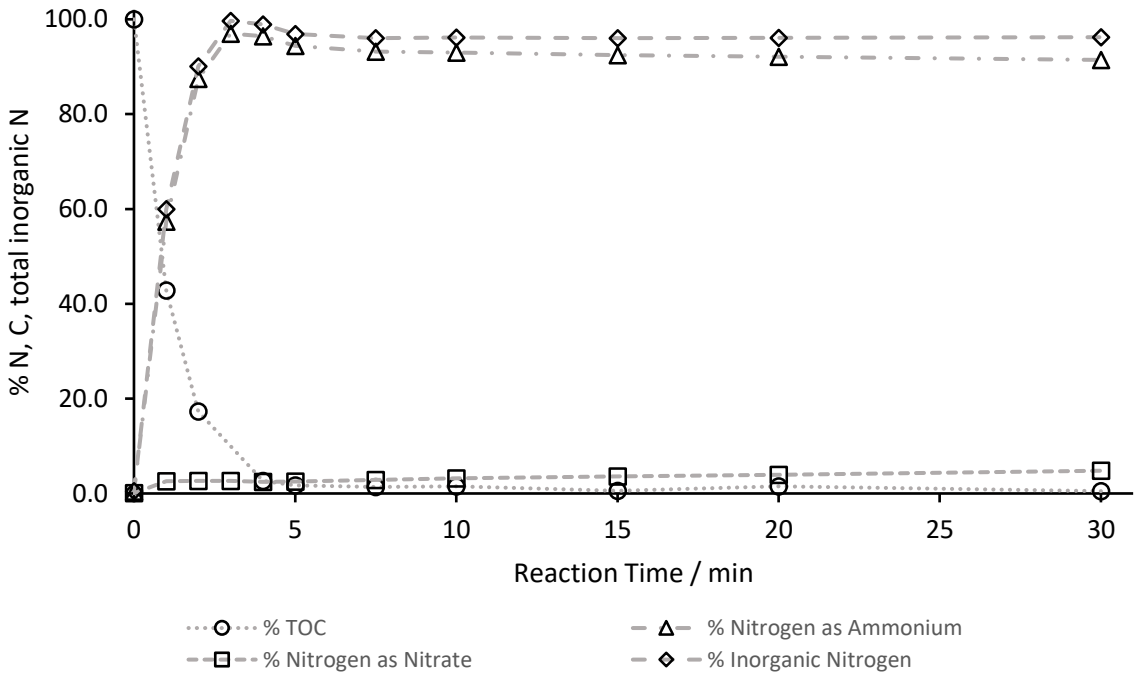

Figure 6.2: Oxidation of glycine by heat activated persulfate at an initial pH of 2 adjusted by sulfuric acid

In comparison, the results obtained under the same experimental conditions except for the adjustment of the initial pH in the system to pH 12 by potassium hydroxide is shown in **Figure 6.3.**

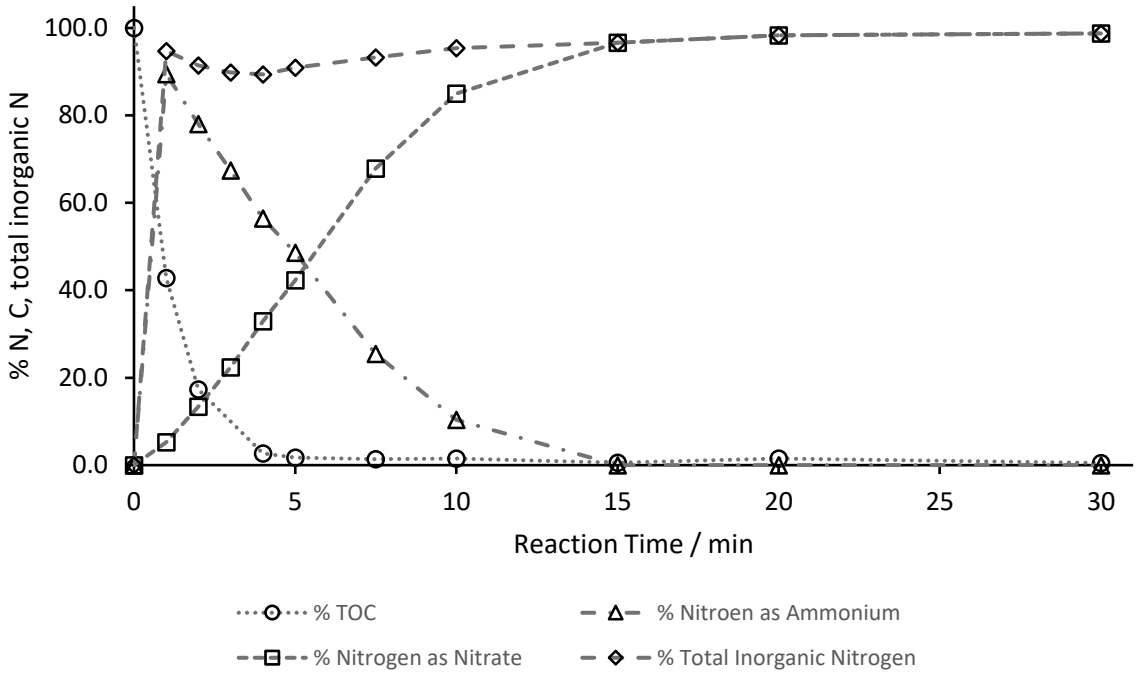

Figure 6.3: Oxidation of glycine by heat activated persulfate at an initial pH of 12 adjusted by potassium hydroxide

Under initially acidic conditions, glycine is almost immediately converted to CO_2 and ammonium in the first three minutes of the experiment. The oxidation of ammonium to nitrate is comparably slower, after 30 min of oxidation, only 4.8 % of the nitrogen is present in the form of nitrate. Under initially alkaline conditions starting at pH 12, 89.5 % of the nitrogen present in the organic analyte is also converted to ammonium within the first minute of the reaction, but the oxidation from ammonium to nitrate is faster than under acidic conditions. Within the first 15 minutes, 96.7 % of the nitrogen is oxidized to nitrate. After 30 min reaction time, 98.8 % of the initially present organic nitrogen can be recovered as nitrate. Surprisingly, literature on the kinetics of the oxidation of ammonium to nitrate by persulfate at different pH conditions is not available as most studies focus solely on the recovery as nitrate after the complete oxidation procedure.[217]

The results from the oxidation of caffeine under acidic and alkaline conditions are shown in **Figure 6.4** and **Figure 6.5** respectively.

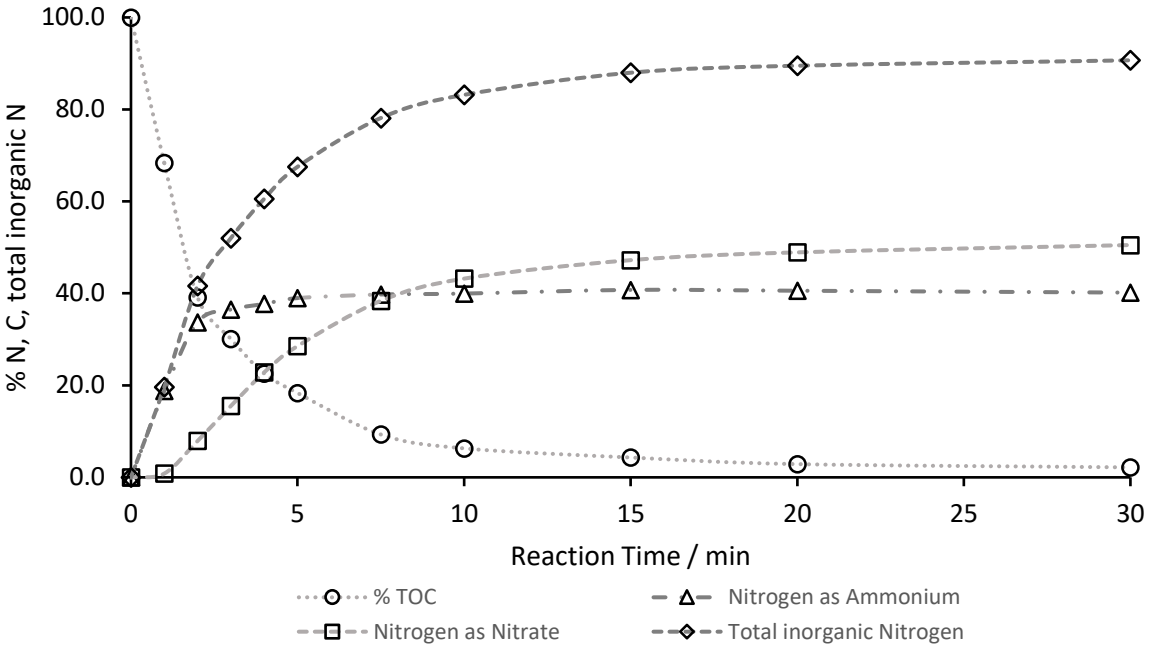

Figure 6.4: Oxidation of caffeine by heat activated persulfate at an initial pH of 2 adjusted by sulfuric acid

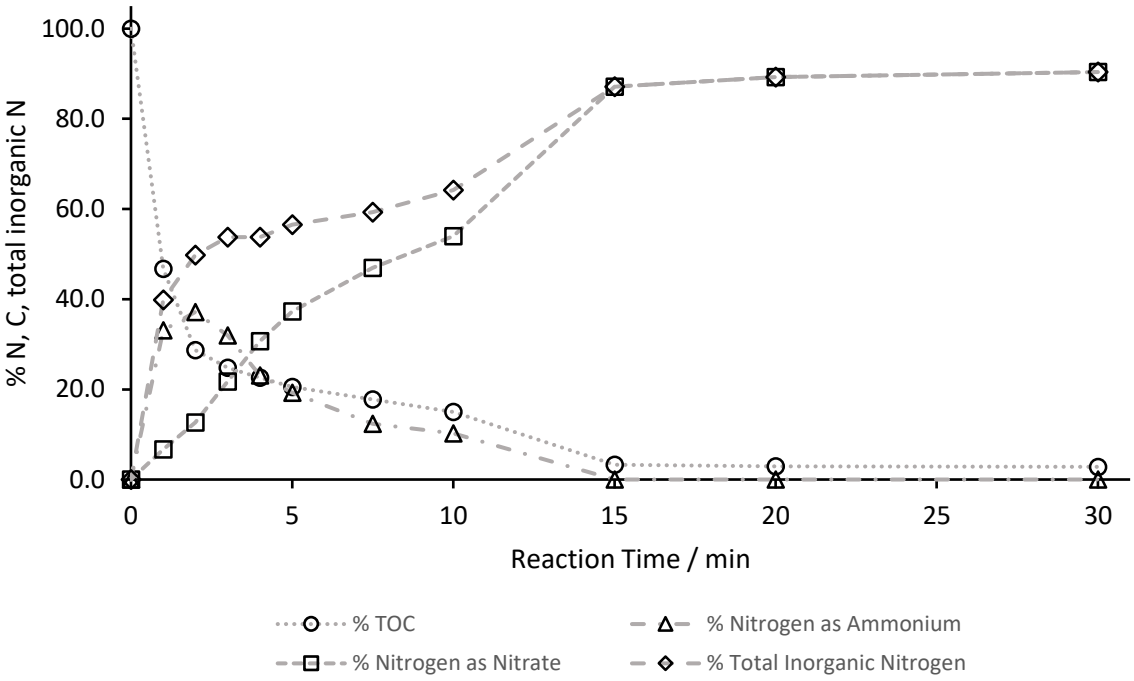

Figure 6.5: Oxidation of caffeine by heat activated persulfate at an initial pH of 12 adjusted by potassium hydroxide

In comparison to glycine, the mineralization of caffeine by heat activated persulfate is overall slower as indicated by the decrease of the organic carbon in the system. This could be due to the fact, that the nitrogen atoms in caffeine are bound in heterocyclic carbon ring systems and

not in a freely accessible amino group. For caffeine, it takes 15 min for the TOC to drop below 5 % of the initially introduced carbon. Even within 30 min of oxidation, 2-3 % of the carbon cannot be oxidized to CO_2 and remain in the system in a non-purgeable carbon form. These results match with the observations from the batch experiment presented in **Chapter 5** as well as for the mineralization experiments in **Chapter 4**, that analytes like caffeine with C-N double bond systems are more resistant to oxidation by heat activated persulfate, than analytes with single C-N bonds like in the amino group of glycine.[156, 215] Under acidic conditions, the reaction of heat activated persulfate and caffeine leads to a mixture of 50.5 % nitrate and 40.2 % ammonium after 30 min. The remaining part of the initially present nitrogen in the analyte is either bound in the remaining organic fraction, or present in a different inorganic form that is not detectable by the present IC method. Nitrite was monitored in all of the measurements but was never present in quantifiable amounts in the batch reactor samples (< 0.5 mg L^{-1}). In the comparison of the formation of nitrate and ammonium between the initially alkaline and acidic reaction of heat activated persulfate with caffeine, parallel formation of both species can be observed in the first 5 min of the reaction. In contrast to the experiment at low pH, in the alkaline system ammonium is oxidized to nitrate in parallel to the mineralization of caffeine. After 15 min, the initially produced ammonium is almost completely oxidized to nitrate, whereas for the low pH system, a mixture of 40.8 % ammonium and 47.2 % nitrate was obtained. From these results, it can be concluded, that the alkaline oxidation can offer significant advantages for the application as an oxidation reaction in the LC-IRMS setup, as one of the major requirements of the oxidation system is the complete transformation of nitrogen in the analyte into a single species that can be used for the subsequent transformation into an IRMS measurable gaseous form to avoid isotopic fractionation during the oxidation step.

In addition to the measurements of TOC and inorganic nitrogen species, the change of the pH in the reactor system was also measured for the alkaline oxidation of glycine and caffeine. The drop of the pH in the system during the oxidation of the respective analyte is shown in **Figure 6.6**.

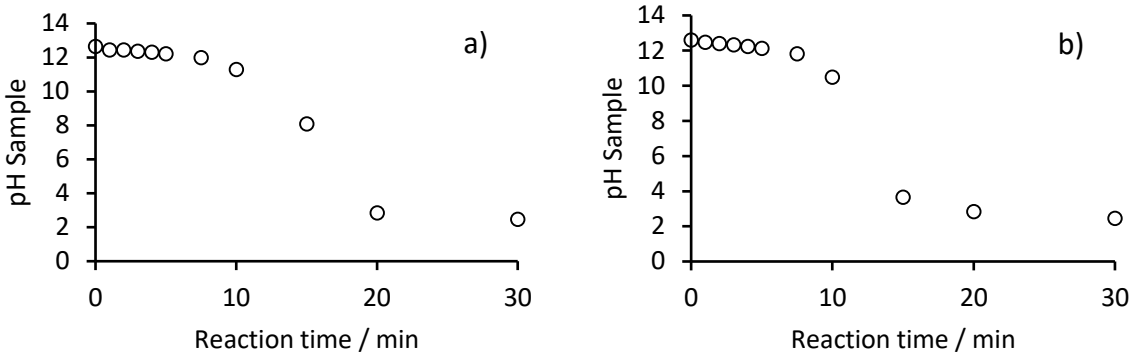

Figure 6.6: Change of the pH in the system during the batch oxidation under initially alkaline conditions, a) Oxidation of glycine, b) Oxidation of caffeine

For both analytes, a significant drop of the pH in the reactor could be observed after 10 min reaction time. The change of the pH in the system can be attributed to the hydrolysis of persulfate at high temperatures in alkaline solutions according to Equation 6.1.[188]

$$S_2O_8{}^{2-} + H_2O \longrightarrow 2\,SO_4{}^{2-} + \tfrac{1}{2}\,O_2 + 2H^+ \qquad \textbf{(6.1)}$$

An application for the shift of the pH in a comparable batch measurement system for the parallel determination of total nitrogen (as nitrate) and phosphorous (as phosphate) has been published by De Borba *et al.* in 2014.[216] For the measurement of total nitrogen and phosphorus, the oxidation is performed at 120 °C in closed vials for around 60 min. Depending on the initial ratio of persulfate to hydroxide in the system, final pH levels of approximately 2 (persulfate to hydroxide ratio of 2:1 and 1:1) or pH 11 (persulfate to hydroxide ratio of 1:2) could be observed. In contrast to the application of De Borba *et al.*, where a shift of the pH from alkaline to acidic was desired due to benefits for the phosphate measurement, in the context of an oxidation setup for the LC-IRMS application, the initial ratio of persulfate to hydroxide has to be chosen in a way that the conditions during the oxidation remain alkaline to favor the oxidation of ammonium to nitrate. As indicated by **Figure 6.6** the pH in the batch system stayed above pH 10 in the first 10 min of the oxidation reaction. Considering the relatively short reaction times currently possible in the LC-IRMS interface reactor (approximately 17-43 s) the conditions should be applicable for the fast oxidation of ammonium to nitrate in the interface setup.

6.4.2 Application of the alkaline oxidation conditions in the IsoLink® LC-IRMS interface

For the oxidation reaction in the flow-through reactor of the LC-IRMS interface, commonly used combinations of LC effluent entering the interface, as well as standard flows and concentrations of oxidation reagent (100 g L^{-1} $Na_2S_2O_8$) and NaOH solution (50 g L^{-1}) were used. The resulting pH values measured after the oxidation reaction at different flow rate from the HPLC (and thereby different NaOH concentration) as well as at different temperatures of the oxidation reactor and in combination with an infusion of organic analyte (glycine, 50 mg L^{-1} (C)) are shown in **Table 6.1.**

Table 6.1: Influence of the HPLC flow, oxidation reactor temperature and presence of an organic analyte (156.3 mg L^{-1} ≙ 50 mg L^{-1} (C)) on the pH of the LC-IRMS interface eluent

Flow (µL min^{-1})						
Water (HPLC)	NaOH (50 g L^{-1})	$Na_2S_2O_8$ (100 g L^{-1})	Total Flow (µL min^{-1})	**pH (30 °C)**	**pH (100 °C)**	**pH (100 °C + Analyte)**
200	50	50	300	12.71	12.61	12.58
300	50	50	400	12.64	12.55	12.53
400	50	50	500	12.57	12.48	12.48
500	50	50	600	12.53	12.46	12.45
600	50	50	700	12.54	12.36	12.43

The pH conditions in the effluent of the interface did not drop below pH 12 for all evaluated combinations of flows from 200 µL min^{-1} (lower than commonly used in LC-IRMS applications) to a total flow of 700 µL min^{-1} which is the maximal flow allowed for the membrane separation unit in the LC-IRMS interface.[158] From the comparison of the pH values obtained at a temperature of 30 °C of the oxidation oven compared to an oxidation at 100 °C, only a relatively low drop of the pH could be observed for all flows. The addition of glycine as an exemplary analyte did also not lead to a significant change of the pH.

To further evaluate the oxidation under alkaline conditions in the LC-IRMS interface, glycine was used as a reference compound, as the batch experiments indicated a fast oxidation of the organic carbon and almost quantitative conversion of the initially present nitrogen to nitrate if the reaction time is long enough for the complete oxidation from ammonium to nitrate. In **Table 6.2**, the results for the oxidation of glycine at a set of different HPLC flow conditions are shown. In part a), the oxidation agent concentration was 100 g L^{-1} $Na_2S_2O_8$, whereas for the results shown in part b), the oxidation agent concentration was increased to 200 g L^{-1}. For each set of flows and oxidation agent concentrations, the nitrogen recovery as % NO_3^- in relation to the initially present organic nitrogen is shown. For the interpretation of the results, the interaction of the changed parameters in the experimental setup have to be taken into account. With an increase of the analyte flow into the system, three parameters are simultaneously changed. With higher infusion flows, the analyte concentration in the oxidation reactor increases (ratio of analyte flow to total flow), at the same time the concentration of the oxidation agent is decreased (lower ratio of oxidation agent flow to HPLC flow) and the residence time of the mixture in the oxidation reactor is decreased (higher overall flow). Thereby, an increased analyte flow negatively affects the oxidation efficiency in three ways. Vice versa, the reduction of the analyte flow should theoretically have a positive effect on the oxidation process.

Table 6.2: Nitrogen recovery as nitrate after the alkaline glycine oxidation in the IsoLink LC-IRMS interface reactor.
a) Oxidation agent concentration of 100 g L^{-1} $Na_2S_2O_8$, b) Oxidation agent concentration of 200 g L^{-1} $Na_2S_2O_8$

a)

Flow (µL min^{-1})				c_0 (Glycine)	c (NO_3^- after Oxidation)	**Recovery N**	**c ($Na_2S_2O_8$)**	Reaction Time
Analyte Flow	NaOH (50 g L^{-1})	**$Na_2S_2O_8$ (100 g L^{-1})**	Total Flow	(mg L^{-1} (N))	(mg L^{-1} (N))	**%**	**(g L^{-1})**	(s)
600	50	50	700	25.0	1.9	**7.5**	**7.1**	17
500	50	50	600	24.3	2.2	**8.9**	**8.3**	20
400	50	50	500	23.3	3.4	**14.5**	**10.0**	24
300	50	50	400	21.9	8.1	**37.1**	**12.5**	29
200	50	50	300	19.4	14.9	**76.6**	**16.7**	39

b)

Flow (µL min^{-1})				c_0 (Glycine)	c (NO_3^- after Oxidation)	**Recovery N**	**c ($Na_2S_2O_8$)**	Reaction Time
Analyte Flow	NaOH (50 g L^{-1})	**$Na_2S_2O_8$ (200 g L^{-1})**	Total Flow	(mg L^{-1} (N))	(mg L^{-1} (N))	**%**	**(g L^{-1})**	(s)
600	50	50	700	25.0	5.1	**20.6**	**14.3**	17
500	50	50	600	24.3	7.9	**32.4**	**16.7**	20
400	50	50	500	23.3	12.6	**54.1**	**20.0**	24
300	50	50	400	21.9	17.5	**80.1**	**25.0**	29
200	50	50	300	19.4	18.6	**95.5**	**33.3**	39

From the results shown in **Table 6.2 a)**, an increase in the nitrate recovery from 7.5 % to 76.6 % could be observed when the flow of the glycine solution were decreased from 600 to 200 µL min^{-1}. At the same time, as a result of the overall lower system flow in the oxidation reactor, the reaction time increased from 17 s to 39 s. In comparison, in **Table 6.2 b)**, the overall concentration of oxidation agent in the system was increased from 100 g L^{-1} $Na_2S_2O_8$ to 200 g L^{-1} $Na_2S_2O_8$ whereas the remaining flow conditions were kept constant. On the one hand, an increased oxidation agent concentration leads to an overall improved nitrogen recovery at each flow level (recoveries presented in **Table 6.2 a)** in comparison to **Table 6.2. b)**). On the other hand, the increased oxidation agent concentration by a factor of two had a lower effect on the nitrogen recovery as an increase in the reaction time from 17 to 39 s.

For low system flows (300 µL mim^{-1}) and high oxidation agent concentrations (200 g L^{-1} $Na_2S_2O_8$), nitrogen recoveries of more than 95 % can be obtained using the standard LC-IMRS interface. Lower flows are not applicable in the context of LC-IRMS, as low sensitivity of the instrument requires high sample amounts to be introduced which cannot be efficiently separated on columns designed for flow conditions in the region below 100 µL min^{-1}. The amount of oxidation agent added in the interface is finally limited by the solubility of $Na_2S_2O_8$, which is 547.6 g L^{-1} at 20 °C.[173] The main drawback of increased oxidation agent concentrations is that the amount of oxygen produced during the oxidation is increased in parallel. For the conventional LC-IMRS setup, this leads to a fast destruction of the filament in the ionization source and decreased precision of the isotope measurements, but excess oxygen was shown to be removable by the use of an additional copper reduction system for the interface which would also have to be applied if gas phase reduction of nitrogen species to N_2 need to be performed as the last step in the transformation of nitrate to the IRMS measurement gas.[46]

As the residence time in the oxidation reactor was identified as one of the main parameters affecting the nitrogen recoveries, the total flow in the system was further reduced by decreasing the flow of the NaOH solution from 50 to 25 µL min^{-1} for the following infusion experiments. Besides glycine, potassium nitrate, ammonium sulfate, caffeine, urea, and acetonitrile were additionally used to obtain individual nitrate recoveries for the LC-IMRS interface under alkaline conditions (**Table 6.3**).

Table 6.3: Oxidation experiments at alkaline pH in the LC-IRMS interface reactor. Initial analyte concentrations were kept constant at 50 mg L^{-1} (N).

a) Potassium nitrate, b) Ammonium sulfate, c) Caffeine, d) Glycine, e) Urea, f) Acetonitrile

a) **Flow (µL min^{-1})**				c_0 KNO_3	c (NO_3^- after Oxidation)	Recovery N	c ($Na_2S_2O_8$)	Reaction Time
Analyte Flow	NaOH (50 mg L^{-1})	$Na_2S_2O_8$ (200 g L^{-1})	Total Flow	(mg L^{-1} (N))	(mg L^{-1} (N))	%	(g L^{-1})	(s)
200	25	50	275	36.4	36.4	101	36.4	43
300	25	50	375	40.0	40.0	102	26.7	31

b)				c_0 $(NH_4)_2SO_4$	c (NO_3^- after Oxidation)	Recovery N	c ($Na_2S_2O_8$)	Reaction Time
Analyte Flow	NaOH (50 mg L^{-1})	$Na_2S_2O_8$ (200 g L^{-1})	Total Flow	(mg L^{-1} (N))	(mg L^{-1} (N))	%	(g L^{-1})	(s)
200	25	50	275	36.4	36.3	99.8	36.4	43
300	25	50	375	40.0	40.1	100	26.7	31

c)				c_0 Caffeine	c (NO_3^- after Oxidation)	Recovery N	c ($Na_2S_2O_8$)	Reaction Time
Analyte Flow	NaOH (50 mg L^{-1})	$Na_2S_2O_8$ (200 g L^{-1})	Total Flow	(mg L^{-1} (N))	(mg L^{-1} (N))	%	(g L^{-1})	(s)
200	25	50	275	36.4	24.0	66.1	36.4	43
300	25	50	375	40.0	14.5	36.2	26.7	31

d)				c_0 Glycine	c (NO_3^- after Oxidation)	Recovery N	c ($Na_2S_2O_8$)	Reaction Time
Analyte Flow	NaOH (50 mg L^{-1})	$Na_2S_2O_8$ (200 g L^{-1})	Total Flow	(mg L^{-1} (N))	(mg L^{-1} (N))	%	(g L^{-1})	(s)
200	25	50	275	36.4	31.1	85.5	36.4	43
300	25	50	375	40.0	20.1	50.2	26.7	31

e)				c_0 Urea	c (NO_3^- after Oxidation)	Recovery N	c ($Na_2S_2O_8$)	Reaction Time
Analyte Flow	NaOH (50 mg L^{-1})	$Na_2S_2O_8$ (200 g L^{-1})	Total Flow	(mg L^{-1} (N))	(mg L^{-1} (N))	%	(g L^{-1})	(s)
200	25	50	275	36.4	28.2	77.4	36.4	43

f)				c_0 Acetonitrile	c (NO_3^- after Oxidation)	Recovery N	c ($Na_2S_2O_8$)	Reaction Time
Analyte Flow	NaOH (50 mg L^{-1})	$Na_2S_2O_8$ (200 g L^{-1})	Total Flow	(mg L^{-1} (N))	(mg L^{-1} (N))	%	(g L^{-1})	(s)
200	25	50	275	36.4	22.7	62.5	36.4	43

From the initially introduced analyte concentration, theoretically maximal achievable nitrate recoveries (100 % N oxidation to nitrate) were calculated. After taking the dilution of the analytes in the interface by the NaOH solution and the oxidation agent into account, nitrate recoveries were determined for each compound and set of reaction conditions. The infusion of nitrate solution (**Table 6.3 a)**) was used as a control experiment to prove the precision of the dilution by the three independent pumps in the system which could have an effect on the results (HPLC infusion pump and interface pumps for the oxidation agent and NaOH solution). For nitrate, recoveries of 101 % and 102 % were determined at system flows of 275 µL min^{-1} and 375 µL min^{-1} respectively. Therefore, it can be concluded that the pump system was optimized to produce exact flows that allow a reliable calculation of the nitrogen recovery after oxidation. In addition, introduction of excess nitrate by the reagent solutions could be excluded. In the next step, an ammonium sulfate solution was infused into the interface (**Table 6.3 b)**). At the given flow conditions, a complete oxidation of the nitrogen introduced as ammonium to nitrate could be achieved. This indicates that for more complex molecules, the initial oxidation of the analyte molecule is the critical step in the oxidation rather than the transformation of ammonium to nitrate. For caffeine (**Table 6.3. c)**), which is known to be comparably recalcitrant to oxidation by heat activated persulfate, nitrate recoveries of 66.1 and 36.2 % for system flows of 275 µL min^{-1} and 375µL min^{-1} could be obtained. [35, 101, 215] For glycine, which is oxidized faster as indicated by the batch experiments, recoveries of 85.5 % and 50.2 % for residence times of 43 s and 31 s respectively were determined. This is comparable to the results presented in **Figure 6.2 b)** for system flows in the interface of 300 µL min^{-1} and 400 µL min^{-1} although the flow of the NaOH solution was decreased by 50 %. For urea and acetonitrile (**Table 6.3 e)** and **f)**), recoveries of 77.4 % and 62.5 % respectively were obtained at system flows of 275 µL min^{-1}. Especially for acetonitrile, the nitrate recovery of 62.5 % is promising, as C-N double bonds are known to be recalcitrant under acidic persulfate oxidation conditions and the bond energy in C-N triple bonds is even higher.[156] To further optimize the oxidation, the concentration of oxidation agent, or the residence time in the oxidation reactor have to be significantly increased in order to apply the oxidation procedure for the measurement of isotope ratios, as a complete conversion would be desirable for sensitive and accurate CSIA. As already shown for $\delta^{13}C$ in **Chapter 4**, correct isotope ratios can also be measured with lower oxidation efficiencies, if identical treatment of the analyte and reference material is ensured. Besides an increase in oxidation agent

concentration, the change of the oxidation reactor design could be necessary to increase the nitrate recovery. In the standard design, the reactor consists of a stainless steel tubing that is coiled around a heating cartridge, the length of this capillary could be increased to allow longer reaction times without changes in the system flows. As increased reactor volumes after the LC separation also increase the longitudinal diffusion and would negatively affect the separation, the changes have to be balanced in a way that close to 100 % recovery is obtained without compromising the previously obtained chromatographic separation. As already observed for the infusion experiments conducted in **Chapter 4.4.4** for the oxidation efficiency of δ^{13}C measurements in the IsoLink® interface, an increase in the observed recoveries can be expected if the sample introduction is switched from continuous infusion to actual chromatographic analyte peaks. If the analytes reach the oxidation reactor after HPLC separation, the local ratio of oxidation agent to analyte is higher as a result of the Gaussian concentration profile of the analyte peak as a result of chromatographic peak broadening. In depth evaluations of the nitrogen recoveries could be performed as presented for the carbonate referencing strategy, with a suitable nitrogen reference compound and an online quantification.

6.5 Conclusion

By comparison of the oxidation products formed during the oxidation by heat activated persulfate at acidic and alkaline conditions, suitable reaction conditions for the transformation of nitrogen bound in organic analytes or present as ammonium to nitrate could be identified. Nitrate could serve as an intermediate species in the transformation to the final nitrogen measurement gas used for the IRMS measurement. The oxidation at alkaline pH conditions could successfully be transferred from a batch reactor system to the continuous oxidation in a flow-through system of a commercially available LC-IRMS interface. By the direct infusion of nitrogen containing analytes into the oxidation reactor and subsequent IC measurements, good nitrate recoveries could be obtained. Further improvements to the nitrate recovery could be realized by increasing the length of the heated zone of the flow-through reactor system. With a subsequent reduction of nitrate to NO, a membrane gas separation and reduction of NO to N_2 in the gas phase, the wet chemical oxidation at alkaline conditions could be an alternative for high temperature catalytic conversion systems for the development of a LC-IRMS system for δ^{15}N measurements.

7 General Conclusion and Outlook

7.1 General Conclusion

One of the main fields of applications for LC-IRMS is in the field of food authenticity. Many recent publications focus on the authenticity of sugars in honey from various sources, although detection of honey adulteration was already established in 2006 by Cabañero *et al.* which indicates the ongoing interest in further developments in this field.[54, 97, 218-219] The analytical method for the authenticity control of xylitol in food products presented in **Chapter 3** offers new possibilities to identify incorrect labelling of the utilized raw materials. With the developed LC-IRMS method, previously published trends in EA-IRMS based measurements on xylitol bulk material could be validated and further elucidated.[143] The identified offset between xylitol and the bulk plant raw material observed with both IRMS techniques is probably due to fractionation between the lignin and hemicellulose fractions. Detailed isotopic information for bulk plant material is present in the literature, but fractionation between different molecule classes in the material is not available and could be subject for more detailed studies in the future.

In the context of the evaluation of oxidation conditions in the LC-IRMS interface for δ^{15}N measurements, problems with incomplete oxidation that were already observed with the standard setup for δ^{13}C measurements were evaluated in **Chapter 4**. The detailed insights into the persulfate based oxidation process in the LC-IMRS interface offer new possibilities for method improvement during the development for compound specific δ^{13}C measurements. With the help of the carbonate referencing strategy, oxidation conditions of target analytes can be systematically evaluated during the method development step to identify recalcitrant compounds that require special oxidation conditions such as nitrogen containing ring systems or halogenated analytes.[45, 61] A detailed evaluation of the oxidation conditions is currently not performed in many published applications, but should be established as an additional quality control tool to improve the trueness of LC-IRMS measurements with newly developed methods.

Besides the application in an LC-IMRS, persulfate oxidation is commonly used in large scale applications such as the removal of environmental contaminants or persistent compounds in wastewater.[178] The speciation of the final mineralization products of nitrogen containing

compounds under different pH conditions as presented in **Chapter 5 and 6** could be of interest in these fields, as nitrate as well as ammonium are of concern in the environment with concentration limits of 50 mg L^{-1} for nitrate and 0.5 mg L^{-1} for ammonium in groundwater in Germany.[220] The unspecific oxidation of nitrogen containing matrix compounds as well as target molecules could lead to significant production of ammonium and nitrate depending on the pH conditions in the water or soil. In addition, high temperature catalytic conversion methods for TOC and TNb measurements are used routinely in environmental monitoring, in the presence of high persulfate concentrations, significantly lower TNb levels are measured for organic nitrogen containing molecules and ammonium as presented in **Chapter 5**. This could lead to an underestimation of the nitrogen load in samples after persulfate treatment for remediation purposes.

The results of the oxidation at alkaline conditions in the LC-IRMS interface reactor presented in **Chapter 6** suggest that the nitrate recovery has to be further improved to reach quantitative recoveries desired for IRMS measurements. Besides the proposed options of increased reaction times through lower flow rates in the reactor, or an increased length of the capillary of the reactor, the addition of metal catalysts to the oxidation reaction could be considered in further experiments. The alkaline activation of persulfate is still not completely understood and experiments with additional catalysts have not been published, in contrast to the oxidation at acidic conditions, where catalysts such as Ag^{+}, Fe^{2+}, Mn^{2+} or Co^{2+} have been evaluated to increase the carbon oxidation efficiency. [155, 178]

7.2 Outlook

Based on the initial literature available for the mineralization of nitrogen containing molecules by sulfate radicals as used for the wet-chemical oxidation in the LC-IRMS interface, the nitrogen containing intermediate and end products were not clearly identified either for acidic nor for alkaline reaction conditions. In order to develop a LC-IMRS interface for δ^{15}N measurements, a single nitrogen containing, IRMS measurable form has to be reached as an intermediate or final species to obtain representative compound specific isotope ratios. The evaluation of the speciation of the nitrogen containing mineralization products and nitrogen mass balances for the oxidation of exemplary analytes lead to the conclusion that the acidic oxidation environment used for δ^{13}C measurements could not be employed for development of the δ^{15}N IRMS setup, as nitrate and ammonium were produced, in parallel as final reaction products in the timespan that would be applicable for an online reaction interface. However, the designed analytical approaches could be transferred for the elucidation of the alkaline mineralization products. Under these conditions, promising results could be obtained, as the intermediately formed ammonium is oxidized to nitrate in a timeframe that could be realized in an online instrument after further optimization. Nitrate would be utilized as an intermediate species after the oxidation, which contains the isotopic N information of previously LC separated analytes.

In order to integrate the wet chemical oxidation at alkaline conditions into the measurement of compound specific nitrogen isotope ratios, the oxidation could be combined with a subsequent wet chemical reduction of NO_3^- to NO followed by a gas separation and reduction to N_2. After the oxidation to nitrate, published techniques such as the nitrate reduction to NO by V(III)Cl_3 solution can be used to transform the nitrate into a gaseous species that can be separated by the membrane system of the LC-IRMS interface.[122, 221] NO could be measured directly on the IRMS system or further reduction to N_2 is performed by a copper filled gas phase reduction oven, which would in addition scavenge excess oxygen produced during the initial oxidation process.[46] In this combination, LC-IRMS could become a powerful tool for the measurement of compound specific dual isotope information of carbon and nitrogen on a single analytical platform. This setup for the compound specific δ^{15}N measurement could be an alternative to the high temperature catalytic conversion LC-IRMS system, which was developed by Federherr and co-workers, but is not commercially available until now.[48]

Regardless of the oxidation technique employed for the transformation in the LC-IRMS interface, the commercial availability of an LC-IRMS interface for the combined measurement of δ^{13}C and δ^{15}N isotope ratios would lead to new possibilities in many fields of research. Dual element studies as for example performed for the herbicide glyphosate by Mogusu *et al.*, can offer a significantly higher power of discrimination than comparisons based on one element alone.[212] As many target molecules for current LC-IRMS investigations like amino acids, pharmaceuticals or pesticides contain nitrogen, an analytical solution for a combined δ^{13}C and δ^{14}N isotope measurement would offer significant advantages for the research in these fields.

Chapter 8: Sources

1. Jochmann, M. A.; Schmidt, T. C., *Compound-specific stable isotope analysis*. Royal Society of Chemistry: Cambridge, 2012.
2. van Grieken, R.; de Bruin, M., Nomenclature for radioanalytical chemistry (IUPAC Recommendations 1994). In *Pure Appl. Chem.*, 1994; Vol. 66, p 2513.
3. Faure, G.; Mensing, T. M., *Isotopes: Principles and Applications, 3rd Edition*. Wiley: Hoboken, NJ, 2004.
4. Fry, B., *Stable isotope ecology*. Springer: New York, NY, 2006.
5. Berglund, M.; Wieser, M. E., Isotopic compositions of the elements 2009 (IUPAC Technical Report). *Pure Appl. Chem.* **2011,** *83* (2), 397-410.
6. Coplen, T. B., Guidelines and recommended terms for expression of stable-isotope-ratio and gas-ratio measurement results. *Rapid Commun. Mass Spectrom.* **2011,** *25* (17), 2538-2560.
7. Muccio, Z.; Jackson, G. P., Isotope ratio mass spectrometry. *Analyst* **2009,** *134* (2), 213-222.
8. McKinney, C. R.; McCrea, J. M.; Epstein, S.; Allen, H. A.; Urey, H. C., Improvements in Mass Spectrometers for the Measurement of Small Differences in Isotope Abundance Ratios. *Rev. Sci. Instrum.* **1950,** *21* (8), 724-730.
9. Brenna, J. T.; Corso, T. N.; Tobias, H. J.; Caimi, R. J., High-precision continuous-flow isotope ratio mass spectrometry. *Mass Spectrom. Rev.* **1997,** *16* (5), 227-258.
10. Aelion, C. M., *Environmental isotopes in biodegradation and bioremediation*. CRC Press: Boca Raton, Fla. [u.a.], 2010.
11. Urey, H. C., The thermodynamic properties of isotopic substances. *Journal of the Chemical Society (Resumed)* **1947,** (0), 562-581.
12. Schauble, E. A.; Ghosh, P.; Eiler, J. M., Preferential formation of 13C–18O bonds in carbonate minerals, estimated using first-principles lattice dynamics. *Geochim. Cosmochim. Acta* **2006,** *70* (10), 2510-2529.
13. Wang, Z.; Schauble, E. A.; Eiler, J. M., Equilibrium thermodynamics of multiply substituted isotopologues of molecular gases. *Geochim. Cosmochim. Acta* **2004,** *68* (23), 4779-4797.

14. Elsner, M.; Zwank, L.; Hunkeler, D.; Schwarzenbach, R. P., A New Concept Linking Observable Stable Isotope Fractionation to Transformation Pathways of Organic Pollutants. *Environ. Sci. Technol.* **2005,** *39* (18), 6896-6916.

15. Crosson, E. R.; Ricci, K. N.; Richman, B. A.; Chilese, F. C.; Owano, T. G.; Provencal, R. A.; Todd, M. W.; Glasser, J.; Kachanov, A. A.; Paldus, B. A.; Spence, T. G.; Zare, R. N., Stable Isotope Ratios Using Cavity Ring-Down Spectroscopy: Determination of 13C/12C for Carbon Dioxide in Human Breath. *Anal. Chem.* **2002,** *74* (9), 2003-2007.

16. van Geldern, R.; Nowak, M. E.; Zimmer, M.; Szizybalski, A.; Myrttinen, A.; Barth, J. A. C.; Jost, H.-J., Field-Based Stable Isotope Analysis of Carbon Dioxide by Mid-Infrared Laser Spectroscopy for Carbon Capture and Storage Monitoring. *Anal. Chem.* **2014,** *86* (24), 12191-12198.

17. Brand, W. A.; Geilmann, H.; Crosson, E. R.; Rella, C. W., Cavity ring-down spectroscopy versus high-temperature conversion isotope ratio mass spectrometry; a case study on δ2H and δ18O of pure water samples and alcohol/water mixtures. *Rapid Commun. Mass Spectrom.* **2009,** *23* (12), 1879-1884.

18. Diomande, D. G.; Martineau, E.; Gilbert, A.; Nun, P.; Murata, A.; Yamada, K.; Watanabe, N.; Tea, I.; Robins, R. J.; Yoshida, N.; Remaud, G. S., Position-Specific Isotope Analysis of Xanthines: A 13C Nuclear Magnetic Resonance Method to Determine the 13C Intramolecular Composition at Natural Abundance. *Anal. Chem.* **2015,** *87* (13), 6600-6606.

19. Rossmann, A.; Butzenlechner, M.; Schmidt, H.-L., Evidence for a Nonstatistical Carbon Isotope Distribution in Natural Glucose. *Plant Physiol.* **1991,** *96* (2), 609.

20. Weilacher, T.; Gleixner, G.; Schmidt, H.-L., Carbon isotope pattern in purine alkaloids a key to isotope discriminations in C1 compounds. *Phytochemistry* **1996,** *41* (4), 1073-1077.

21. Vanhaecke, F.; Degryse, P., *Isotopic Analysis : Fundamentals and Applications Using ICP-MS*. John Wiley & Sons: Weinheim, 2012.

22. Newman, A., Product Review: The Precise World of Isotope Ratio Mass Spectrometry. *Anal. Chem.* **1996,** *68* (11), 373A-377A.

23. Werner, R. A.; Brand, W. A., Referencing strategies and techniques in stable isotope ratio analysis. *Rapid Commun. Mass Spectrom.* **2001,** *15* (7), 501-519.

24. Murphey, B. F., The Temperature Variation of the Thermal Diffusion Factors for Binary Mixtures of Hydrogen, Deuterium, and Helium. *Physical Review* **1947,** *72* (9), 834-837.

25. Fraser, I.; Meier-Augenstein, W.; Kalin, R. M., The role of stable isotopes in human identification: a longitudinal study into the variability of isotopic signals in human hair and nails. *Rapid Commun. Mass Spectrom.* **2006,** *20* (7), 1109-1116.

26. Nachev, M.; Jochmann, M. A.; Walter, F.; Wolbert, J. B.; Schulte, S. M.; Schmidt, T. C.; Sures, B., Understanding trophic interactions in host-parasite associations using stable isotopes of carbon and nitrogen. *Parasites & Vectors* **2017,** *10* (1), 90.

27. Benson, S.; Lennard, C.; Maynard, P.; Roux, C., Forensic applications of isotope ratio mass spectrometry—A review. *Forensic Sci. Int.* **2006,** *157* (1), 1-22.

28. Grassineau, N. V.; Mattey, D. P.; Lowry, D., Sulfur Isotope Analysis of Sulfide and Sulfate Minerals by Continuous Flow-Isotope Ratio Mass Spectrometry. *Anal. Chem.* **2001,** *73* (2), 220-225.

29. Schmidt, T.; Zwank, L.; Elsner, M.; Berg, M.; Meckenstock, R.; Haderlein, S., Compound-specific stable isotope analysis of organic contaminants in natural environments: a critical review of the state of the art, prospects, and future challenges. *Anal. Bioanal. Chem.* **2004,** *378* (2), 283-300.

30. Meier-Augenstein, W., Applied gas chromatography coupled to isotope ratio mass spectrometry. *J. Chromatogr. A* **1999,** *842* (1), 351-371.

31. Aguilar-Cisneros, B. O.; López, M. G.; Richling, E.; Heckel, F.; Schreier, P., Tequila Authenticity Assessment by Headspace SPME-HRGC-IRMS Analysis of 13C/12C and 18O/16O Ratios of Ethanol. *J. Agric. Food. Chem.* **2002,** *50* (26), 7520-7523.

32. Rieley, G., Derivatization of organic compounds prior to gas chromatographic-combustion-isotope ratio mass spectrometric analysis: identification of isotope fractionation processes. *Analyst* **1994,** *119* (5), 915-919.

33. Mogusu, E. O.; Wolbert, J. B.; Kujawinski, D. M.; Jochmann, M. A.; Elsner, M., Dual element (15N/14N, 13C/12C) isotope analysis of glyphosate and AMPA by derivatization-gas chromatography isotope ratio mass spectrometry (GC/IRMS) combined with LC/IRMS. *Anal. Bioanal. Chem.* **2015,** *407* (18), 5249-5260.

34. Reinnicke, S.; Juchelka, D.; Steinbeiss, S.; Meyer, A.; Hilkert, A.; Elsner, M., Gas chromatography/isotope ratio mass spectrometry of recalcitrant target compounds: performance of different combustion reactors and strategies for standardization. *Rapid Commun. Mass Spectrom.* **2012,** *26* (9), 1053-1060.

35. Zhang, L.; Kujawinski, D. M.; Jochmann, M. A.; Schmidt, T. C., High-temperature reversed-phase liquid chromatography coupled to isotope ratio mass spectrometry. *Rapid Commun. Mass Spectrom.* **2011,** *25* (20), 2971-2980.

36. Krummen, M.; Hilkert, A. W.; Juchelka, D.; Duhr, A.; Schlüter, H.-J.; Pesch, R., A new concept for isotope ratio monitoring liquid chromatography/mass spectrometry. *Rapid Commun. Mass Spectrom.* **2004,** *18* (19), 2260-2266.

37. Sano, M.; Yotsui, Y.; Abe, H.; Sasaki, S., A new technique for the detection of metabolites labelled by the isotope 13C using mass fragmentography. *Biomed. Mass Spectrom.* **1976,** *3* (1), 1-3.

38. Matthews, D. E.; Hayes, J. M., Isotope-ratio-monitoring gas chromatography-mass spectrometry. *Anal. Chem.* **1978,** *50* (11), 1465-1473.

39. Caimi, R. J.; Brenna, J. T., High-precision liquid chromatography-combustion isotope ratio mass spectrometry. *Anal. Chem.* **1993,** *65* (23), 3497-3500.

40. Godin, J.-P.; Hau, J.; Fay, L.-B.; Hopfgartner, G., Isotope ratio monitoring of small molecules and macromolecules by liquid chromatography coupled to isotope ratio mass spectrometry. *Rapid Commun. Mass Spectrom.* **2005,** *19* (18), 2689-2698.

41. Teffera, Y.; Kusmierz, J. J.; Abramson, F. P., Continuous-Flow Isotope Ratio Mass Spectrometry Using the Chemical Reaction Interface with Either Gas or Liquid Chromatographic Introduction. *Anal. Chem.* **1996,** *68* (11), 1888-1894.

42. Teffera, Y.; Abramson, F. P.; McLean, M.; Vestal, M., Development of an isotope-selective high-performance liquid chromatography detector using chemical-reaction-interface mass spectrometry: application to deuterated cortisol metabolites in urine. *J. Chromatogr. B Biomed. Sci. Appl.* **1993,** *620* (1), 89-96.

43. Bronk, D. A.; Lomas, M. W.; Glibert, P. M.; Schukert, K. J.; Sanderson, M. P., Total dissolved nitrogen analysis: comparisons between the persulfate, UV and high temperature oxidation methods. *Mar. Chem.* **2000,** *69* (1), 163-178.

44. St-Jean, G., Automated quantitative and isotopic (13C) analysis of dissolved inorganic carbon and dissolved organic carbon in continuous-flow using a total organic carbon analyser. *Rapid Commun. Mass Spectrom.* **2003,** *17* (5), 419-428.

45. Kujawinski, D. M.; Zhang, L.; Schmidt, T. C.; Jochmann, M. A., When Other Separation Techniques Fail: Compound-Specific Carbon Isotope Ratio Analysis of Sulfonamide

Containing Pharmaceuticals by High-Temperature-Liquid Chromatography-Isotope Ratio Mass Spectrometry. *Anal. Chem.* **2012,** *84* (18), 7656-7663.

46. Hettmann, E.; Brand, W. A.; Gleixner, G., Improved isotope ratio measurement performance in liquid chromatography/isotope ratio mass spectrometry by removing excess oxygen. *Rapid Commun. Mass Spectrom.* **2007,** *21* (24), 4135-4141.

47. Morrison, D. J.; Taylor, K.; Preston, T., Strong anion-exchange liquid chromatography coupled with isotope ratio mass spectrometry using a Liquiface interface. *Rapid Commun. Mass Spectrom.* **2010,** *24* (12), 1755-1762.

48. Federherr, E.; Willach, S.; Roos, N.; Lange, L.; Molt, K.; Schmidt, T. C., A novel high-temperature combustion interface for compound-specific stable isotope analysis of carbon and nitrogen via high-performance liquid chromatography/isotope ratio mass spectrometry. *Rapid Commun. Mass Spectrom.* **2016,** *30* (7), 944-952.

49. Federherr, E.; Cerli, C.; Kirkels, F. M. S. A.; Kalbitz, K.; Kupka, H. J.; Dunsbach, R.; Lange, L.; Schmidt, T. C., A novel high-temperature combustion based system for stable isotope analysis of dissolved organic carbon in aqueous samples. I: development and validation. *Rapid Commun. Mass Spectrom.* **2014,** *28* (23), 2559-2573.

50. Kirkels, F. M. S. A.; Cerli, C.; Federherr, E.; Gao, J.; Kalbitz, K., A novel high-temperature combustion based system for stable isotope analysis of dissolved organic carbon in aqueous samples. II: optimization and assessment of analytical performance. *Rapid Commun. Mass Spectrom.* **2014,** *28* (23), 2574-2586.

51. Schierbeek, H.; Moerdijk-Poortvliet, T. C. W.; van den Akker, C. H. P.; te Braake, F. W. J.; Boschker, H. T. S.; van Goudoever, J. B., Analysis of [U-13C6]glucose in human plasma using liquid chromatography/isotope ratio mass spectrometry compared with two other mass spectrometry techniques. *Rapid Commun. Mass Spectrom.* **2009,** *23* (23), 3824-3830.

52. Morrison, D. J.; O'Hara, J. P.; King, R. F. G. J.; Preston, T., Quantitation of plasma 13C-galactose and 13C-glucose during exercise by liquid chromatography/isotope ratio mass spectrometry. *Rapid Commun. Mass Spectrom.* **2011,** *25* (17), 2484-2488.

53. Boschker, H. T. S.; Moerdijk-Poortvliet, T. C. W.; van Breugel, P.; Houtekamer, M.; Middelburg, J. J., A versatile method for stable carbon isotope analysis of carbohydrates by high-performance liquid chromatography/isotope ratio mass spectrometry. *Rapid Commun. Mass Spectrom.* **2008,** *22* (23), 3902-3908.

54. Cabañero, A. I.; Recio, J. L.; Rupérez, M., Liquid Chromatography Coupled to Isotope Ratio Mass Spectrometry: A New Perspective on Honey Adulteration Detection. *J. Agric. Food. Chem.* **2006,** *54* (26), 9719-9727.

55. Cabañero, A. I.; Recio, J. L.; Rupérez, M., Simultaneous Stable Carbon Isotopic Analysis of Wine Glycerol and Ethanol by Liquid Chromatography Coupled to Isotope Ratio Mass Spectrometry. *J. Agric. Food. Chem.* **2010,** *58* (2), 722-728.

56. Köster, D.; Wolbert, J.-B.; Schulte, M. S.; Jochmann, M. A.; Schmidt, T. C., Origin of Xylitol in Chewing Gum: A Compound-Specific Isotope Technique for the Differentiation of Corn- and Wood-Based Xylitol by LC-IRMS. *J. Agric. Food. Chem.* **2018,** *66* (8), 2015-2020.

57. McCullagh, J.; Gaye-Siessegger, J.; Focken, U., Determination of underivatized amino acid δ13C by liquid chromatography/isotope ratio mass spectrometry for nutritional studies: the effect of dietary non-essential amino acid profile on the isotopic signature of individual amino acids in fish. *Rapid Commun. Mass Spectrom.* **2008,** *22* (12), 1817-1822.

58. Smith, C. I.; Fuller, B. T.; Choy, K.; Richards, M. P., A three-phase liquid chromatographic method for δ13C analysis of amino acids from biological protein hydrolysates using liquid chromatography–isotope ratio mass spectrometry. *Anal. Biochem.* **2009,** *390* (2), 165-172.

59. Mora, A.; Arriaza, B. T.; Standen, V. G.; Valdiosera, C.; Salim, A.; Smith, C., High-resolution palaeodietary reconstruction: Amino acid δ13C analysis of keratin from single hairs of mummified human individuals. *Quaternary International* **2017,** *436* (Part A), 96-113.

60. Wei, X.; Gilevska, T.; Wetzig, F.; Dorer, C.; Richnow, H.-H.; Vogt, C., Characterization of phenol and cresol biodegradation by compound-specific stable isotope analysis. *Environ. Pollut.* **2016,** *210* (Supplement C), 166-173.

61. Franke, S.; Kümmel, S.; Nijenhuis, I., Liquid chromatography/isotope ratio mass spectrometry analysis of halogenated benzoates for characterization of the underlying degradation reaction in Thauera chlorobenzoica CB-1T. *Rapid Commun. Mass Spectrom.* **2018,** *32* (11), 906-912.

62. Godin, J.-P.; Hopfgartner, G.; Fay, L., Temperature-Programmed High-Performance Liquid Chromatography Coupled to Isotope Ratio Mass Spectrometry. *Anal. Chem.* **2008,** *80* (18), 7144-7152.

63. Zhang, L.; Thevis, M.; Piper, T.; Jochmann, M. A.; Wolbert, J. B.; Kujawinski, D. M.; Wiese, S.; Teutenberg, T.; Schmidt, T. C., Carbon Isotope Ratio Analysis of Steroids by High-

Temperature Liquid Chromatography-Isotope Ratio Mass Spectrometry. *Anal. Chem.* **2014,** *86* (5), 2297-2302.

64. Bada, J. L.; Gillespie, R.; Gowlett, J. A. J.; Hedges, R. E. M., Accelerator mass spectrometry radiocarbon ages of amino acid extracts from Californian palaeoindian skeletons. *Nature* **1984,** *312*, 442.

65. O'Connell, T. C.; Hedges, R. E. M., Investigations into the effect of diet on modern human hair isotopic values. *Am. J. Phys. Anthropol.* **1999,** *108* (4), 409-425.

66. Corr, L. T.; Sealy, J. C.; Horton, M. C.; Evershed, R. P., A novel marine dietary indicator utilising compound-specific bone collagen amino acid δ13C values of ancient humans. *Journal of Archaeological Science* **2005,** *32* (3), 321-330.

67. Dunn, P. J. H.; Honch, N. V.; Evershed, R. P., Comparison of liquid chromatography–isotope ratio mass spectrometry (LC/IRMS) and gas chromatography–combustion–isotope ratio mass spectrometry (GC/C/IRMS) for the determination of collagen amino acid δ13C values for palaeodietary and palaeoecological reconstruction. *Rapid Commun. Mass Spectrom.* **2011,** *25* (20), 2995-3011.

68. McCullagh, J. S. O.; Juchelka, D.; Hedges, R. E. M., Analysis of amino acid 13C abundance from human and faunal bone collagen using liquid chromatography/isotope ratio mass spectrometry. *Rapid Commun. Mass Spectrom.* **2006,** *20* (18), 2761-2768.

69. Choy, K.; Smith, C. I.; Fuller, B. T.; Richards, M. P., Investigation of amino acid δ13C signatures in bone collagen to reconstruct human palaeodiets using liquid chromatography–isotope ratio mass spectrometry. *Geochim. Cosmochim. Acta* **2010,** *74* (21), 6093-6111.

70. Raghavan, M.; McCullagh, J. S. O.; Lynnerup, N.; Hedges, R. E. M., Amino acid δ13C analysis of hair proteins and bone collagen using liquid chromatography/isotope ratio mass spectrometry: paleodietary implications from intra-individual comparisons. *Rapid Commun. Mass Spectrom.* **2010,** *24* (5), 541-548.

71. Blyth, A. J.; Shutova, Y.; Smith, C., δ13C analysis of bulk organic matter in speleothems using liquid chromatography–isotope ratio mass spectrometry. *Org. Geochem.* **2013,** *55* (Supplement C), 22-25.

72. Blyth, A. J.; Smith, C. I.; Drysdale, R. N., A new perspective on the δ13C signal preserved in speleothems using LC–IRMS analysis of bulk organic matter and compound specific stable isotope analysis. *Quat. Sci. Rev.* **2013,** *75* (Supplement C), 143-149.

73. Godin, J.-P.; McCullagh, J. S. O., Review: Current applications and challenges for liquid chromatography coupled to isotope ratio mass spectrometry (LC/IRMS). *Rapid Commun. Mass Spectrom.* **2011,** *25* (20), 3019-3028.

74. Schierbeek, H.; te Braake, F.; Godin, J.-P.; Fay, L.-B.; van Goudoever, J. B., Novel method for measurement of glutathione kinetics in neonates using liquid chromatography coupled to isotope ratio mass spectrometry. *Rapid Commun. Mass Spectrom.* **2007,** *21* (17), 2805-2812.

75. Schierbeek, H.; Rook, D.; te Braake, F. W. J.; Dorst, K. Y.; Voortman, G.; Godin, J.-P.; Fay, L.-B.; van Goudoever, J. B., Simultaneous analysis of 13C-glutathione as its dimeric form GSSG and its precursor [1-13C]glycine using liquid chromatography/isotope ratio mass spectrometry. *Rapid Commun. Mass Spectrom.* **2009,** *23* (18), 2897-2902.

76. Braun, A.; Spona-Friedl, M.; Griebler, C.; Elsner, M., Isotopomics in Saliva - Towards Non-Invasive Diabetes Diagnosis. *Presentation at Isotopes 2017 Ascona, Switzerland* **2017**.

77. Gaye-Siessegger, J.; McCullagh, J. S. O.; Focken, U., The effect of dietary amino acid abundance and isotopic composition on the growth rate, metabolism and tissue δ13C of rainbow trout. *Br. J. Nutr.* **2011,** *105* (12), 1764-1771.

78. Heuer, V.; Elvert, M.; Tille, S.; Krummen, M.; Mollar, X. P.; Hmelo, L. R.; Hinrichs, K.-U., Online δ13C analysis of volatile fatty acids in sediment/porewater systems by liquid chromatography-isotope ratio mass spectrometry. *Limnol. Oceanogr. Methods* **2006,** *4* (10), 346-357.

79. Heuer, V. B.; Pohlman, J. W.; Torres, M. E.; Elvert, M.; Hinrichs, K.-U., The stable carbon isotope biogeochemistry of acetate and other dissolved carbon species in deep subseafloor sediments at the northern Cascadia Margin. *Geochim. Cosmochim. Acta* **2009,** *73* (11), 3323-3336.

80. Bodé, S.; Denef, K.; Boeckx, P., Development and evaluation of a high-performance liquid chromatography/isotope ratio mass spectrometry methodology for δ13C analyses of amino sugars in soil. *Rapid Commun. Mass Spectrom.* **2009,** *23* (16), 2519-2526.

81. Bai, Z.; Bodé, S.; Huygens, D.; Zhang, X.; Boeckx, P., Kinetics of amino sugar formation from organic residues of different quality. *Soil Biol. Biochem.* **2013,** *57*, 814-821.

82. Bodé, S.; Fancy, R.; Boeckx, P., Stable isotope probing of amino sugars – a promising tool to assess microbial interactions in soils. *Rapid Commun. Mass Spectrom.* **2013,** *27* (12), 1367-1379.

83. Hatton, P.-J.; Bodé, S.; Angeli, N.; Boeckx, P.; Zeller, B.; Boiry, S.; Gelhaye, L.; Derrien, D., Assimilation and accumulation of C by fungi and bacteria attached to soil density fractions. *Soil Biol. Biochem.* **2014,** *79* (Supplement C), 132-139.

84. Albéric, P., Liquid chromatography/mass spectrometry stable isotope analysis of dissolved organic carbon in stream and soil waters. *Rapid Commun. Mass Spectrom.* **2011,** *25* (20), 3012-3018.

85. Scheibe, A.; Krantz, L.; Gleixner, G., Simultaneous determination of the quantity and isotopic signature of dissolved organic matter from soil water using high-performance liquid chromatography/isotope ratio mass spectrometry. *Rapid Commun. Mass Spectrom.* **2012,** *26* (2), 173-180.

86. Powers, L. C.; Brandes, J. A.; Miller, W. L.; Stubbins, A., Using liquid chromatography-isotope ratio mass spectrometry to measure the δ13C of dissolved inorganic carbon photochemically produced from dissolved organic carbon. *Limnol. Oceanogr. Methods* **2017,** *15* (1), 103-115.

87. Powers, L. C.; Brandes, J. A.; Stubbins, A.; Miller, W. L., MoDIE: Moderate dissolved inorganic carbon (DI13C) isotope enrichment for improved evaluation of DIC photochemical production in natural waters. *Mar. Chem.* **2017,** *194* (Supplement C), 1-9.

88. Malik, A.; Scheibe, A.; LokaBharathi, P. A.; Gleixner, G., Online Stable Isotope Analysis of Dissolved Organic Carbon Size Classes Using Size Exclusion Chromatography Coupled to an Isotope Ratio Mass Spectrometer. *Environ. Sci. Technol.* **2012,** *46* (18), 10123-10129.

89. Malik, A.; Gleixner, G., Importance of microbial soil organic matter processing in dissolved organic carbon production. *FEMS Microbiol. Ecol.* **2013,** *86* (1), 139-148.

90. Smith, B. N.; Epstein, S., Two Categories of (13)C/(12)C Ratios for Higher Plants. *Plant Physiol.* **1971,** *47* (3), 380-384.

91. Sternberg, L. O.; Deniro, M. J.; Johnson, H. B., Isotope Ratios of Cellulose from Plants Having Different Photosynthetic Pathways. *Plant Physiol.* **1984,** *74* (3), 557-561.

92. Bender, M. M., Variations in the 13C/12C ratios of plants in relation to the pathway of photosynthetic carbon dioxide fixation. *Phytochemistry* **1971,** *10* (6), 1239-1244.

93. Osmond, C. B.; Allaway, W. G.; Sutton, B. G.; Troughton, J. H.; Queiroz, O.; LÜTtge, U.; Winter, K., Carbon Isotope Discrimination in Photosynthesis of CAM Plants. *Nature* **1973,** *246*, 41.

94. Elflein, L.; Raezke, K.-P., Improved detection of honey adulteration by measuring differences between 13C/12C stable carbon isotope ratios of protein and sugar compounds with a combination of elemental analyzer — isotope ratio mass spectrometry and liquid chromatography — isotope ratio mass spectrometry (δ13C-EA/LC-IRMS). *Apidologie* **2008,** *39* (5), 574-587.

95. Dong, H.; Luo, D.; Xian, Y.; Luo, H.; Guo, X.; Li, C.; Zhao, M., Adulteration Identification of Commercial Honey with the C-4 Sugar Content of Negative Values by an Elemental Analyzer and Liquid Chromatography Coupled to Isotope Ratio Mass Spectroscopy. *J. Agric. Food. Chem.* **2016,** *64* (16), 3258-3265.

96. Luo, D.; Luo, H.; Dong, H.; Xian, Y.; Guo, X.; Wu, Y., Hydrogen (2H/1H) Combined with Carbon (13C/12C) Isotope Ratios Analysis to Determine the Adulteration of Commercial Honey. *Food. Anal. Method.* **2016,** *9* (1), 255-262.

97. Dong, H.; Xiao, K.; Xian, Y.; Wu, Y., Authenticity determination of honeys with non-extractable proteins by means of elemental analyzer (EA) and liquid chromatography (LC) coupled to isotope ratio mass spectroscopy (IRMS). *Food Chem.* **2018,** *240* (Supplement C), 717-724.

98. Cabañero, A. I.; Recio, J. L.; Rupérez, M., Isotope ratio mass spectrometry coupled to liquid and gas chromatography for wine ethanol characterization. *Rapid Commun. Mass Spectrom.* **2008,** *22* (20), 3111-3118.

99. Guyon, F.; Gaillard, L.; Brault, A.; Gaultier, N.; Salagoïty, M.-H.; Médina, B., Potential of ion chromatography coupled to isotope ratio mass spectrometry via a liquid interface for beverages authentication. *J. Chromatogr. A* **2013,** *1322* (Supplement C), 62-68.

100. Jochmann, M. A.; Steinmann, D.; Stephan, M.; Schmidt, T. C., Flow Injection Analysis−Isotope Ratio Mass Spectrometry for Bulk Carbon Stable Isotope Analysis of Alcoholic Beverages. *J. Agric. Food. Chem.* **2009,** *57* (22), 10489-10496.

101. Zhang, L.; Kujawinski, D. M.; Federherr, E.; Schmidt, T. C.; Jochmann, M. A., Caffeine in Your Drink: Natural or Synthetic? *Anal. Chem.* **2012,** *84* (6), 2805-2810.

102. Bononi, M.; Quaglia, G.; Tateo, F., Easy Extraction Method To Evaluate δ13C Vanillin by Liquid Chromatography–Isotopic Ratio Mass Spectrometry in Chocolate Bars and Chocolate Snack Foods. *J. Agric. Food. Chem.* **2015,** *63* (19), 4777-4781.

103. Bononi, M.; Quaglia, G.; Tateo, F., Preliminary LC-IRMS Characterization of Italian Pure Lemon Juices and Evaluation of Commercial Juices Distributed in the Italian Market. *Food. Anal. Method.* **2016,** *9* (10), 2824-2831.

104. Guyon, F.; Auberger, P.; Gaillard, L.; Loublanches, C.; Viateau, M.; Sabathié, N.; Salagoïty, M.-H.; Médina, B., 13C/12C isotope ratios of organic acids, glucose and fructose determined by HPLC-co-IRMS for lemon juices authenticity. *Food Chem.* **2014,** *146* (Supplement C), 36-40.

105. Zhang, Q.; Chang, T.; Li, W., A calibrated measurement of the atomic-weight of carbon. *Chin. Sci. Bull.* **1990,** *35* (4), 290-296.

106. Coplen, T. B.; Brand, W. A.; Gehre, M.; Gröning, M.; Meijer, H. A. J.; Toman, B.; Verkouteren, R. M., New Guidelines for δ13C Measurements. *Anal. Chem.* **2006,** *78* (7), 2439-2441.

107. Brand Willi, A.; Coplen Tyler, B.; Vogl, J.; Rosner, M.; Prohaska, T., Assessment of international reference materials for isotope-ratio analysis (IUPAC Technical Report). In *Pure Appl. Chem.*, 2014; Vol. 86, p 425.

108. Paul, D.; Skrzypek, G.; Fórizs, I., Normalization of measured stable isotopic compositions to isotope reference scales – a review. *Rapid Commun. Mass Spectrom.* **2007,** *21* (18), 3006-3014.

109. Grootes, P. M.; Mook, W. G.; Vogel, J. C., Isotopic fractionation between gaseous and condensed carbon dioxide. *Zeitschrift für Physik A Hadrons and nuclei* **1969,** *221* (3), 257-273.

110. Verkouteren, R. M.; Lee, J. N., web-based interactive data processing: application to stable isotope metrology. *Fresenius J. Anal. Chem.* **2001,** *370* (7), 803-810.

111. Meija, J.; Chartrand, M. M. G., Uncertainty evaluation in normalization of isotope delta measurement results against international reference materials. *Anal. Bioanal. Chem.* **2018,** *410* (3), 1061-1069.

112. Kjeldahl, J., Neue Methode zur Bestimmung des Stickstoffs in organischen Körpern. *Zeitschrift für analytische Chemie* **1883,** *22* (1), 366-382.

113. Sáez-Plaza, P.; Michałowski, T.; Navas, M. J.; Asuero, A. G.; Wybraniec, S., An Overview of the Kjeldahl Method of Nitrogen Determination. Part I. Early History, Chemistry of the Procedure, and Titrimetric Finish. *Crit. Rev. Anal. Chem.* **2013,** *43* (4), 178-223.

114. Smart, M. M.; Reid, F. A.; Jones, J. R., A comparison of a persulfate digestion and the Kjeldahl procedure for determination of total nitrogen in freshwater samples. *Water Res.* **1981,** *15* (7), 919-921.

115. Xue, D.; Botte, J.; De Baets, B.; Accoe, F.; Nestler, A.; Taylor, P.; Van Cleemput, O.; Berglund, M.; Boeckx, P., Present limitations and future prospects of stable isotope methods for nitrate source identification in surface- and groundwater. *Water Res.* **2009,** *43* (5), 1159-1170.

116. Henriksen, A., Bestemmelse av totalnitrogen i avlopsvann. *Nordforsk, Miljövardssekretariatet, Publikation* **1973,** *Vol. 3*, 41-43.

117. Koroleff, F., Bestämning av total nitrogen i naturliga vatten genom persulfatoxidation. *International council for the Exploration of the Sea, 1969 Concil Meeting* **1970,** *Paper C:8, revised version*.

118. Koroleff, F., Bestämning av total nitrogen i vatten. *Nordforsk, Miljövardssekretariatet, Publikation* **1973,** *Vol. 3*, 39-40.

119. D'Elia, C. F.; Steudler, P. A., Determination of total nitrogen in aqueous samples using persulfate digestion. *Limnol. Oceanogr.* **1977,** *22* (4), 760-764.

120. Nydahl, F., On the peroxodisulphate oxidation of total nitrogen in waters to nitrate. *Water Res.* **1978,** *12* (12), 1123-1130.

121. Rossi, G.; Savarese, M., On-line determination of total nitrogen in natural sea water samples by alkaline persulphate oxidation. *Mar. Pollut. Bull.* **1997,** *35* (1), 174-175.

122. Yang, F.; Troncy, E.; Francœur, M.; Vinet, B.; Vinay, P.; Czaika, G.; Blaise, G., Effects of reducing reagents and temperature on conversion of nitrite and nitrate to nitric oxide and detection of NO by chemiluminescence. *Clin. Chem.* **1997,** *43* (4), 657-662.

123. Melsbach, A.; Ponsin, V.; Torrentó, C.; Lihl, C.; Hofstetter, T. B.; Hunkeler, D.; Elsner, M., 13C- and 15N-Isotope Analysis of Desphenylchloridazon by Liquid Chromatography–Isotope-Ratio Mass Spectrometry and Derivatization Gas Chromatography–Isotope-Ratio Mass Spectrometry. *Anal. Chem.* **2019,** *91* (5), 3412-3420.

124. Hartenbach, A. E.; Hofstetter, T. B.; Tentscher, P. R.; Canonica, S.; Berg, M.; Schwarzenbach, R. P., Carbon, Hydrogen, and Nitrogen Isotope Fractionation During Light-Induced Transformations of Atrazine. *Environ. Sci. Technol.* **2008,** *42* (21), 7751-7756.

125. Maier, M. P.; Prasse, C.; Pati, S. G.; Nitsche, S.; Li, Z.; Radke, M.; Meyer, A.; Hofstetter, T. B.; Ternes, T. A.; Elsner, M., Exploring Trends of C and N Isotope Fractionation to Trace

Transformation Reactions of Diclofenac in Natural and Engineered Systems. *Environ. Sci. Technol.* **2016,** *50* (20), 10933-10942.

126. Chikaraishi, Y.; Ogawa, N. O.; Kashiyama, Y.; Takano, Y.; Suga, H.; Tomitani, A.; Miyashita, H.; Kitazato, H.; Ohkouchi, N., Determination of aquatic food-web structure based on compound-specific nitrogen isotopic composition of amino acids. *Limnol. Oceanogr. Methods* **2009,** *7* (11), 740-750.

127. Grembecka, M., Sugar alcohols—their role in the modern world of sweeteners: a review. *Eur. Food Res. Technol.* **2015,** *241* (1), 1-14.

128. Granström, T. B.; Izumori, K.; Leisola, M., A rare sugar xylitol. Part II: biotechnological production and future applications of xylitol. *Appl. Microbiol. Biotechnol.* **2007,** *74* (2), 273.

129. Carocho, M.; Morales, P.; Ferreira, I. C. F. R., Sweeteners as food additives in the XXI century: A review of what is known, and what is to come. *Food Chem. Toxicol.* **2017,** *107* (Part A), 302-317.

130. Scheller, H. V.; Ulvskov, P., Hemicelluloses. *Annu. Rev. Plant Biol.* **2010,** *61* (1), 263-289.

131. Albuquerque, T. L. d.; da Silva, I. J.; de Macedo, G. R.; Rocha, M. V. P., Biotechnological production of xylitol from lignocellulosic wastes: A review. *Process Biochem.* **2014,** *49* (11), 1779-1789.

132. Rivas, B.; Torre, P.; Domínguez, J. M.; Converti, A.; Parajó, J. C., Purification of Xylitol Obtained by Fermentation of Corncob Hydrolysates. *J. Agric. Food. Chem.* **2006,** *54* (12), 4430-4435.

133. Rafiqul, I. S. M.; Sakinah, A. M. M., Processes for the Production of Xylitol—A Review. *Food Rev. Int.* **2013,** *29* (2), 127-156.

134. Parajó, J. C.; Domínguez, H.; Domínguez, J., Biotechnological production of xylitol. Part 1: Interest of xylitol and fundamentals of its biosynthesis. *Bioresour. Technol.* **1998,** *65* (3), 191-201.

135. Hernández-Pérez, A. F.; de Arruda, P. V.; Felipe, M. d. G. d. A., Sugarcane straw as a feedstock for xylitol production by Candida guilliermondii FTI 20037. *Braz. J. Microbiol.* **2016,** *47* (2), 489-496.

136. Canilha, L.; de Almeida e Silva, J. B.; Solenzal, A. I. N., Eucalyptus hydrolysate detoxification with activated charcoal adsorption or ion-exchange resins for xylitol production. *Process Biochem.* **2004,** *39* (12), 1909-1912.

137. Swain, M. R.; Krishnan, C., Improved conversion of rice straw to ethanol and xylitol by combination of moderate temperature ammonia pretreatment and sequential fermentation using Candida tropicalis. *Ind. Crops Prod.* **2015,** *77*, 1039-1046.

138. Pourmir, A.; Noor-Mohammadi, S.; Johannes, T. W., Production of xylitol by recombinant microalgae. *J. Biotechnol.* **2013,** *165* (3–4), 178-183.

139. Liavoga, A. B.; Bian, Y.; Seib, P. A., Release of D-Xylose from Wheat Straw by Acid and Xylanase Hydrolysis and Purification of Xylitol. *J. Agric. Food. Chem.* **2007,** *55* (19), 7758-7766.

140. Cerling, T. E.; Harris, J. M.; MacFadden, B. J.; Leakey, M. G.; Quade, J.; Eisenmann, V.; Ehleringer, J. R., Global vegetation change through the Miocene/Pliocene boundary. *Nature* **1997,** *389* (6647), 153-158.

141. van der Merwe, N. J.; Tschauner, H., C4 Plants and the Development of Human Societies. In *C4 Plant Biology*, Monson, R. K., Ed. Academic Press: San Diego, 1999; pp 509-549.

142. Brand, W. A.; Dobberstein, P., Isotope-Ratio-Monitoring Liquid Chromatography Mass Spectrometry (IRM-LCMS): First Results from a Moving Wire Interface System. *Isotopes Environ. Health Stud.* **1996,** *32* (2-3), 275-283.

143. Symes, C.; Loubser, E.; Woodborne, S., Stable isotope (δ13C) profiling of xylitol and sugar in South Africa. *S. Afr. J. Sci.* **2017,** *113* (5/6), 83-87.

144. Directive 2011/83/EU of the European Parliament and of the Council of 25 October 2011 on consumer rights, amending Council Directive 93/13/EEC and Directive 1999/44/EC of the European Parliament and of the Council and repealing Council Directive 85/577/EEC and Directive 97/7/EC of the European Parliament and of the Council Text with EEA relevance. *Off. J. Eur. Union* **2011,** *L 304*, 30.

145. Goodman, K. J.; Brenna, J. T., Curve Fitting for Restoration of Accuracy for Overlapping Peaks in Gas Chromatography/Combustion Isotope Ratio Mass Spectrometry. *Anal. Chem.* **1994,** *66* (8), 1294-1301.

146. J. DeNiro, M.; Hastorf, C., Alteration of 15N /14N and 13C /12C ratios of plant matter during the initial stages of diagenesis: Studies utilizing archaeological specimens from Peru. *Geochim. Cosmochim. Acta* **1985,** *49* (1), 97-115.

147. Voronin, P. Y.; Mukhin, V. A.; Velivetskaya, T. A.; Ignat'ev, A. V.; Kuznetsov, V. V., Isotope composition of carbon and nitrogen in tissues and organs of Betula pendula. *Russ. J. Plant Physiol.* **2017,** *64* (2), 184-189.

148. Wilson, A. T.; Grinsted, M. J., 12C/13C in cellulose and lignin as palaeothermometers. *Nature* **1977,** *265* (5590), 133-135.

149. Loader, N. J.; Robertson, I.; McCarroll, D., Comparison of stable carbon isotope ratios in the whole wood, cellulose and lignin of oak tree-rings. *Palaeogeogr., Palaeoclimatol., Palaeoecol.* **2003,** *196* (3), 395-407.

150. Godin, J. P.; Hau, J.; Fay, L. B.; Hopfgartner, G., Isotope ratio monitoring of small molecules and macromolecules by liquid chromatography coupled to isotope ratio mass spectrometry. *Rapid Commun. Mass Spectrom.* **2005,** *19* (18), 2689-2698.

151. Brandes, J. A., Rapid and precise δ13C measurement of dissolved inorganic carbon in natural waters using liquid chromatography coupled to an isotope-ratio mass spectrometer. *Limnol. Oceanogr. Methods* **2009,** *7* (11), 730-739.

152. Godin, J.-P.; Fay, L.-B.; Hopfgartner, G., Liquid chromatography combined with mass spectrometry for 13C isotopic analysis in life science research. *Mass Spectrom. Rev.* **2007,** *26* (6), 751-774.

153. Caimi, R. J.; Brenna, J. T., Direct analysis of carbon isotope variability in albumins by liquid flow-injection isotope ratio mass spectrometry. *J. Am. Soc. Mass. Spectrom.* **1996,** *7* (6), 605-610.

154. Abaye, D. A.; Morrison, D. J.; Preston, T., Strong anion exchange liquid chromatographic separation of protein amino acids for natural 13C-abundance determination by isotope ratio mass spectrometry. *Rapid Commun. Mass Spectrom.* **2011,** *25* (3), 429-435.

155. Gilevska, T.; Gehre, M.; Richnow, H. H., Performance of the Wet Oxidation Unit of the HPLC Isotope Ratio Mass Spectrometry System for Halogenated Compounds. *Anal. Chem.* **2014,** *86* (15), 7252-7257.

156. Cueto Díaz, S.; Encinar, J. R.; Sanz-Medel, A.; Alonso, J. I. G., Liquid Chromatography, Chemical Oxidation, and Online Carbon Isotope Dilution Mass Spectrometry as a Universal Quantification System for Nonvolatile Organic Compounds. *Anal. Chem.* **2013,** *85* (3), 1873-1879.

157. Skrzypek, G.; Ford, D., Reference materials selection for the stable carbon isotope analysis of dissolved carbon using a wet oxidation system. *Rapid Commun. Mass Spectrom.* **2018,** *doi:10.1002/rcm.8351*.

158. *Thermo Fisher Scientific LC IsoLink Operating Manual Revision C - 1156140*. Thermo Fisher Scientific Inc.: Bremen, Germany, 2011.

159. Basler, A.; Dyckmans, J., Compound-specific δ13C analysis of monosaccharides from soil extracts by high-performance liquid chromatography/isotope ratio mass spectrometry. *Rapid Commun. Mass Spectrom.* **2013,** *27* (22), 2546-2550.

160. Godin, J.-P.; Breuillé, D.; Obled, C.; Papet, I.; Schierbeek, H.; Hopfgartner, G.; Fay, L.-B., Liquid and gas chromatography coupled to isotope ratio mass spectrometry for the determination of 13C–valine isotopic ratios in complex biological samples. *J. Mass Spectrom.* **2008,** *43* (10), 1334-1343.

161. Tagami, K.; Uchida, S., Online stable carbon isotope ratio measurement in formic acid, acetic acid, methanol and ethanol in water by high performance liquid chromatography–isotope ratio mass spectrometry. *Anal. Chim. Acta* **2008,** *614* (2), 165-172.

162. Godin, J.-P.; Stellingwerff, T.; Actis-Goretta, L.; Mermoud, A.-F.; Kochhar, S.; Rezzi, S., The role of liquid chromatography and flow injection analyses coupled to isotope ratio mass spectrometry for studying human in vivo glucose metabolism. *Rapid Commun. Mass Spectrom.* **2011,** *25* (20), 2989-2994.

163. Lynch, A. H.; McCullagh, J. S. O.; Hedges, R. E. M., Liquid chromatography/isotope ratio mass spectrometry measurement of δ13C of amino acids in plant proteins. *Rapid Commun. Mass Spectrom.* **2011,** *25* (20), 2981-2988.

164. Pollard, A. M.; Ditchfield, P.; McCullagh, J. S. O.; Allen, T. G.; Gibson, M.; Boston, C.; Clough, S.; Marquez-Grant, N.; Nicholson, R. A., "These boots were made for walking": The isotopic analysis of a C4 Roman inhumation from Gravesend, Kent, UK. *Am. J. Phys. Anthropol.* **2011,** *146* (3), 446-456.

165. Kujawinski, D. M.; Wolbert, J. B.; Zhang, L.; Jochmann, M. A.; Widory, D.; Baran, N.; Schmidt, T. C., Carbon isotope ratio measurements of glyphosate and AMPA by liquid chromatography coupled to isotope ratio mass spectrometry. *Anal. Bioanal. Chem.* **2013,** *405* (9), 2869-2878.

166. Malik, A.; Blagodatskaya, E.; Gleixner, G., Soil microbial carbon turnover decreases with increasing molecular size. *Soil Biol. Biochem.* **2013,** *62* (Supplement C), 115-118.

167. Moerdijk-Poortvliet, T. C. W.; Stal, L. J.; Boschker, H. T. S., LC/IRMS analysis: A powerful technique to trace carbon flow in microphytobenthic communities in intertidal sediments. *J. Sea Res.* **2014,** *92* (Supplement C), 19-25.

168. Moerdijk-Poortvliet, T. C. W.; Brasser, J.; de Ruiter, G.; Houtekamer, M.; Bolhuis, H.; Stal, L. J.; Boschker, H. T. S., A versatile method for simultaneous stable carbon isotope analysis of DNA and RNA nucleotides by liquid chromatography/isotope ratio mass spectrometry. *Rapid Commun. Mass Spectrom.* **2014,** *28* (12), 1401-1411.

169. Grosse, J.; van Breugel, P.; Boschker, H. T. S., Tracing carbon fixation in phytoplankton—compound specific and total 13C incorporation rates. *Limnol. Oceanogr. Methods* **2015,** *13* (6), 288-302.

170. Moerdijk-Poortvliet, T. C. W.; Schierbeek, H.; Houtekamer, M.; van Engeland, T.; Derrien, D.; Stal, L. J.; Boschker, H. T. S., Comparison of gas chromatography/isotope ratio mass spectrometry and liquid chromatography/isotope ratio mass spectrometry for carbon stable-isotope analysis of carbohydrates. *Rapid Commun. Mass Spectrom.* **2015,** *29* (13), 1205-1214.

171. Birkigt, J.; Gilevska, T.; Ricken, B.; Richnow, H.-H.; Vione, D.; Corvini, P. F. X.; Nijenhuis, I.; Cichocka, D., Carbon Stable Isotope Fractionation of Sulfamethoxazole during Biodegradation by Microbacterium sp. Strain BR1 and upon Direct Photolysis. *Environ. Sci. Technol.* **2015,** *49* (10), 6029-6036.

172. Raghavan, M.; McCullagh James, S. O.; Lynnerup, N.; Hedges Robert, E. M., Amino acid δ13C analysis of hair proteins and bone collagen using liquid chromatography/isotope ratio mass spectrometry: paleodietary implications from intra-individual comparisons. *Rapid Commun. Mass Spectrom.* **2010,** *24* (5), 541-548.

173. Behrman, E. J.; Dean, D. H., Sodium peroxydisulfate is a stable and cheap substitute for ammonium peroxydisulfate (persulfate) in polyacrylamide gel electrophoresis. *J. Chromatogr. B Biomed. Sci. Appl.* **1999,** *723* (1), 325-326.

174. Köster, D.; Jochmann, M. A.; Lutze, H. V.; Schmidt, T. C., Monitoring of the total carbon and nitrogen balance during the mineralization of nitrogen containing compounds by heat activated persulfate. *Chem. Eng. J.* **2019,** *367*, 160-168.

175. Johnson, R. L.; Tratnyek, P. G.; Johnson, R. O. B., Persulfate Persistence under Thermal Activation Conditions. *Environ. Sci. Technol.* **2008,** *42* (24), 9350-9356.

176. Merritt, D. A.; Freeman, K. H.; Ricci, M. P.; Studley, S. A.; Hayes, J. M., Performance and Optimization of a Combustion Interface for Isotope Ratio Monitoring Gas Chromatography/Mass Spectrometry. *Anal. Chem.* **1995,** *67* (14), 2461-2473.

177. Tsitonaki, A.; Petri, B.; Crimi, M.; MosbÆK, H.; Siegrist, R. L.; Bjerg, P. L., In Situ Chemical Oxidation of Contaminated Soil and Groundwater Using Persulfate: A Review. *Crit. Rev. Environ. Sci. Technol.* **2010,** *40* (1), 55-91.

178. Wacławek, S.; Lutze, H. V.; Grübel, K.; Padil, V. V. T.; Černík, M.; Dionysiou, D. D., Chemistry of persulfates in water and wastewater treatment: A review. *Chem. Eng. J.* **2017,** *330*, 44-62.

179. Matzek, L. W.; Carter, K. E., Activated persulfate for organic chemical degradation: A review. *Chemosphere* **2016,** *151*, 178-188.

180. Lutze, H. V.; Bircher, S.; Rapp, I.; Kerlin, N.; Bakkour, R.; Geisler, M.; von Sonntag, C.; Schmidt, T. C., Degradation of Chlorotriazine Pesticides by Sulfate Radicals and the Influence of Organic Matter. *Environ. Sci. Technol.* **2015,** *49* (3), 1673-1680.

181. Ji, Y.; Dong, C.; Kong, D.; Lu, J.; Zhou, Q., Heat-activated persulfate oxidation of atrazine: Implications for remediation of groundwater contaminated by herbicides. *Chem. Eng. J.* **2015,** *263* (0), 45-54.

182. Ji, Y.; Fan, Y.; Liu, K.; Kong, D.; Lu, J., Thermo activated persulfate oxidation of antibiotic sulfamethoxazole and structurally related compounds. *Water Res.* **2015,** *87*, 1-9.

183. Jiang, C.; Ji, Y.; Shi, Y.; Chen, J.; Cai, T., Sulfate radical-based oxidation of fluoroquinolone antibiotics: Kinetics, mechanisms and effects of natural water matrices. *Water Res.* **2016,** *106*, 507-517.

184. Lee, Y.-C.; Lo, S.-L.; Kuo, J.; Lin, Y.-L., Persulfate oxidation of perfluorooctanoic acid under the temperatures of 20–40°C. *Chem. Eng. J.* **2012,** *198-199*, 27-32.

185. Ghauch, A.; Tuqan, A. M.; Kibbi, N.; Geryes, S., Methylene blue discoloration by heated persulfate in aqueous solution. *Chem. Eng. J.* **2012,** *213*, 259-271.

186. EN-1484, EN 1484 (1997-05-00) Water analysis - Guidelines for the determination of total organic carbon (TOC) and dissolved organic carbon (DOC). *CEN European Committee for Standardization* **1997**.

187. Peyton, G. R., The free-radical chemistry of persulfate-based total organic carbon analyzers. *Mar. Chem.* **1993,** *41* (1), 91-103.

188. House, D. A., Kinetics and Mechanism of Oxidations by Peroxydisulfate. *Chem. Rev.* **1962,** *62* (3), 185-203.

189. Huang, K.-C.; Couttenye, R. A.; Hoag, G. E., Kinetics of heat-assisted persulfate oxidation of methyl tert-butyl ether (MTBE). *Chemosphere* **2002,** *49* (4), 413-420.

190. Anipsitakis, G. P.; Dionysiou, D. D., Radical Generation by the Interaction of Transition Metals with Common Oxidants. *Environ. Sci. Technol.* **2004,** *38* (13), 3705-3712.

191. Kolthoff, I. M.; Miller, I. K., The Chemistry of Persulfate. I. The Kinetics and Mechanism of the Decomposition of the Persulfate Ion in Aqueous Medium. *J. Am. Chem. Soc.* **1951,** *73* (7), 3055-3059.

192. Neta, P.; Madhavan, V.; Zemel, H.; Fessenden, R. W., Rate constants and mechanism of reaction of sulfate radical anion with aromatic compounds. *J. Am. Chem. Soc.* **1977,** *99* (1), 163-164.

193. Lutze, H. V.; Kerlin, N.; Schmidt, T. C., Sulfate radical-based water treatment in presence of chloride: Formation of chlorate, inter-conversion of sulfate radicals into hydroxyl radicals and influence of bicarbonate. *Water Res.* **2015,** *72*, 349-360.

194. Wangersky, P. J., Dissolved organic carbon methods: a critical review. *Mar. Chem.* **1993,** *41* (1), 61-74.

195. Ebina, J.; Tsutsui, T.; Shirai, T., Simultaneous determination of total nitrogen and total phosphorus in water using peroxodisulfate oxidation. *Water Res.* **1983,** *17* (12), 1721-1726.

196. Low, G. K. C.; McEvoy, S. R.; Matthews, R. W., Formation of nitrate and ammonium ions in titanium dioxide mediated photocatalytic degradation of organic compounds containing nitrogen atoms. *Environ. Sci. Technol.* **1991,** *25* (3), 460-467.

197. Durán, A.; Monteagudo, J. M.; San Martín, I.; Amunategui, F. J.; Patterson, D. A., Mineralization of aniline using hydroxyl/sulfate radical-based technology in a waterfall reactor. *Chemosphere* **2017,** *186*, 177-184.

198. Vicente, F.; Santos, A.; Romero, A.; Rodriguez, S., Kinetic study of diuron oxidation and mineralization by persulphate: Effects of temperature, oxidant concentration and iron dosage method. *Chem. Eng. J.* **2011,** *170* (1), 127-135.

199. Pohl, C.; Rey, M.; Jensen, D.; Kerth, J., Determination of sodium and ammonium ions in disproportionate concentration ratios by ion chromatography. *J. Chromatogr. A* **1999,** *850* (1), 239-245.

200. DIN-32645, DIN 32645:2008-11, Chemical analysis – Decision limit, detection limit and determination limit under repeatability conditions – Terms, methods, evaluation. Beuth-Verlag: Berlin, 2008.

201. Wine, P. H.; Tang, Y.; Thorn, R. P.; Wells, J. R.; Davis, D. D., Kinetics of aqueous phase reactions of the SO4− radical with potential importance in cloud chemistry. *J. Geophys. Res. Atmos.* **1989,** *94* (D1), 1085-1094.

202. Maruthamuthu, P.; Neta, P., Phosphate radicals. Spectra, acid-base equilibriums, and reactions with inorganic compounds. *J. Phys. Chem.* **1978,** *82* (6), 710-713.

203. Clifton, C. L.; Huie, R. E., Rate constants for hydrogen abstraction reactions of the sulfate radical, SO4−. Alcohols. *Int. J. Chem. Kinet.* **1989,** *21* (8), 677-687.

204. Ammann, A. A.; Rüttimann, T. B.; Bürgi, F., Simultaneous determination of TOC and TNb in surface and wastewater by optimised high temperature catalytic combustion. *Water Res.* **2000,** *34* (14), 3573-3579.

205. Goulden, P. D.; Anthony, D. H. J., Kinetics of uncatalyzed peroxydisulfate oxidation of organic material in fresh water. *Anal. Chem.* **1978,** *50* (7), 953-958.

206. Schlögl, R.; Wagner, E.; Fetzer, T.; Wagner, J.; Nehb, W.; Adlkofer, J.; Pachaly, B.; Keim, W., Inorganic Reactions. In *Handbook of Heterogeneous Catalysis*, Wiley-VCH Verlag GmbH: 2008; pp 1697-1799.

207. Peterson, B. J.; Fry, B., Stable Isotopes in Ecosystem Studies. *Annu. Rev. Ecol. Syst.* **1987,** *18* (1), 293-320.

208. Minagawa, M.; Wada, E., Stepwise enrichment of 15N along food chains: Further evidence and the relation between δ15N and animal age. *Geochim. Cosmochim. Acta* **1984,** *48* (5), 1135-1140.

209. Nachev, M.; Jochmann, M. A.; Walter, F.; Wolbert, J. B.; Schulte, S. M.; Schmidt, T. C.; Sures, B., Understanding trophic interactions in host-parasite associations using stable isotopes of carbon and nitrogen. *Parasites & Vectors* **2017,** *10*, 90.

210. Sures, B.; Nachev, M.; Gilbert, B. M.; Dos Santos, Q. M.; Jochmann, M. A.; Köster, D.; Schmidt, T. C.; Avenant-Oldewage, A., The monogenean Paradiplozoon ichthyoxanthon behaves like a micropredator on two of its hosts, as indicated by stable isotopes. *J. Helminthol.* **2018,** *93* (1), 71-75.

211. Ohkouchi, N.; Chikaraishi, Y.; Close, H. G.; Fry, B.; Larsen, T.; Madigan, D. J.; McCarthy, M. D.; McMahon, K. W.; Nagata, T.; Naito, Y. I.; Ogawa, N. O.; Popp, B. N.; Steffan, S.;

Takano, Y.; Tayasu, I.; Wyatt, A. S. J.; Yamaguchi, Y. T.; Yokoyama, Y., Advances in the application of amino acid nitrogen isotopic analysis in ecological and biogeochemical studies. *Org. Geochem.* **2017,** *113*, 150-174.

212. Mogusu, E.; Wolbert, J. B.; Kujawinski, D.; Jochmann, M.; Elsner, M., Dual element (15N/14N, 13C/12C) isotope analysis of glyphosate and AMPA by derivatization-gas chromatography isotope ratio mass spectrometry (GC/IRMS) combined with LC/IRMS. *Anal. Bioanal. Chem.* **2015,** *407* (18), 5249-5260.

213. Reinnicke, S.; Bernstein, A.; Elsner, M., Small and Reproducible Isotope Effects during Methylation with Trimethylsulfonium Hydroxide (TMSH): A Convenient Derivatization Method for Isotope Analysis of Negatively Charged Molecules. *Anal. Chem.* **2010,** *82* (5), 2013-2019.

214. Broek, T. A. B.; Walker, B. D.; Andreasen, D. H.; McCarthy, M. D., High-precision measurement of phenylalanine δ15N values for environmental samples: A new approach coupling high-pressure liquid chromatography purification and elemental analyzer isotope ratio mass spectrometry. *Rapid Commun. Mass Spectrom.* **2013,** *27* (21), 2327-2337.

215. Köster, D.; Sanchez Villalobos, I. M.; Jochmann, M. A.; Brand, W. A.; Schmidt, T. C., New Concepts for the Determination of Oxidation Efficiencies in Liquid Chromatography–Isotope Ratio Mass Spectrometry. *Anal. Chem.* **2019,** *91* (8), 5067-5073.

216. De Borba, B. M.; Jack, R. F.; Rohrer, J. S.; Wirt, J.; Wang, D., Simultaneous determination of total nitrogen and total phosphorus in environmental waters using alkaline persulfate digestion and ion chromatography. *J. Chromatogr. A* **2014,** *1369*, 131-137.

217. Minella, M.; Tartari, G. A.; Rogora, M.; Frigione, M.; Vione, D.; Minero, C.; Maurino, V., Influence of nitrogen speciation on the TDN measurement in fresh waters by high temperature catalytic oxidation and persulfate digestion. *Int. J. Environ. Anal. Chem.* **2016,** *96* (5), 474-489.

218. Kawashima, H.; Suto, M.; Suto, N., Determination of carbon isotope ratios for honey samples by means of a liquid chromatography/isotope ratio mass spectrometry system coupled with a post-column pump. *Rapid Commun. Mass Spectrom.* **2018,** *32* (15), 1271-1279.

219. She, S.; Chen, L.; Song, H.; Lin, G.; Li, Y.; Zhou, J.; Liu, C., Discrimination of geographical origins of Chinese acacia honey using complex 13C/12C, oligosaccharides and polyphenols. *Food Chem.* **2019,** *272*, 580-585.

220. Arle, J.; Blondzik, K.; Claussen, U.; Duffek, A.; Grimm, S.; Hilliges, F.; Kirschbaum, B.; Kirst, I.; Koch, D.; Koschorreck, J.; Lepom, P.; Leujak, W.; Mohaupt, V.; Naumann, S.; Pirntke, U.; Rechenberg, J.; Schilling, P.; Ullrich, A.; Wellmitz, J.; Werner, S.; Wolter, R., Waters in Germany: Status and assessment. *German Environment Agency* **2017**.

221. Stange, F. C.; Spott, O.; Apelt, B.; Russow, R. W. B., Automated and rapid online determination of 15N abundance and concentration of ammonium, nitrite, or nitrate in aqueous samples by the SPINMAS technique. *Isotopes Environ. Health Stud.* **2007,** *43* (3), 227-236.

Chapter 9: List of Figures

Figure 4.3: Infusion and oxidation of different concentration levels of caffeine under identical oxidation conditions with measurement of the remaining organic carbon after oxidation. a) Correlation of the oxidized carbon in relation to the initially introduced analyte concentration; b) Molar ratio of oxidation agent to the analyte concentration in relation to the oxidation efficiency; Error bars indicate 99 % confidence intervals after Gaussian error propagation for the carbon fractions

Figure 4.4: Linearity of the obtained peak areas by IRMS in relation to the injected DIC concentration. Flow injection experiments were carried out at three different system flow conditions: (system flow of 300 µL min^{-1}: 200 µL min^{-1} HPLC, 50 µL min^{-1} oxidation agent, 50 µL min^{-1} H_3PO_4), (system flow of 500 µL min^{-1}: 400 µL min^{-1} HPLC, 50 µL min^{-1} oxidation agent, 50 µL min^{-1} H_3PO_4), (system flow of 700 µL min^{-1}: 600 µL min^{-1} HPLC, 50 µL min^{-1} oxidation agent, 50 µL min^{-1} H_3PO_4)

Figure 4.5: Flow injection of common LC-IRMS analytes at identical oxidation conditions and varying concentrations; circles indicate the peak area obtained by IRMS, horizontal bars correspond to the calculated oxidation efficiency compared to the DIC reference measurement. Flow rate HPLC, 600 µL min^{-1}, $Na_2S_2O_8$ (0.42 M, 50 µL min^{-1}), H_3PO_4 (1M, 50 µL min^{-1}). Error bars might be smaller than the symbols (99 % confidence intervals)

Figure 4.6: Comparison of the $\delta^{13}C$ values obtained for the compounds analyzed by flow injection. Dotted lined represent the ± 0.5 ‰ range around the mean $\delta^{13}C$ value. Error bars indicate the 99 % confidence interval. Results for the concentration level of 50 mg L^{-1} could not be obtained as the signal intensity was below the threshold of 1 V (m/z 44, 3 x 10^8 Ω) *n=2 no calculation of confidence interval possible. $\delta^{13}C$ values were calculated using CO_2 reference gas set to 0 ‰ and are not normalized to the VPDB scale as they were inteded to be used to monitor the stability of the $\delta^{13}C$ signal only and are not used for further interpreatation of the data.

Figure 4.7: Peak areas and $\delta^{13}C$ values obtained for methanol and xylitol by LC-IRMS at different flow and oxidation conditions; circles indicate the peak area obtained by IRMS, diamonds correspond to the $\delta^{13}C$ ratio measured against the CO_2 reference gas. Instrumental parameters: (a, b: HPLC flow, 500 µL min^{-1}; H_3PO_4 1.5 M, 50 µL min^{-1}; $Na_2S_2O_8$ 0.84 M, 50 µL min^{-1}), (c, d: HPLC flow, 500 µL min^{-1}; H_3PO_4 1.5 M, 50 µL min^{-1}; $Na_2S_2O_8$ 0.42 M, 50 µL min^{-1}), (e, f: HPLC flow, 200 µL min^{-1}; H_3PO_4 0.75 M, 50 µL min^{-1}; $Na_2S_2O_8$ 0.21 M, 50 µL min^{-1}) Error bars might be smaller than the symbols (99 % confidence intervals)

Figure 4.8: Peak areas and $\delta^{13}C$ values obtained for caffeine by LC-IRMS at different oxidation conditions; circles indicate the peak area obtained by IRMS, diamonds correspond to the $\delta^{13}C$ ratio measured against the CO_2 reference gas. Instrumental parameters: (a: HPLC flow, 500 µL min^{-1}; H_3PO_4 1.5 M, 50 µL min^{-1}; $Na_2S_2O_8$ 0.84 M, 50 µL min^{-1}), (b: HPLC flow, 500 µL min^{-1}; H_3PO_4 1.5 M, 50 µL min^{-1}; $Na_2S_2O_8$ 0.42 M, 50 µL min^{-1}) Error bars might be smaller than the symbols (99 % confidence intervals)

Figure 4.9: $\delta^{13}C$ values obtained for different concentrations of xylitol (a) and methanol (b) oxidized at 100 °C (diamonds) in contrast to the reduced peak areas obtained by a reduction of the oxidation temperature (spheres). Error bars indicate the 99 % confidence interval and may be smaller than the symbols. $\delta^{13}C$ values were calculated using CO_2 reference gas set to 0 ‰ and are not normalized to the VPDB scale as they were intended to be used to monitor the stability of the $\delta^{13}C$ signal only and are not used for further interpretation of the data.

Figure 5.1: Setup for the mineralization experiments: triple-necked glass flask with reflux cooler, heating plate with automatic temperature control, manual three-port valve, and crushed ice cooling system

Figure 5.2: Cation chromatogram of solutions containing $Na_2S_2O_8$ (30 mmol L^{-1}), $K_2S_2O_8$ (30 mmol L^{-1}), and NH_4Cl (50 mg L^{-1} (N))

Figure 5.3: Effect of the injection volume on the chromatographic separation of ammonium and potassium by cation chromatography ($c(K^+)$=60 mmol L^{-1}) a) injection volume of 4 µL b) injection volume of 10 µL

Figure 5.4: Recovery rates obtained for the determination of TOC and TNb from glycine, NH_4Cl, and $NaNO_3$ at different $K_2S_2O_8$ concentration in the sample matrix. Error bars indicate the 95 % confidence interval after error propagation of the individual measurement uncertainties. *used to calculate the correction factor in section 5.6.4

Figure 5.5: Recovery rates obtained for the determination of TOC and TNb from glycine, NH_4Cl, and $NaNO_3$ at different NaCl (a) and K_2SO_4 (b) concentration in the sample matrix. Error bars indicate the 95 % confidence interval after error propagation of the individual measurement uncertainties

Figure 5.6: PDS concentration during the mineralization of organic compounds as a result of the heat induced decomposition and further transformation to sulfate. The dashed line indicates the 7.5 mmol L^{-1} threshold above which a constant effect of the PDS on the TNb measurements was observed. k_1 (batch experiment 96-98 °C) = 0.74 x 10^{-3} s^{-1}

Chapter 10: List of Tables

Chapter 11: List of Abbreviations

LC-IRMS	Liquid chromatography isotope ratio mass spectrometry
TOC	Total organic carbon
TNb	Total nitrogen bound (Total dissolved nitrogen except for dissolved N_2)
IC	Ion chromatography / Inorganic carbon
SIA	Stable Isotope Analysis
CSIA	Compound-specific isotope analysis
GC-IRMS	Gas chromatography isotope ratio mass spectrometry
C3 plants	Plant type employing the Calvin cycle for photosynthesis
C4 plant	Plant type employing the Hatch-Slack pathway for photosynthesis
EIE	Equilibrium Isotope Effect
KIE	Kinetic Isotope Effect
NMR	Nuclear magnetic resonance
SNIF-NMR	Site specific natural-isotope fractionation nuclear magnetic resonance
MS	Mass spectrometry
TIMS	Thermal ionization mass spectrometry
ICP-MS	Inductively coupled plasma mass spectrometry
GIRMS	Gas isotope ratio mass spectrometry
EI	Electron impact ionization
EA-IRMS	Elemental analyzer isotope ratio mass spectrometry
TCD	Thermal conductivity detector
GC	Gas chromatography
HPLC	High performance liquid chromatography
RP	Reversed phase

WCO	Wet chemical oxidation
HTC	High temperature combustion
CRI	Chemical reaction interface
BSIA	Bulk stable isotope analysis
FIA	Flow injection analysis
GSSG	Glutathione disulfide
DOC	Dissolved organic carbon
EPS	Extracellular polymeric substances
DIC	Dissolved inorganic carbon
CAM	Plant employing the Crassulacean Acid Metabolism
PDB	Pee Dee Belemnite
VPDB	Vienna Pee Dee Belemnite
IAEA	International Atomic Energy Agency
TN	Total nitrogen
PTFE	Polytetrafluoroethylene
PDS	Peroxydisulfate
TC	Total carbon
NPOC	Non-purgeable organic carbon

Chapter 12: List of Publications

12.1 Publications in peer-reviewed journals

2020 T.L.V. Bornemann, P.S. Adam, V. Turzynski, U. Schreiber, P.A. Figueroa-Gonzalez, J. Rahlff, D. Köster, T.C. Schmidt, R. Schunk, B. Krauthausen, A.J. Probst, *Geological degassing enhances microbial metabolism in the continental subsurface*, Submitted to Nature Communications

2020 B.M. Gilbert, M. Nachev, M.A. Jochmann, T.C. Schmidt, D. Köster, B. Sures, A. Avenant-Oldewage, *You are what you eat. Differences in trophic levels of two parasite species infecting a single host according to stable isotopes,* Parasitology Research, https://doi.org/10.1007/s00436-020-06619-1

2019 D. Köster, I.M. Sanchez Villalobos, M.A. Jochmann, W.A. Brand, T.C. Schmidt, *New Concepts for the Determination of Oxidation Efficiencies in Liquid Chromatography-Isotope Ratio Mass Spectrometry*, Analytical Chemistry, 91 (8), pp. 5067–5073

2019 D. Köster, M.A. Jochmann, H.V. Lutze, T.C. Schmidt, *Monitoring of the total carbon and nitrogen balance during the mineralization of nitrogen containing compounds by heat activated persulfate,* Chemical Engineering Journal, 367, pp. 160-168

2019 S.M. Schulte, D. Köster, M.A. Jochmann, R.U. Meckenstock, *Applying reverse stable isotope labeling analysis by mid-infrared laser spectroscopy to monitor BDOC in recycled wastewater,* Science of the Total Environment, 665, pp. 1064-1072

2019 C. Koch, M. Nachev, J. Klein, D. Köster, O.J. Schmitz, T.C. Schmidt, B. Sures, *Degradation of the Polymeric Brominated Flame Retardant "Polymeric FR" by Heat and UV Exposure*, Environmental Science and Technology, 53(3), pp. 1453-1462

2019 B. Sures, M. Nachev, B.M. Gilbert, Q.M. Dos Santos, M.A. Jochmann, D. Köster, T.C. Schmidt, A. Avenant-Oldewage, *The monogenean Paradiplozoon ichthyoxanthon behaves like a micropredator on two of its hosts, as indicated by stable isotopes,* Journal of Helminthology, 93(1), pp. 71-75

2018 D. Köster, J.B. Wolbert, M.S. Schulte, M.A. Jochmann, T. C. Schmidt, *Origin of Xylitol in Chewing Gum: A Compound-Specific Isotope Technique for the Differentiation of Corn- and Wood-Based Xylitol by LC-IRMS, Journal of Agricultural and Food Chemistry, 2018, 66 (8)*

12.2 Poster Presentations

2018	D. Köster, M.A. Jochmann, H.V. Lutze, T.C. Schmidt, *Monitoring of the total carbon and nitrogen balance during the mineralization of nitrogen containing compounds by sulfate radicals,* 3. Wasseranalytische Seminar, Mülheim an der Ruhr
2017	J.B. Wolbert, D. Köster, M.A. Jochmann, T.C. Schmidt, *Coupling LC-IMRS with high resolution mass spectrometry,* Isotopes 2017, Mt. Verità, Ascona, Schweiz
2017	D. Köster, J.-B. Wolbert, M.A. Jochmann, T.C. Schmidt, *Determination of compound specific carbon isotope ratios for xylitol in chewing gum by LC-IRMS*, ANAKON 2017, Tübingen
2016	D. Köster, T. Hesse, M.A. Jochmann, T.C. Schmidt, *Determination of the inorganic nitrogen species formed during the oxidation of organic compounds formed by sulfate radicals,* 2016, Analytica Conference, München

12.3 Presentations

2018	D. Köster, J.B. Wolbert, M.A. Jochmann, T.C. Schmidt, *The origin of xylitol in chewing gum – a compound-specific isotope technique for the differentiation of corn and wood based xylitol by LC-IRMS,* 28. Doktorandenseminar, Hohenroda

13 Lebenslauf

Der Lebenslauf ist in der Online-Version aus Gründen des Datenschutzes nicht enthalten.

Der Lebenslauf ist in der Online-Version aus Gründen des Datenschutzes nicht enthalten.

14 Erklärung

Hiermit versichere ich, dass ich die vorliegende Arbeit mit dem Titel:

„Applications for liquid chromatography coupled to isotope ratio mass spectrometry and evaluation of the oxidation processes towards compound specific δ^{15}N analysis"

selbst verfasst und keine außer den angegebenen Hilfsmitteln und Quellen benutzt habe, und dass die Arbeit in dieser oder ähnlicher Form noch bei keiner anderen Universität eingereicht wurde.

Essen, den 18.03.2020

Daniel Köster

15 Declaration of scientific contributions

The present thesis includes work that has been published in cooperation with Co-authors, with my own contributions declared as follows:

D. Köster, J.B. Wolbert, M.S. Schulte, M.A. Jochmann, T. C. Schmidt, *Origin of Xylitol in Chewing Gum: A Compound-Specific Isotope Technique for the Differentiation of Corn- and Wood-Based Xylitol by LC-IRMS, Journal of Agricultural and Food Chemistry, 2018, 66 (8)*

Declaration of own contributions: The experiments were conducted by D. Köster, J.B. Wolbert and M.S. Schulte. The evaluation of the experimental data was performed by D. Köster. The draft and corrections to the manuscript were written by D. Köster. The manuscript was revised by D. Köster, J.B. Wolbert, M.S. Schulte, M.A. Jochmann, and T. C. Schmidt.

D. Köster, M.A. Jochmann, H.V. Lutze, T.C. Schmidt, *Monitoring of the total carbon and nitrogen balance during the mineralization of nitrogen containing compounds by heat activated persulfate,* Chemical Engineering Journal, 367, pp. 160-168

Declaration of own contributions: The experiments were conducted by D. Köster. The evaluation of the experimental data was performed by D. Köster. The draft and corrections to the manuscript were written by D. Köster. The manuscript was revised by D. Köster, M.A. Jochmann, H.V. Lutze, and T.C. Schmidt.

D. Köster, I.M. Sanchez Villalobos, M.A. Jochmann, W.A. Brand, T.C. Schmidt, *New Concepts for the Determination of Oxidation Efficiencies in Liquid Chromatography-Isotope Ratio Mass Spectrometry*, Analytical Chemistry, 91 (8), pp. 5067–5073

Declaration of own contributions: The experiments were conducted by D. Köster and I.M. Sanchez Villalobos. The evaluation of the experimental data was performed by D. Köster. The draft and corrections to the manuscript were written by D. Köster. The manuscript was revised by D. Köster, M.A. Jochmann, W.A. Brand, T.C. Schmidt.

16 Danksagung

Zuallererst möchte ich meinen großen Dank an Professor Torsten C. Schmidt aussprechen, für die Betreuung meiner Promotion und der damit verbundenen langjährigen Zusammenarbeit sowie der Begutachtung meiner Dissertation.

Für die Übernahme des Zweitgutachtens möchte ich Herrn Professor Oliver J. Schmitz danken.

Bei Herrn Dr. Maik A. Jochmann möchte ich mich für die fachliche Unterstützung bei der Erarbeitung meines Promotionsthemas, die Begleitung der Arbeiten im Labor, sowie für die moralische Unterstützung über die gesamte Dauer der Promotion bedanken.

Herrn Willi A. Brand möchte ich für die fachlichen Diskussionen, die Unterstützung bei der Erarbeitung des Projektes und der Mitarbeit an der Publikation der Ergebnisse aus dieser Promotion danken.

Für viele hilfreiche Diskussionen, moralische Unterstützung und Zusammenarbeit im Labor möchte ich Marcel, Benny, Christian, Kamil, Xochitli, Tobias, Lotta, Wiebke, Irene, Nenad, Sajjad und Nerea ausdrücklich danken. Außerdem möchte ich mich bei allen Mitarbeitern der Instrumentellen Analytischen Chemie der Universität Duisburg-Essen für die gute Zusammenarbeit und die lange Zeit, die mich viele seit dem Masterstudium begleitet haben bedanken - ich werde die gemeinsame Zeit immer in guter Erinnerung behalten.

Bei meiner Familie bedanke ich mich von ganzem Herzen für ihre langjährige Unterstützung durch mein komplettes Studium und während der Promotion. Insbesondere danke ich Cornelia für ihr Vertrauen in mich und die Unterstützung durch alle Höhen und Tiefen die man bei der Verwirklichung eines solchen Projekts durchläuft.